METAL SPECIFICITY AND THE MECHANISM OF ALLOSTERIC REGULATION IN METAL-SENSING METAL-RESPONSIVE TRANSCRIPTIONAL REPRESSORS *Staphylococcus aureus* CzrA AND *Mycobacterium tuberculosis* NmtR

A Dissertation

by

MARIO ANTONIO PENNELLA

Submitted to the Office of Graduate Studies of
Texas A&M University
in partial fulfillment of the requirements for the degree of

DOCTOR OF PHILOSOPHY

May 2005

Major Subject: Biochemistry

METAL SPECIFICITY AND THE MECHANISM OF ALLOSTERIC REGULATION IN METAL-SENSING METAL-RESPONSIVE TRANSCRIPTIONAL REPRESSORS *Staphylococcus aureus* CzrA AND *Mycobacterium tuberculosis* NmtR

A Dissertation

by

MARIO ANTONIO PENNELLA

Submitted to Texas A&M University
in partial fulfillment of the requirements
for the degree of

DOCTOR OF PHILOSOPHY

Approved as to style and content by:

David P. Giedroc
(Chair of Committee)

Gary R. Kunkel
(Member)

J. Martin Scholtz
(Member)

Patricia LiWang
(Member)

Gregory D. Reinhart
(Head of Department)

May 2005

Major Subject: Biochemistry

ABSTRACT

Metal Specificity and the Mechanism of Allosteric Regulation in Metal-Sensing Metal-Responsive Transcriptional Repressors *Staphylococcus aureus* CzrA and *Mycobacterium tuberculosis* NmtR. (May 2005)

Mario Antonio Pennella, B.S., University of Oklahoma

Chair of Advisory Committee: Dr. David P. Giedroc

The metal-responsive transcriptional repressors of the SmtB/ArsR family repress the expression of their respective operons in the absence of metal and are released from the operator/promoter region when metal ions bind, thus allowing RNA polymerase to bind and transcribe the operon, which encodes genes involved in homeostasis and resistance. To elucidate the determinants of metal ion selectivity, comparative metal-binding and DNA-binding properties of *S. aureus* CzrA and *M. tuberculosis* NmtR were characterized. The structure of the metal coordination complexes of CzrA and NmtR reveal that CzrA forms a 4-coordinate, tetrahedral complex with both Zn(II) and Co(II) potent regulators of *czr* operator/promoter (O/P) binding *in vitro* and de-repression *in vivo*. In contrast, NmtR adopts 5- or 6-coordinate complexes with Ni(II) and Co(II), the strongest allosteric regulators of *nmt* O/P binding *in vitro* and de-repression *in vivo.* Zn(II), a non-inducer *in vivo* and poor regulator *in vitro*, binds NmtR with high affinity and forms a non-native 4-coordinate complex. These studies suggest that metal coordination geometries (number), not metal binding affinities, are primary determinants of functionality.

To gain molecular insight into the mechanism of allosteric regulation of O/P binding by metal ions, NMR and X-ray crystallographic studies of apo- and zinc forms of CzrA, and another ArsR/SmtB zinc sensor, *Synechococcus PCC7942* SmtB, were performed. These studies showed that formation of the metal chelate drives a quaternary structural switch mediated by an intersubunit hydrogen-binding network that originates with the nonliganding $N^{\varepsilon 2}$ face of His97 in CzrA (His117 in SmtB) that stabilizes a low affinity DNA-binding conformation.

Mutagenesis experiments reveal that substitution of D84 and H97 in CzrA, results in the formation of higher coordination number complexes that are nonfunctional in driving zinc-mediated allosteric regulation of DNA binding. In contrast, conservative mutations of H86 and H100 in CzrA bind Co(II) or Zn(II) in a tetrahedral manner, albeit with greatly reduced affinity, and allosterically regulate O/P binding with significant lower coupling free energies compared to wild-type CzrA. These findings further reinforce the notion that metal coordination geometry is the primary determinant for functional sites in metal-sensing transcriptional repressors.

DEDICATION

I would like to dedicate this work to my parents, Dr. Filippo Pennella and Barbara Pennella. They've supported me continuously through my entire life. Anytime I've needed anything or have had any trouble they have helped me. I cannot express how much this has meant to me, especially the last seven years. I would also like to express my gratitude to my wife, Dr. Min Xu, and my step-son Dingwen (Bao Bao) Li. They've made the last two years of my life the best years in my life. I love all of you.

ACKNOWLEDGMENTS

I would like to thank my advisor Dr. David P. Giedroc for the opportunity to work under his supervision in his laboratory. His guidance and patience allowed me to work through several projects before working on this main project presented here, which has been a fruitful experience. I would also like to thank current and former members of the Giedroc laboratory including Xiaohua Chen, Laura Busenlehner, Michael VanZile, Paul Nixon, Julius Apuy, Peter Cornish, Raza Kahn, Suzanne Stammler, Lichun Li, Yun Wang, Tong Liu, Sun-Bae Lee, Hermes Reyes Caballeros, and Arun Kumar. I would like to also acknowledge the help and comments of the members of my committee: Dr. Gary Kunkel, Dr. Patricia LiWang, and Dr. J. Martin Scholtz. I would like to also give thanks to collaborators including Dr. Toshiko Ohta (University of Tsukuba), Dr. Robert Scott, Dr. Nate Cosper, and Jacob Shokes (University of Georgia), Dr. Karl Koshlap (University of North Carolina), Dr. James Sacchettini (Texas A&M University) and especially Dr. Christoph Eicken (Institute of Biosciences and Technology-Houston, Texas A&M University) and his work on solving the high resolution 3-D crystal structures of apo and zinc forms of SmtB and CzrA, which were integral for much of the work presented here.

TABLE OF CONTENTS

CHAPTER Page

I INTRODUCTION 1

Regulatory metals in metalloregulatory proteins 4
MerR family 7
DtxR family 11
Fur family 16
NikR family 21
SmtB/ArsR family 24
Metal binding sites of SmtB/ArsR proteins 27
α3N sensors: CadC 29
α5 sensors: SmtB, NmtR, and CzrA 31
Scope of the research 34

II STRUCTURAL ELEMENTS OF METAL SELECTIVITY IN METAL SENSOR PROTEINS 37

Introduction 37
Materials and methods 40
Results 46
Discussion 58

III A METAL-LIGAND MEDIATED INTERSUBUNIT ALLOSTERIC SWITCH IN RELATED SmtB/ArsR ZINC SENSOR PROTEINS 63

Introduction 63
Materials and methods 66
Results 72
Discussion 85

IV FUNCTIONAL ROLES OF INDIVIDUAL ZINC LIGANDS IN MEDIATING ALLOSTERIC REGULATION OF DNA BINDING *S. aureus* CzrA 88

Introduction 88
Materials and methods 92
Results 96
Discussion 108

CHAPTER Page

V SUMMARY AND PERSPECTIVES 114

REFERENCES 123

VITA 136

LIST OF FIGURES

FIGURE Page

1.1 Coordination chelates of CueR and ZntR with a sequence alignment of selected members of the MerR family.. 9

1.2 Coordination chelates of wt and D8M MntR and a sequence alignment of four members of the DtxR family..14

1.3 Coordination chelate of *P. aeruginosa* Fur and sequence alignment of selected members of the Fur family 19

1.4 Coordination chelate of *E. coli* NikR and a sequence alignment of selected members of the NikR family 23

1.5 Coordination chelate of Zn_2 SmtB and a sequence alignment of three representative members from the SmtB/ArsR family........................28

1.6 The general operon structure regulated by SmtB/ArsR Family transcriptional repressors and the core 12-2-12 inverted repeat motifs of the SmtB/ArsR-regulated O/Ps 30

2.1 Multiple sequence alignment SmtB, CzrA, and NmtR from the SmtB/ArsR family 39

2.2 CzrA and NmtR DNA binding experiments 48

2.3 Optical spectroscopy of CzrA, NmtR, and SmtB......................................52

2.4 Spectroscopic analysis of metallated NmtR..53

2.5 EXAFS of CzrA, NmtR, and SmtB...55

3.1 Structure of cyanobacterial SmtB...67

3.2 Structure of *S. aureus* CzrA 75

3.3 An intersubunit hydrogen-bonding network in Zn_2 α5-SmtB involved in allosteric coupling of Zn and DNA binding sites 78

3.4 NMR evidence in support of a metal-ligand mediated hydrogen-bonding network in Zn_2 CzrA in solution.................................80

FIGURE Page

3.5 Main-chain amide hydrogen-deuterium exchange rates of apoCzrA and Zn_2 CzrA.......... 82

3.6 Structure of Zn_1 SmtB and zinc binding properties of CzrA 84

4.1 Sequence alignment of members from the SmtB/ArsR family.......... 90

4.2 Cobalt uv-vis spectroscopy on CzrA variants.......... 97

4.3 Representative titrations of Zn(II) into a mixture of competitor (mag-fura-2 or quin-2) and variant CzrAs with the overall K_{Zn} for each variant CzrA plotted 101

4.4 NMR Spectroscopy of wild-type and variant CzrAs.......... 104

4.5 Representative binding isotherms of apo and zinc forms of variant CzrAs (H86D, H86N, and H97N) to fluorescein-labeled DNA oligonucleotide containing the czr O/P sequence 106

4.6 An amino acid sequence alignment of the $\alpha5$ metal binding sites of selected proteins from the SmtB/ArsR family.......... 111

5.1 Model of CzrA regulation of Zn(II) 120

LIST OF TABLES

TABLE Page

1.1 Families of Metalloregulatory Proteins in Prokaryotes 6

2.1 Sedimentation Equilibrium Ultracentrifugation Analysis of CzrA and NmtR.. 45

2.2 Curve Fitting Results for EXAFS... 57

3.1 Data Collection and Refinement Statistics 69

4.1 Equilibrium Association Constants for the Binding of Co(II) (K_{Co}) and Zn(II) (K_{Zn}) to CzrA Variants.................................... 99

CHAPTER I

INTRODUCTION

The folding of small globular domains within gene regulatory proteins is required for sequence-specific DNA binding, an event that underlies gene expression in all kingdoms of life (Spolar and Record, 1994). The formation of zinc-ligand coordination bonds provides the major driving force for the folding of these mini-domains that lack an appreciable hydrophobic core (Berg and Godwin, 1997). Over the last two decades, an explosion in our knowledge of the diverse roles that the essential trace element zinc plays in DNA metabolism, chromatin remodeling, transcriptional regulation, nucleic acid packaging and ribosome biogenesis has taken place (Blencowe and Morby, 2003; Fingerman *et al.*, 2003; Frausto da Silva and Williams, 2001; Katz and Jentoft, 1989; Maret, 2001).

Zinc is found in all human body tissues with 30-40% found in the nucleus, 50% in the cytosol, with the remainder found in organelles, vesicles, and the cell membrane (Tapiero and Tew, 2003). Zinc plays critical roles in the reduction of common infections, helps in the prevention of stunting growth, and supports neurobehavioral development among other attributes (Hotz *et al.*, 2003). Zinc is an essential trace element in all organisms, and the unique combination of structural and thermodynamic properties of zinc make it ideally suited for a diverse array of biological roles. These

---

This dissertation follows the style and format of *Molecular Microbiology*.

properties include its ready availability, Lewis acidity, high concentration of charge (atomic radii of 0.65 Å), lack of redox reactivity and stable oxidation state (2+). Zn(II) is a d^{10} transition metal ion that forms metal complexes of high thermodynamic stability that are often characterized by facile ligand exchange (Frausto da Silva and Williams, 2001).

Zinc binds nearly exclusively to three types of amino acid side chains in proteins. These are cysteines, histidines, and carboxylates (Asp and Glu) with thiolate sulfurs and imidazole nitrogens by far the most common donor atoms. Zinc sites in proteins adopt a variety of coordination structures that differ in the number of ligands bound (coordination number), the type of ligands, metal-ligand bond lengths, dihedral ligand-metal-ligand bond angles, and in some cases, second shell interactions (Frausto da Silva and Williams, 2001). The Metalloprotein Database and Browser hosted by The Scripps Research Institute (http://metallo.scripps.edu/) reveals that among the approximately 3100 structurally characterized zinc coordination sites deposited in the Protein Data Bank (http://www.rcsb.org/pdb), the most prominent coordination number is four (1726), the most common liganding pattern tetrathiolate (C_4 or S_4) (484), with tetrahedral or distorted tetrahedral coordination geometries by far the most prevalent for zinc sites classified as of April 2004 (Castagnetto *et al.*, 2002).

Zinc complexes in proteins perform structural, catalytic and regulatory functions. Structural zinc sites typically adopt tetrahedral or distorted tetrahedral coordination geometries formed by four protein-derived ligands with no bound water molecules. Cysteines and histidines are by far the preferred ligands in such sites (*e.g.* zinc fingers)

(Auld, 2001). Catalytic and regulatory Zn(II) sites utilize the same amino acid ligands as structural sites, but include a greater percentage of carboxylate ligands derived from aspartate and glutamate, as well as solvent molecules (H_2O), which are almost always found in catalytic sites in enzymes (*e.g*. carbonic anhydrase) (Auld, 2001). Co-catalytic sites, defined as catalytic metal sites that coordinate two metal ions via a bridging ligand(s) (*e.g.,* phosphotriesterase), are formed by ligand sets similar to those found in catalytic sites, except that cysteine residues that typify structural zinc cluster sites (*e.g*., metallothioneins) are never found as a bridging ligand in metalloenzymes (Auld, 2001).

Structural zinc ions stabilize protein tertiary structure, protein-protein, and protein-nucleic acid interfaces. The zinc coordination bonds induce thermal and conformational rigidity to these important domains of proteins much like disulfide bonds do in oxidizing environments. In the absence of zinc, these protein domains are unfolded and exist in a predominantly random coil conformation and are presumably subjected to rapid degradation and clearance by the cell. The most striking and seminal illustration of how “structural zinc” stabilizes tertiary structure formation in DNA binding proteins is in zinc finger (zf) proteins (Krishna *et al.*, 2003). Classical C_2H_2 (Cys_2His_2) zinc finger domains, which mainly include DNA-binding proteins (they also mediate protein-RNA, protein-protein, and protein-lipid interactions) are small (~30 amino acid residues) domains that fold around one or more zinc ions, and are nearly exclusively found in eukaryotic organisms (Jantz *et al.*, 2004; Matthews and Sunde, 2002). Recent findings reveal that canonical C_2H_2 zinc finger domains in transcriptional regulatory proteins in eukaryotes are not exclusively involved in structural stability but have also been implicated in regulating the concentration of bio-available zinc in cells (Bird *et al.*, 2003; Giedroc *et al.*, 2001).

Sub-optimal or toxic (above normal physiological levels) concentrations of intracellular zinc have adverse affects on many aspects of cellular metabolism. Zinc is now known to function at the level of transcription by binding directly to regulatory proteins, *i.e.,* metal sensor proteins that repress, de-repress, or activate the transcription of genes that encode metal transporters (importers/exporters) and/or metal chelators. This helps cells maintain homeostasis, or an optimal steady-state concentration of zinc within the cytosol and other intracellular organelles (Blencowe and Morby, 2003; Eide, 2003).

REGULATORY METALS IN METALLOREGULATORY PROTEINS

Transition metal ions, including Zn(II) are essential for survival, but become toxic at high intracellular concentrations. In all kingdoms of life, cells must therefore be capable of regulating the steady-state concentration or available pool of individual metal ions via the coordinate regulation of specific metal import and metal efflux or chelation systems. This metal homeostasis is established by metalloregulatory proteins which "sense" when the concentration or pool of a particular transition metal ion in the cytosol or an intracellular compartment becomes either deficient or exceeds critical levels required for normal cellular metabolism. These proteins are almost always involved in regulating an operon that encodes a metal-specific efflux pump or membrane bound transporters, metal reductases, cytoplasmic or periplasmic metal transport proteins, or metal-sequestering proteins as well as the metal-responsive transcriptional regulator for the operon (Silver and Phung, 1996). These transcriptional regulators can function as repressors or activators. Through extensive biochemical, molecular genetic and more recently, whole genome sequencing efforts, a large number of known or putative metal-responsive regulator proteins have been identified, especially in eubacteria and archeabacteria. Five distinct subfamilies of prokaryotic metal sensing transcriptional regulators have emerged from these studies and include the ArsR (or SmtB/ArsR), DtxR, Fur, MerR, and NikR families of metalloregulators (Table 1.1). Zinc-specific metalloregulators in four of the five families (NikR family as of 2004 only contains nickel-specific regulators) have been discovered, and in some cases extensively characterized as to the structure of the coordination chelate, how individual family members recognize or detect a specific metal ion, and how metal binding positively or negatively allosterically regulates DNA binding and transcription of the resistance or uptake operons. Metal sensor proteins and the determinants of their coordination chelates (number of ligands, types of ligands, and coordination geometry) are discussed as are important factors that determine metal selectivity (zinc vs. other metal ions) in these families of related sensor proteins. These aspects of metal regulation in prokaryotes are discussed in turn.

TABLE 1.1. Families of Metalloregulatory Proteins in Prokaryotes

Family	Fold/DNA binding motif	Example(s)[a]	States[b]	Structure[c]
ArsR/ SmtB	ααααββα/Winged HTH	ArsR (As, Ab) CadC (Cd, Pb) CzrA, SmtB (Zn) NmtR (Ni)	apo - Repressor metal - Weak repressor	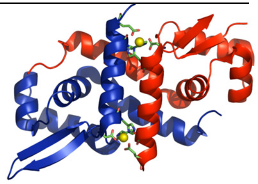
DtxR	αααββαααα/ N-terminal Winged Helix	DtxR (Fe) IdeR (Fe) MntR (Mn)	apo - weak repressor metal - co-repressor	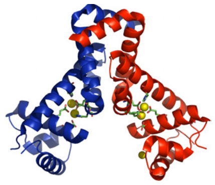
Fur	ααααββββαβ/ N-term Winged Helix	Fur (Fe) Zur (Zn)	apo - weak repressor metal - co-repressor	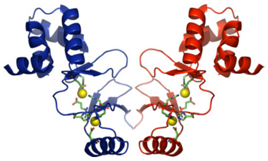
MerR	βααββαααα/ N-term Winged Helix	CueR (Cu) MerR (Hg) PbrR (Pb) ZntR (Zn)	apo - repressor metal - activator	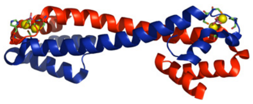
NikR	βααβαββαβ/ Ribbon-helix-helix	NikR (Ni)	apo - weak repressor Metal - co-repressor	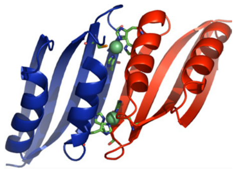

---

[a] Includes examples of proteins and the predominant metal(s) they regulate *in vivo* and *in vitro*.

[b] Represents the functional states of the apo- and metallated forms of the repressors.

[c] The following are representative crystal structures from each family: the ArsR family is the Zn_2 form of SmtB; the DtxR family is Mn(II)-bound wtMntR; the Fur family is Zn(II)-bound Fur; the MerR family is Zn(II) bound ZntR; and the NikR family is Ni(II) bound C-terminal NikR. For each structure one protomer is colored blue and the other protomer is red. Small yellow, red, and green spheres that appear in the structures represent bound metal ions.

MerR FAMILY

The MerR family of regulators activate gene expression by distorting the operator DNA sequence and cause RNA polymerase to initiate transcription at an otherwise suboptimal promoter (Brown *et al.*, 2003). Members of this family are characterized by N-terminal winged-helix DNA binding domains, followed by a long coiled-coil region. The C-terminal helical domain is the effector binding domain (Brown *et al.*, 2003). MerR orthologs that bind a wide range of inducers including metal ions, lipophilic drugs, nitric oxide and superoxide (induced by oxidative stress) are known. The paradigm of this family and hence where the name derives comes from the seminal studies of *merR* genes of transposons Tn*501* from *P. aeruginosa* and Tn*21* from *Shigella flexneri* R100 plasmid. In Gram-negative systems, MerR regulates expression of the mercury resistance divergon (*merTP(C/F)AD(E)* and *merR*) from the major regulated promoter (Barkay *et al.*, 2003). MerR has been shown to bind to the operator/promoter region of the *mer* operon which contains a 7-4-7 inverted repeat. MerR activates the transcription of the operon in the presence of Hg(II) and acts as a weak repressor in the absence of Hg(II) (Brown *et al.*, 2003). A unifying feature of the family of MerR is that repression and activation requires the regulator bound on the -35 and -10 regions of the promoter. The -35 and -10 region is separated by a longer spacer than normal (19 bp versus 17 bp). This suggested that the promoter structure was important to the regulatory mechanism. Activation distorts the DNA at the center of the operator to realign the –35 and -10 sequence, allowing RNA polymerase to transcribe the genes upon activation (Ansari *et al.*, 1992). Insertions or deletions (1 to 2 bp) in the 19 bp spacer have shown to abolish promoter activity or increase constitutive promoter activity, respectively, indicating the 19 bp spacer is essential for regulation (Brown *et al.*, 2003).

Although the structure of MerR has not yet been solved, the x-ray crystallographic structures of BmrR and MtaN, two MerR orthologs that regulate multi-drug resistance in pathogenic bacteria have been determined (Godsey *et al.*, 2001; Heldwein and Brennan, 2001). More recently, the crystal structures of two *E. coli*-derived metal-regulators from the MerR family have been reported. These include the zinc-specific regulator ZntR (Table 1.1) to 1.9 Å resolution, and CueR, a Cu(I) sensor to 2.2 Å resolution, which regulates the expression of the efflux pump CopA and periplasmic copper oxidase CueO in response to moderate copper stress. Au(I)- and Ag(I)-liganded complexes of CueR (to 2.5 and 2.1 Å resolution, respectively) have also been determined (Changela *et al.*, 2003). The metal coordination environment of these proteins is likely essential for determining metal specificity of MerR proteins.

E. coli ZntR: A Zn(II)-dependent MerR family regulator. *E. coli* ZntR is mainly zinc inducible and regulates the expression of *zntA*, which encodes a Zn(II)/Cd(II)/Pb(II) ATPase. The ZntR operator is uniquely defined by a 20 bp sequence spacer between the canonical -35 and -10 regions of the promoter. ZntR exists as a dimer, binds two zinc ions per monomer (as determined by x-ray crystallography), and utilizes a MerR-like DNA distortion mechanism to activate the expression of *zntA* (Changela *et al.*, 2003; Outten *et al.*, 1999). Strikingly, x-ray crystallography reveals a binuclear zinc site with

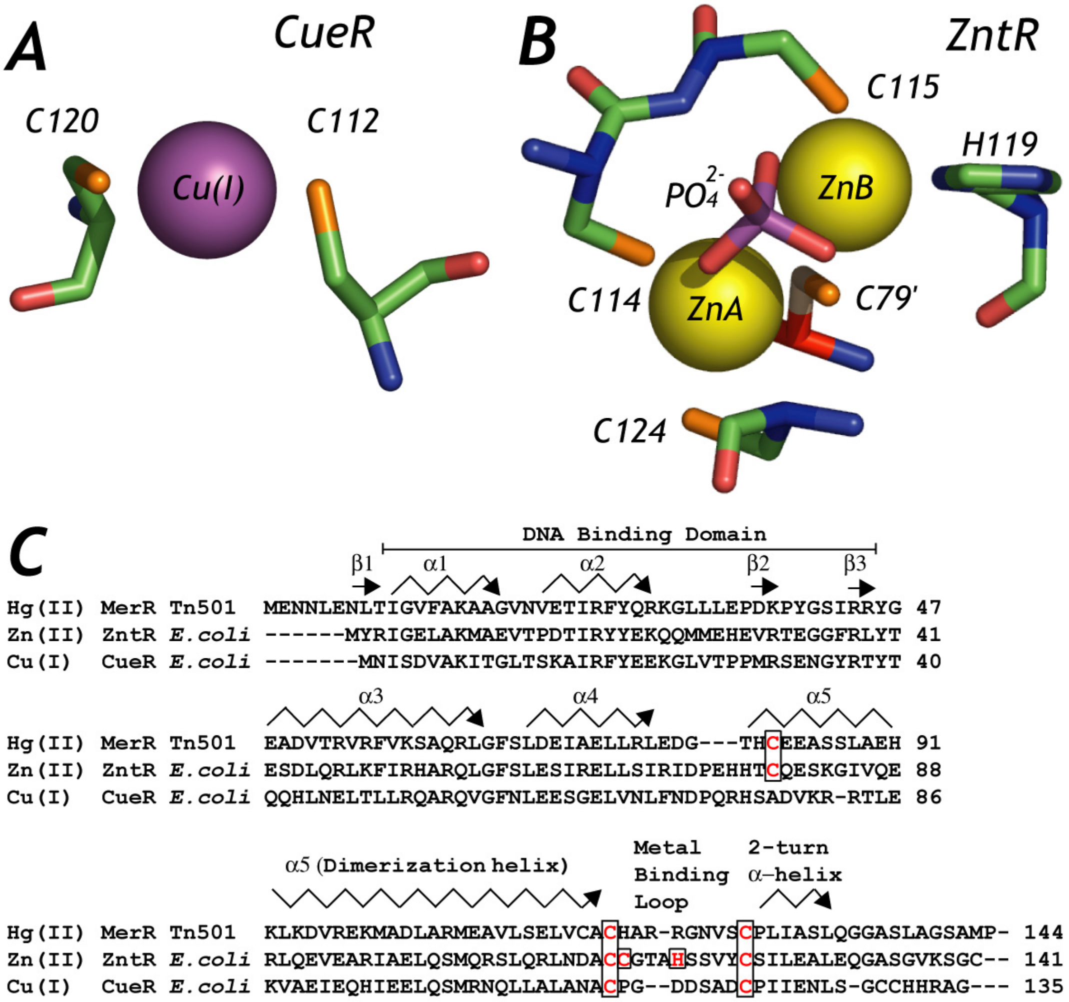
A
CueR
C120
Cu(I)
C112
B
ZntR
C115
H119
PO_4^{2-}
ZnB
C114
ZnA
C79'
C124
C
DNA Binding Domain
β1
α1
α2
β2
β3
Hg(II) MerR Tn501 MENNLENLTIGVFAKAAGVNVETIRFYQRKGLLLEPDKPYGSIRRYG 47
Zn(II) ZntR E.coli ------MYRIGELAKMAEVTPDTIRYYEKQQMMEHEVRTEGGFRLYT 41
Cu(I) CueR E.coli -------MNISDVAKITGLTSKAIRFYEEKGLVTPPMRSENGYRTYT 40
α3
α4
α5
Hg(II) MerR Tn501 EADVTRVRFVKSAQRLGFSLDEIAELLRLEDG---THCEEASSLAEH 91
Zn(II) ZntR E.coli ESDLQRLKFIRHARQLGFSLESIRELLSIRIDPEHHTCQESKGIVQE 88
Cu(I) CueR E.coli QQHLNELTLLRQARQVGFNLEESGELVNLFNDPQRHSADVKR-RTLE 86
α5 (Dimerization helix)
Metal Binding Loop
2-turn α–helix
Hg(II) MerR Tn501 KLKDVREKMADLARMEAVLSELVCACHAR-RGNVSCPLIASLQGGASLAGSAMP- 144
Zn(II) ZntR E.coli RLQEVEARIAELQSMQRSLQRLNDACCGTAHSSVYCSILEALEQGASGVKSGC-- 141
Cu(I) CueR E.coli KVAEIEQHIEELQSMRNQLLALANACPG--DDSADCPIIENLS-GCCHHRAG--- 135

Figure 1.1. Coordination chelates of CueR and ZntR with a sequence alignment of selected members of the MerR family. **(A.)** Close-up of the metal binding domain of CueR with one bound copper shown as a purple sphere and two cysteine residues from the same monomer (C112 and C120) ligating the metal ion with linear coordination geometry (Changela *et al.*, 2003). **(B.)** Close-up of the metal binding domain of ZntR with two bound zinc ions shown as *yellow* spheres. Four zinc-ligating residues are derived from the one protomer (C114, C115, H119, and C124), while a phosphate (or sulfate) anion and the side chain of C79' from the other protomer bridge the two zinc ions. **(C.)** Sequence alignment of Hg(II)-specific Tn501 MerR, Zn(II)-specific *E. coli* ZntR, and Cu(I)-specific *E. coli* CueR (Changela *et al.*, 2003). Known metal binding residues are colored *red* and are boxed. Secondary structure elements are represented above the sequence: β strands, horizontal arrows; α-helices, zig-zag arrows.

each zinc ion bound in a tetrahedral coordination environment and an internuclear Zn-Zn distance of 3.6 Å (Changela *et al.*, 2003). One zinc ion (designated as A) is ligated by Cys114 and Cys124 of the metal binding loop while the other zinc ion (designated as B) is ligated by Cys115 and His119 of same metal binding loop (Figure 1.1) (Changela *et al.*, 2003). The two zinc ions are bridged by the oxygen atoms of a phosphate (or sulfate) anion and by the sulfur of Cys79' from the other protomer. This binuclear Zn(II) coordination complex in ZntR, coupled with the bound anion, was totally unexpected since Hg-MerR requires just one trigonally coordinated Hg(II) ion that bridges the MerR dimer to effect metalloregulation of the *mer* operon (Brown *et al.*, 2003). The extent to which occupancy of one or both metal sites in each of two symmetry-related metal-binding loops in ZntR regulates transcriptional activation has yet to be firmly established, although substitution of all five protein-derived zinc ligands reduces or abrogates the Zn(II) response *in vivo* (Khan *et al.*, 2002). Interestingly, inspection of the ZntR structure and sequence alignment of known ZntRs suggests that a $C_3H(D)$ mononuclear, tetrahedral Zn(II) complex involving Cys114, His(Asp)119, Cys124 and Cys79' could also be readily accommodated by ZntR. Also, His29 and His53 are also required for metalloregulation, although these additional residues likely play a role in mediating DNA distortion by Zn(II)-ZntR (Khan *et al.*, 2002). Three of the four metal binding cysteines in ZntR (Cys79', Cys114, and Cys124) are conserved in Hg-sensing MerRs, and likely constitute the donor atoms to the subunit-bridging *tris*-thiolato Hg(II) complex. In Cu(I)-CueR, cysteines analogous to Cys114 and Cys124 form a linear S-Cu-S regulatory complex (Figure 1.1). Only in known zinc-sensing

ZntRs are His29, His53 and His119 invariant or conserved. Hence, the metal selectivity of MerR family members appears to derive from differences in coordination number and type of metal ligands utilized by different proteins (see Figure 1.1), a finding exactly analogous to that previously demonstrated for two members of the ArsR/SmtB family, a zinc-sensing *S. aureus* CzrA vs. the nickel-sensing NmtR (Pennella *et al.*, 2003).

As a further test of the inducer-specificity of the metal-binding domains in MerR proteins, a chimeric protein has been characterized in which the N-terminal winged-helix DNA-binding domain (44 residues) of *Tn501* MerR was fused to the C-terminal 103 amino acids of ZntR and transcriptional activation measured from a *mer* operator/promoter that contained a 20 bp –10/-35 spacer uniquely characteristic of the *zntA* promoter rather than the wild-type 19-bp spacer in the *mer* operon (Brocklehurst *et al.*, 1999). This hybrid protein responded to Zn(II), but not Hg(II), consistent with the hypothesis that the C-terminal metal-binding domain of MerR proteins plays a major role in metal selectivity and adjustment of the appropriate degree of DNA distortion required by various operator-promoters (Brown *et al.*, 2003).

DtxR FAMILY

The DtxR family of regulators is named after its founding member DtxR from *Cornybacterium diphtheria*. DtxR and a homolog found in *M. tuberculosis*, IdeR, function as Fe(II)-dependent repressors that bind to a hyphenated palindromic sequence as a dimer (Andrews *et al.*, 2003). DtxR negatively regulates genes required for iron acquisition, and expression of a major virulence factor, diphtheria toxin, in response to its co-repressor iron. DtxR contains an N-terminal winged-helix (αααββα) DNA binding domain followed by a helical dimerization domain; some DtxRs also contain a C-terminal Src homology 3 (SH3)-like domain that is rare in bacterial proteins (White *et al.*, 1998). At least 18 crystallographic structures of *C. diphtheria* DtxR and *M. tuberculosis* IdeR have been reported with a variety of divalent metal ions bound, in the presence and absence of DNA. While the coordination structures and functional importance of these bound metal ions is controversial, two distinct metal sites in DtxR/IdeR, termed site 1 and site 2, emerge from these studies. Metal site 1 adopts a distorted octahedral coordination geometry and is coordinated by three residues derived from the α4 (H79, E83) and α5 (H98) helices (see Figure 1.2C), and two residues contributed by the C-terminal SH3 domain (E170 and Q173). Metal site 2 is the putative metalloregulatory site, and adopts a distorted pentacoordinate geometry formed by three closely-spaced and invariant residues in the α5 helix (C102, E105, and H106) as well as M10 from helix α1 (Figure 1.2C) (White *et al.*, 1998).

DtxR (IdeR) orthologs have recently been discovered that are involved in the regulation of genes that encode metal transporters apparently specific for other divalent metal ions, including Mn(II) and perhaps Zn(II). These include *Bacillus subtilis* MntR, highly specific for Mn(II), and *Treponema pallidum* TroR. *B. subtilis* MntR regulates the expression of two manganese transporters, the Nramp-type transporter MntH under high Mn(II) and the ABC-type transporter MntABCD under low Mn(II) conditions (Glasfeld *et al.*, 2003; Kehres and Maguire, 2003). In high manganese, Mn(II)-MntR functions as a repressor by binding to operators upstream of the coding regions of both *mntH* and *mntABCD* operons. MntR is selective for manganese while DtxR is activated to bind DNA by various divalent metals including manganese *in vitro*.

MntR. Strikingly, the high resolution crystallographic structure of Mn(II)-bound MntR (to 1.75 Å resolution) reveals a binuclear Mn(II) center, with the two Mn(II) ions bridged by two glutamates, E102 and E11, the latter unique to MntR, and a solvent molecule (Figure 1.2A) (Glasfeld *et al.*, 2003). The other ligands to the site A Mn(II) ion are H77 and E99 (C102 in DtxR) and two water molecules, creating a distorted octahedral coordination geometry (Glasfeld *et al.*, 2003). Mn_B also adopts an octahedral geometry and is ligated by D8, which is M10 in Fe(II)-sensing DtxR, H103, and two solvent molecules, in addition to the bridging ligands E11 and E102 (Glasfeld *et al.*, 2003). Mn_B is roughly positioned in the same place as a Co(II) ion bound to metal site 1 in IdeR.

In an effort to understand the molecular basis of metal ion discrimination between DtxR/IdeR and MntR, a D8M substitution mutant of MntR was functionally and structurally characterized. D8M MntR shows relaxed specificity for Mn(II) and is activated by both Fe(II) and Mn(II) *in vivo* (Guedon and Helmann, 2003). The high resolution crystallographic structure of D8M MntR (to 1.6 Å resolution) reveals why (Table 1.1, Figure 1.2) D8M MntR retains just one of the two Mn(II) ions and is coordinated by E11, H77, E102, and a solvent molecule (the introduced M8 is *not* ligated to the metal) in a distorted trigonal bipyramidal geometry, closer to the position of Mn_A in wild-type MntR (Glasfeld *et al.*, 2003). These findings suggest that metal

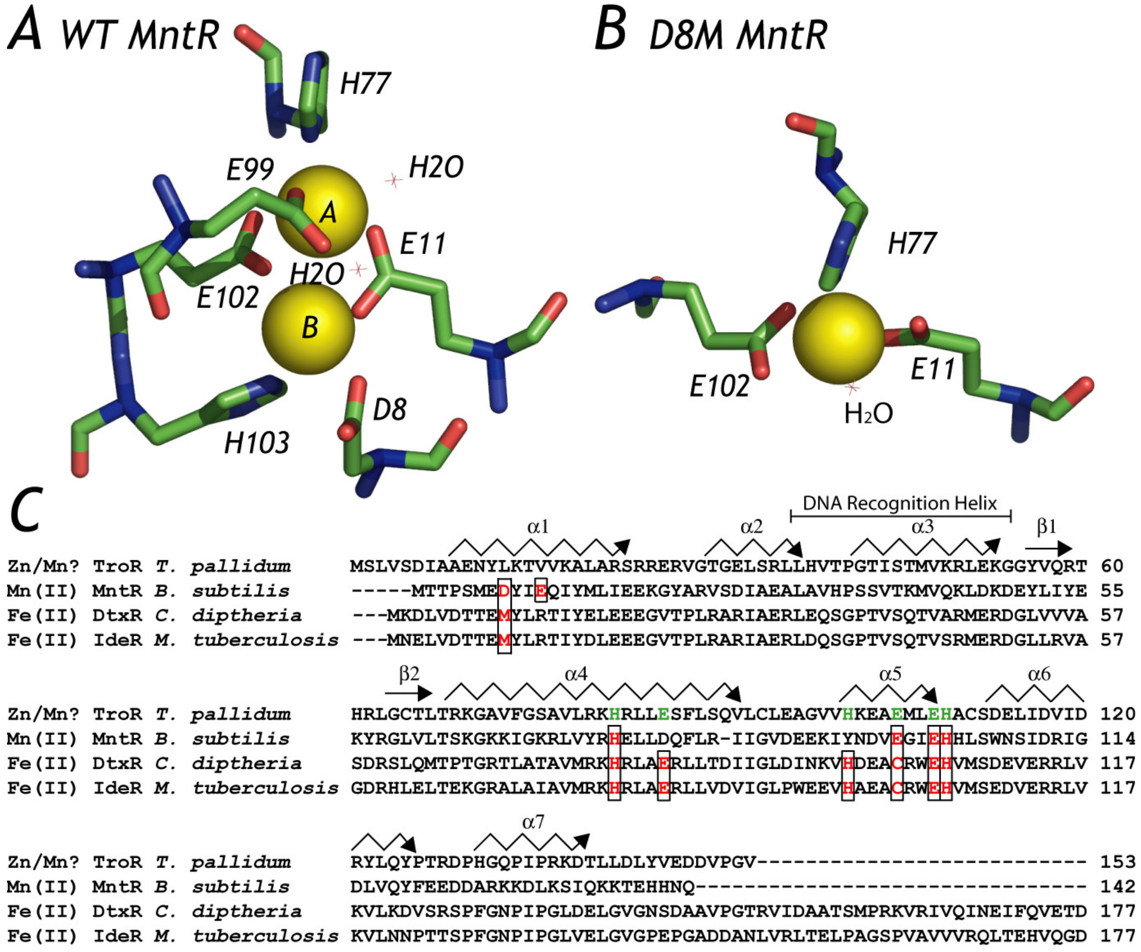

```
Zn/Mn? TroR T. pallidum       MSLVSDIAAENYLKTVVKALARSRRERVGTGELSRLLHVTPGTISTMVKRLEKGGYVQRT 60
Mn(II) MntR B. subtilis       -----MTTPSMEDYIEQIYMLIEEKGYARVSDIAEALAVHPSSVTKMVQKLDKDEYLIYE 55
Fe(II) DtxR C. diptheria      ---MKDLVDTTEMYLRTIYELEEEGVTPLRARIAERLEQSGPTVSQTVARMERDGLVVVA 57
Fe(II) IdeR M. tuberculosis   ---MNELVDTTEMYLRTIYDLEEEGVTPLRARIAERLDQSGPTVSQTVSRMERDGLLRVA 57

Zn/Mn? TroR T. pallidum       HRLGCTLTRKGAVFGSAVLRKHRLLESFLSQVLCLEAGVVHKEAEMLEHACSDELIDVID 120
Mn(II) MntR B. subtilis       KYRGLVLTSKGKKIGKRLVYRHELLDQFLR-IIGVDEEKIYNDVEGIEHHLSWNSIDRIG 114
Fe(II) DtxR C. diptheria      SDRSLQMTPTGRTLATAVMRKHRLAERLLTDIIGLDINKVHDEACRWEHVMSDEVERRLV 117
Fe(II) IdeR M. tuberculosis   GDRHLELTEKGRALAIAVMRKHRLAERLLVDVIGLPWEEVHAEACRWEHVMSEDVERRLV 117

Zn/Mn? TroR T. pallidum       RYLQYPTRDPHGQPIPRKDTLLDLYVEDDVPGV--------------------------- 153
Mn(II) MntR B. subtilis       DLVQYFEEDDARKKDLKSIQKKTEHHNQ-------------------------------- 142
Fe(II) DtxR C. diptheria      KVLKDVSRSPFGNPIPGLDELGVGNSDAAVPGTRVIDAATSMPRKVRIVQINEIFQVETD 177
Fe(II) IdeR M. tuberculosis   KVLNNPTTSPFGNPIPGLVELGVGPEPGADDANLVRLTELPAGSPVAVVVRQLTEHVQGD 177
```

Figure 1.2. Coordination chelates of wt and D8M MntR and a sequence alignment of four members of the DtxR family. **(A.)** Close-up of the metal binding domain of wild-type *B. subtilis* MntR with two Mn(II) ions (shown as *yellow* spheres) bound per protomer in a binuclear cluster. Residues E11, H77, E99, E102, and a solvent molecule (designated as small red x's and labeled H_2O) coordinate the Mn(II) ion designated as Mn_A while D8, E11, E102, and H103 coordinate the Mn(II) ion designated as Mn_B. The Mn(II) ions are bridged by bidentate interactions of E11, E102, and another solvent molecule. **(B.)** Close-up of the metal binding domain of D8M MntR with one Mn(II) bound per protomer. Residues E11, H77, and E102 coordinate the Mn(II) ion along with a solvent molecule. **(C.)** Sequence alignment of *T. pallidum* TroR, *B. subtilis* MntR, *C. diphtheria* DtxR, and *M. tuberculosis* IdeR with the secondary structure regions (based upon crystal structure of MntR) shown as above (Figure 1.1). Known metal binding residues are colored *red* and boxed. Proposed metal binding residues of TroR are shaded *green*.

selectivity in the DtxR family is governed by the number and type of ligands bound to the metal, exactly analogous to findings in the MerR- SmtB/ArsR-family regulators. Interestingly, the amino acid sequence of the putative Zn(II) regulator *T. pallidum* TroR lacks all N-terminal α1-derived metal binding residues that play critical roles in DtxR/IdeR and MntR (Figure 1.2C); this might explain its reported ability to respond to Zn(II) vs. other divalent transition metal ions.

TroR. In 1997, Hardham *et al.* discovered a six gene cluster termed the transport-related operon (*tro*) from *Treponema pallidum* (Hardham *et al.*, 1997). Two genes of the operon include *troA*, which encodes the solute-binding protein (SBP) component of an ATP-binding cassette transporter, and TroR, a DtxR-like metalloregulator (Hardham *et al.*, 1997; Lee *et al.*, 1999). TroR is similar to MntR in sequence (Figure 1.2C), and has been characterized as both a Mn(II)-specific, (Benoit *et al.*, 2001; Posey *et al.*, 1999) and a Zn(II)-specific (Hardham *et al.*, 1997; Hazlett *et al.*, 2003) regulator *in vivo*. Only limited metal-binding experiments have been reported for TroR, and there is currently no available structure. However, the crystallographic structure of Zn(II)-bound TroA, (Lee *et al.*, 1999; Lee *et al.*, 2002) the SBP whose expression is metalloregulated by TroR, may provide some insight as to the natural metal ligand(s) for TroR.

TroA coordinates a single Zn(II) ion in a pentavalent coordination geometry formed by H68, H133, H199 and D279(Oδ1 and Oδ2) (Lee *et al.*, 1999). This coordination structure differs from that recently reported for Zn(II)-bound *Synechocystis* 6803 ZnuA, the SBP of the ZnuABC metal transporter, which is highly selective for

Zn(II). In ZnuA, Zn(II) is bound in a distorted tetrahedral coordination geometry with just three protein-derived histidines, exactly analogous to H68, H133 and H199 in TroA, and a solvent molecule; the bidentate ligand D279 in TroA is conserved in ZnuAs. Although both ZnuA and TroA belong to the same cluster 9 family of ABC transporters, it has been argued that ZnuA preferentially binds Zn(II) over Mn(II) by providing just three protein-derived ligands, since Mn(II) complexes with low coordination numbers are essentially inaccessible due to ligand-field destabilization arguments and the well-understood Irving-Williams series; Zn(II) with its full *d*-shell readily adopts four-coordinate complexes (Banerjee *et al.*, 2003). Since TroA apparently binds Zn(II) in a five-coordinate geometry, Mn(II) should bind to TroA with high affinity as well; this will effectively relax the metal selectivity of this transporter system. This is in fact the case since the measured metal binding affinities of Zn(II) and Mn(II) ($K_d = 1.3 \pm 0.4$ µM and $K_d = 1.0 \pm 0.2$ µM, respectively) are identical within experimental error (Hazlett *et al.*, 2003). One would expect that the metalloregulator TroR would have evolved to sense both Zn(II) and Mn(II) as well.

Fur FAMILY

E. coli Fur and homologs in other prokaryotes regulate the transcription of genes required for iron acquisition, including a host of distinct iron scavenging systems as well as the enzymes for siderophore biosynthesis (Andrews *et al.*, 2003). In addition, the expression of key virulence factors in pathogenic bacteria is also regulated by Fur. The working model is that the iron-bound form of Fur binds to specific target sequences in the promoter of iron-regulated genes, collectively known as “iron boxes”, blocking access by RNA polymerase. Like the DtxR family regulators, iron functions as a co-repressor of the expression of those genes linked to iron acquisition; in iron-starved conditions, these genes are constitutively expressed. The high resolution crystallographic structure of *Pseudomonas aeruginosa* Fur complexed with Zn(II) (rather than iron) has recently been reported to 1.8 Å resolution, with a ribbon representation of the structure shown in Table 1.1 (Pohl *et al.*, 2003). As can be seen the global structure of the Fur homodimer is superficially similar to that of DtxR; in fact the winged-helix DNA-binding domains superimpose with a backbone rmsd of 1.8 Å from helix α2-α4 through the β1-β2 hairpin. The dimerization domain of each protomer is an α/β domain consisting of a 3-stranded β-sheet topped by the C-terminal α5 helix. Dimerization results in a six-stranded β-barrel capped by an antiparallel coiled-coil formed by the α5 helices.

Two metal ions are bound per protomer for a total of four metal ions per dimer, designated Zn1 and Zn2. Zn1 is coordinated by residues located exclusively in the dimerization domain and adopts a distorted octahedral geometry with four protein-derived ligands (H86, D88, E107 and H124), and includes one bidentate carboxylate (D88) and a well-ordered water molecule (see Figure 1.3A). Zn2 bridges the DNA-binding and dimerization domains and adopts distorted tetrahedral coordination geometry (H32, E80, H89 and E100) (Pohl *et al.*, 2003) (see Figure 1.3A). Fe(II) exchange experiments and characterization of the resulting Zn/Fe hybrid protein by x-ray absorption spectroscopy reveals that Zn1 is readily exchanged with Fe(II) and adopts a coordination complex that is isostructural with Zn1, with coordination of Zn2 unchanged. Therefore, the authors argue that in PA Fur, the regulatory metal site corresponds to Zn1 located exclusively in the dimerization domain, while Zn2 is an unusual structural Zn(II) site, which forms part of the long-range allosteric pathway of communication between the regulatory sites and the DNA-binding domains of PA Fur (Pohl *et al.*, 2003). It seems plausible that metal binding to site 1 might globally alter the orientation of one subunit relative to the other, stabilizing a high-affinity binding conformation. All Fur homologs contain the full complement of metal sites structurally characterized in PA Fur.

Interestingly, many Fur homologs, including *E. coli* Fur, contain two pairs of cysteine residues not present in PA Fur. One pair is C92 and C95, just C-terminal to H86 and D88 of the Zn1(Fe) site and H89 of the Zn2 site, and N-terminal to E100 of Zn2 site in PA Fur; PA Fur contains a residue analogous to C92 only which does not participate in metal binding (see Figure 1.3B). In addition, most Fur homologs contain a short C-terminal extension that contains a C-X_4-C sequence that is not present in PA Fur (Figure 1.3B). X-ray absorption studies of *E. coli* Fur suggest at least one sulfur-containing Zn(II) coordination complex; spectroscopic studies of mutants suggest that C92 and C95 ligate this Zn(II) ion in the formation of a structural $S_2(N/O)_2$ complex, although this remains to be definitely determined (Gonzalez de Peredo *et al.*, 1999; Jacquamet *et al.*, 1998).

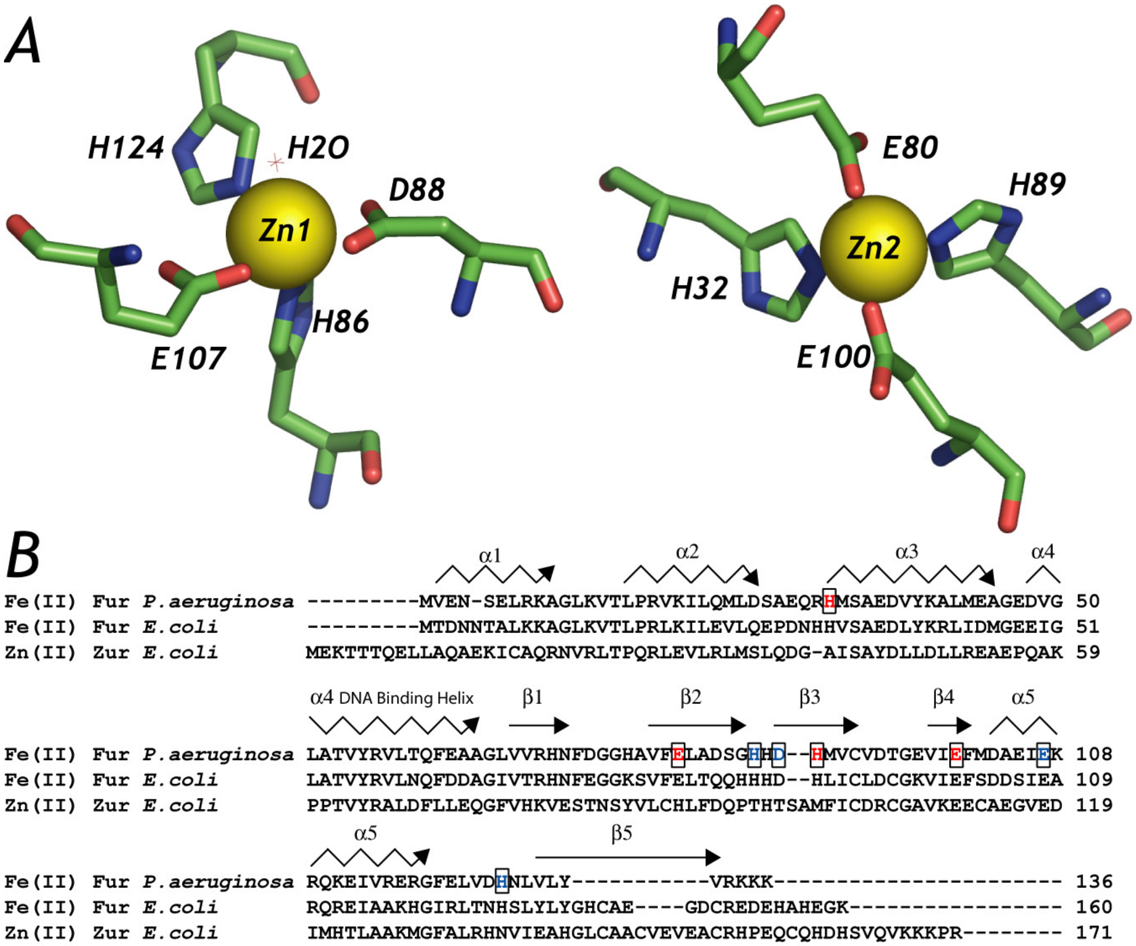

```
Fe(II) Fur P.aeruginosa ---------MVEN-SELRKAGLKVTLPRVKILQMLDSAEQRHMSAEDVYKALMEAGEDVG 50
Fe(II) Fur E.coli       ---------MTDNNTALKKAGLKVTLPRLKILEVLQEPDNHHVSAEDLYKRLIDMGEEIG 51
Zn(II) Zur E.coli       MEKTTTQELLAQAEKICAQRNVRLTPQRLEVLRLMSLQDG-AISAYDLLDLLREAEPQAK 59

Fe(II) Fur P.aeruginosa LATVYRVLTQFEAAGLVVRHNFDGGHAVFELADSGHHD--HMVCVDTGEVIEFMDAEIEK 108
Fe(II) Fur E.coli       LATVYRVLNQFDDAGIVTRHNFEGGKSVFELTQQHHHD--HLICLDCGKVIEFSDDSIEA 109
Zn(II) Zur E.coli       PPTVYRALDFLLEQGFVHKVESTNSYVLCHLFDQPTHTSAMFICDRCGAVKEECAEGVED 119

Fe(II) Fur P.aeruginosa RQKEIVRERGFELVDHNLVLY-----------VRKKK----------------------- 136
Fe(II) Fur E.coli       RQREIAAKHGIRLTNHSLYLYGHCAE----GDCREDEHAHEGK----------------- 160
Zn(II) Zur E.coli       IMHTLAAKMGFALRHNVIEAHGLCAACVEVEACRHPEQCQHDHSVQVKKKPR-------- 171
```

Figure 1.3. Coordination chelate of *P. aeruginosa* Fur and sequence alignment of selected members of the Fur family. **(A.)** Close-up of the metal binding domains of the Zn_4 PA-Fur dimer. Zinc ions shown are represented as yellow spheres. Residues H86, D88, E107 and H124, which includes one bidentate carboxylate (D88) and a well-ordered water molecule coordinate Zn1. Residues H32, E80, H89 and E100 bind Zn2 with a distorted tetrahedral coordination geometry. **(B.)** Sequence alignment of *Pseudomonas aeruginosa* Fur, *E. coli* Fur, and *E. coli* Zur using ClustalW (http://www.ebi.ac.uk/clustalw) (Thompson *et al.*, 1997). Known metal binding ligands are boxed and the secondary structural elements are defined as above (Figure 1.1). *Blue* residues in *P. aeruginosa* Fur represent the proposed regulatory Fe binding site; *Red* residues in *P. aeruginosa* represent the proposed structural Zn binding site.

E. coli Zur. Zur is a recently discovered Fur ortholog (27% sequence identity) that regulates the expression of a divergently transcribed operon that encodes the high affinity zinc uptake system, *znuBC* and *znuA*, in a highly Zn(II)-specific fashion (Patzer and Hantke, 1998, 2000). The high resolution structure of Zur is not yet available and the molecular basis for metal ion discrimination by *E. coli* Zur remains unclear. However, it is possible to speculate on metal selectivity on the basis of an amino acid sequence alignment and limited spectroscopic findings reported for the Zn(II) and Co(II) metalloderivatives of *E. coli* Zur. Zur binds two metal ions per subunit and four per dimer in two spectroscopically distinguishable tetrahedral sites (Outten *et al.*, 2001). One Zn(II) ion, ZnA, is tightly bound in an S_3(N/O) coordination environment and is refractory to metal exchange with Co(II). This site is likely analogous to the structural Zn2 site in Fur homologs that contain the C92-X_2-C95 cysteine pair. The other site, ZnB, is readily exchanged with Co(II) and is characterized by tetrahedral $S(N/O)_3$ coordination geometry, in striking contrast to the octahedral, putative Fe(II)-sensing Zn1(Fe) site of Fur (Outten *et al.*, 2001). Although the four donor atoms to this putative Zn(II)-sensing site remain unknown, at least two cysteine residues just C-terminal to the α5 helix in PA Fur appear to be uniquely conserved in all functionally characterized Zur proteins (Figure 1.3B); one of these may well correspond to the thiolate donor in the ZnB site. Regardless of the details, these comparative structural studies of Fur and Zur emphasize the recurring theme that the primary determinant for metal selectivity in metal sensor proteins is coordination number and geometry, with a lesser role played by the nature of the donor atoms. This is exactly in accord with the conclusions reached by the Fierke group from a careful investigation of the metal affinities and structural studies of a extensive panel of carbonic anhydrase mutants (McCall and Fierke, 2004).

NikR FAMILY

NikR is another metal-responsive transcriptional protein which regulates the uptake of Ni(II) in Gram-negative bacteria and archaea by mediating the repression of the *nik* operon (*nikABCDE*), which encodes a high affinity nickel specific permease that belongs to the ABC transporter family (De Pina *et al.*, 1999; Navarro *et al.*, 1993). NikR contains a ribbon-helix-helix motif, and has been shown to be a homotetramer in the presence or absence of metal (Chivers and Sauer, 1999, 2002). NikR binds an operator sequence within the *nik* promoter with high affinity under conditions of saturating Ni(II) in the cell (Chivers and Sauer, 2002). The apo-form of NikR has not been shown to bind DNA, and it is surmised that it does not. The crystal structure of apo-NikR reveals that the dimeric ribbon-helix-turn-helix domains responsible for DNA binding are on distal ends of the tetrameric C-terminal regulatory domain (Schreiter *et al.*, 2003).

NikR has been shown to possess two nickel-binding sites per monomer (8 per tetramer), one that is high affinity (pM), which allows NikR binding to ~40 base pairs of operator DNA with nanomolar DNA binding affinity, and the other nickel binding site is a low affinity site (µM) that increases the DNA binding site of NikR from 40 bp to ~65 bp, and increases DNA binding affinity to the pM range (Carrington *et al.*, 2003; Chivers and Sauer, 2000, 2002). The operator/promoter sequence contains an imperfect 16-6-16 inverted repeat that possesses dyad-symmetric half-sites 5’-GTATGA-3’. The coordination geometry of the high affinity nickel site in the absence of DNA has been determined for the full-length protein and the C-terminal regulatory domain (residues 48-133; this is the metal binding and tetramerization domain) to be a square planar site that contains one thiolate and three imidazole ligands as determined by x-ray absorption spectroscopy and x-ray crystallography (Carrington *et al.*, 2003; Schreiter *et al.*, 2003). In fact, this site utilizes three ligands (His 87, His89, and Cys95) from one protomer and one ligand (His76) from another protomer (see Figure 1.4A).

Interestingly, a superposition of the C^{α} traces of the Ni(II) bound C-terminal domain crystal structure with the C-terminal regulatory domain from the full-length apo-NikR don’t reveal large quaternary structural changes but do show the ordering and formation of the α3-helix in the nickel bound protein, and the position of the loop between β3 and β4 coming closer to the metal binding site in the metal bound form (Schreiter *et al.*, 2003). However, the native form of the nickel bound state of this protein has been shown to have high affinity for DNA. Surprisingly, the coordination geometry of the nickel binding site in the presence of operator containing DNA has been shown to be six-coordinate and utilizing N/O donors presumably via imidazole and carboxylate ligands (with the possibility of solvent being a donor) (Carrington *et al.*, 2003). This change in coordination number and ligand type suggests that Ni(II) binding “communicates” and induces conformational changes in the N-terminal DNA binding domains of the apo-protein that allow the metallated form to bind DNA with high affinity.

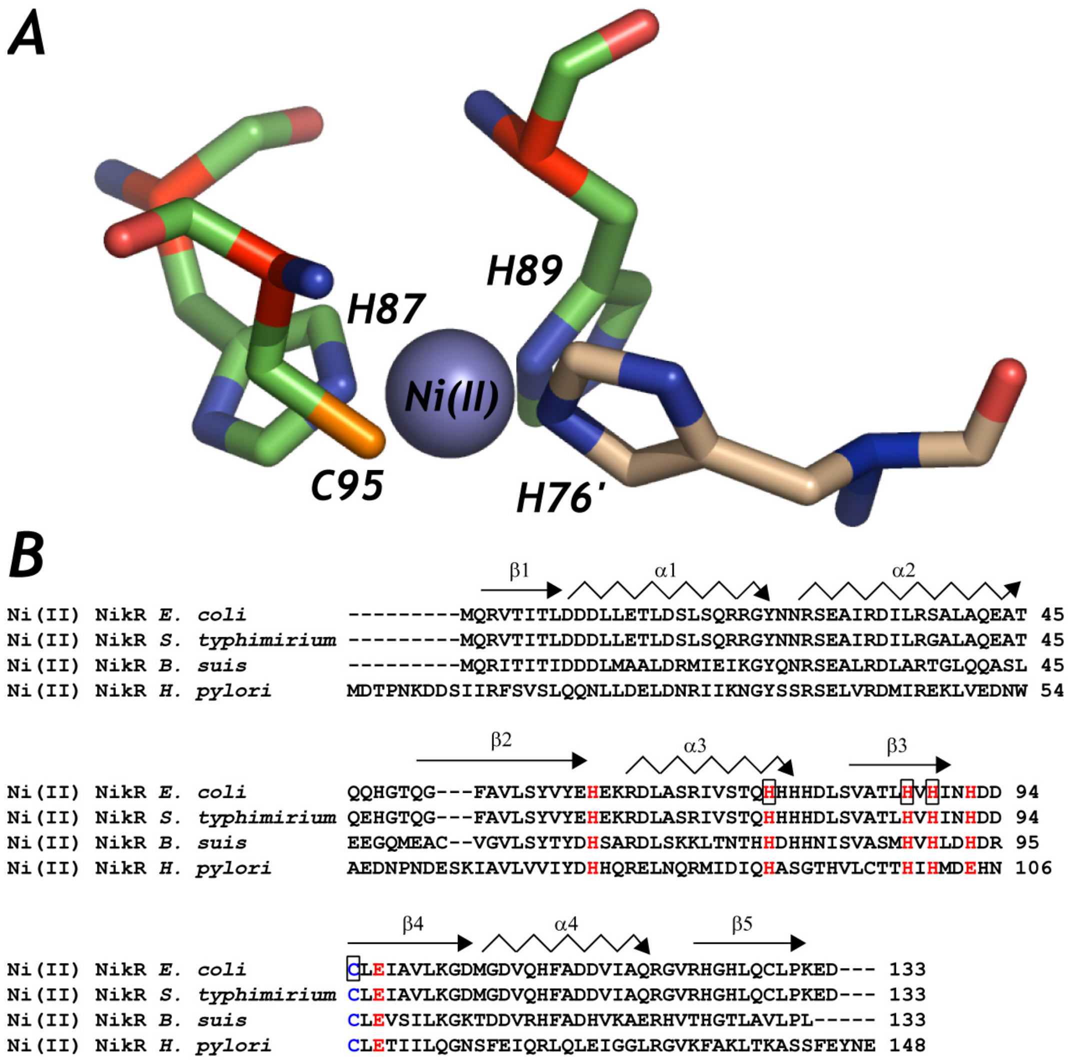

```
Ni(II) NikR E. coli       ---------MQRVTITLDDDLLETLDSLSQRRGYNNRSEAIRDILRSALAQEAT 45
Ni(II) NikR S. typhimirium ---------MQRVTITLDDDLLETLDSLSQRRGYNNRSEAIRDILRGALAQEAT 45
Ni(II) NikR B. suis       ---------MQRITITIDDDLMAALDRMIEIKGYQNRSEALRDLARTGLQQASL 45
Ni(II) NikR H. pylori     MDTPNKDDSIIRFSVSLQQNLLDELDNRIIKNGYSSRSELVRDMIREKLVEDNW 54

Ni(II) NikR E. coli       QQHGTQG---FAVLSYVYEHEKRDLASRIVSTQHHHHDLSVATLHVHINHDD 94
Ni(II) NikR S. typhimirium QEHGTQG---FAVLSYVYEHEKRDLASRIVSTQHHHHDLSVATLHVHINHDD 94
Ni(II) NikR B. suis       EEGQMEAC--VGVLSYTYDHSARDLSKKLTNTHHDHHNISVASMHVHLDHDR 95
Ni(II) NikR H. pylori     AEDNPNDESKIAVLVVIYDHHQRELNQRMIDIQHASGTHVLCTTHIHMDEHN 106

Ni(II) NikR E. coli       CLEIAVLKGDMGDVQHFADDVIAQRGVRHGHLQCLPKED--- 133
Ni(II) NikR S. typhimirium CLEIAVLKGDMGDVQHFADDVIAQRGVRHGHLQCLPKED--- 133
Ni(II) NikR B. suis       CLEVSILKGKTDDVRHFADHVKAERHVTHGTLAVLPL----- 133
Ni(II) NikR H. pylori     CLETIILQGNSFEIQRLQLEIGGLRGVKFAKLTKASSFEYNE 148
```

Figure 1.4. Coordination chelate of *E. coli* NikR and a sequence alignment of selected members of the NikR family. **(A.)** Close-up of the metal binding domain of the NikR C-terminal domain. Nickel ion shown is represented as a slate colored sphere. Three nickel ligating residues derived from one protomer (H87, H89, and C95), and H76' from the other protomer coordinate the nickel ion in a square planar geometry. **(B.)** Sequence alignment of *E. coli* NikR, *S. typhimirium* NikR, *B. suis* NikR, and *H. pylori* NikR using ClustalW (http://www.ebi.ac.uk/clustalw) (Thompson *et al.*, 1997). Metal binding residues that are boxed represent residues in the nickel bound form of NikR in the absence of binding DNA. Residues surmised to be involved in nickel binding under conditions of DNA binding are colored *red*. *Blue* residues bind metal ions in the absence of DNA. Secondary structure elements are based upon the apo crystal structure of NikR and defined as in Figure 1.1.

Even though the NikR family of proteins has only been shown to regulate only one metal ion, Ni(II), this does glean some insight into the specificity of these proteins. Similar to the other metalloregulatory protein families discussed in this chapter, the coordination number and geometries of Ni(II) bound NikR appear to play key roles in determinants of metal specificity and therefore regulation. The novel three imidazole and one thiolate square planar coordination of non-DNA bound NikR and the six-coordinate geometry of DNA bound NikR probably confer specificity for nickel over other metal ions that usually do not adopt this coordination geometry. Additional members of this family are beginning to be characterized, including NikR from B. suis, a bacterial parasite that invades mammalian macrophages, and NikR from H. pylori, a human gastric pathogen (Jubier-Maurin *et al.*, 2001; van Vliet *et al.*, 2002; van Vliet *et al.*, 2004). They appear to have additional functions beside nickel transport including regulation of other proteins important for the survival of the organism (van Vliet *et al.*, 2004). However, sequence alignments of members of this protein family reveal that known metal binding ligands and putative metal binding ligands are strictly conserved, suggesting that the coordination and specificity of nickel binding is similar for all members assigned so far (Figure 1.4B).

SmtB/ArsR FAMILY

The SmtB/ArsR family consists of homodimeric “winged” helix-turn-helix (HTH) transcriptional repressors that are specifically bound to their operator/promoter

(O/P) DNA binding sites in the metal-free apo state. Metal binding allosterically negatively regulates DNA binding and de-represses transcription (Busenlehner *et al.*, 2003). Most of the O/P sequences of this family contain one or two imperfect 12-2-12 inverted repeats but little is known at the molecular level of how apo-repressor binds to these sites. Individual members of this family share between 25-50% amino acid sequence identity, and a conserved helix-turn-helix DNA binding motif and metal binding residues are the determinants that characterize members of this family.

The name of this family is derived from its two founding members, ArsR from *E. coli* and *Synechococcus PCC 7942* SmtB. ArsR is an arsenic/antimony-responsive repressor of the *ars* operon which encodes an arsenate reductase, as well as proteins required for metal export (Busenlehner *et al.*, 2003; Shi *et al.*, 1994; Wu and Rosen, 1993). SmtB functions as a zinc-responsive repressor that represses transcription of a divergently transcribed operon containing both the *smtA* gene (encodes a class II metallothionein) and the *smtB* gene (Busenlehner *et al.*, 2003; Huckle *et al.*, 1993; Morby *et al.*, 1993). *Synechocystis* ZiaR, a repressor from another cyanobacteria, was identified as highly zinc-responsive and regulates the ziaR and ziaA genes, the latter encodes a membrane bound P_{1B}-type ATPase metal-efflux pump that belongs to the subgroup IB-2, which are considered Cd(II)/Pb(II)/Zn(II)-specific proteins (Thelwell *et al.*, 1998). BxmR, which has been identified and characterized from the cyanobacterium *Oscillatoria brevis*, represses the expression of both *bxa1*, a P_{1B}-type ATPase from subgroup IB-2, as well as a divergently transcribed operon encoding *bxmR* and *bmtA*, a heavy metal sequestering metallothionein. De-repression of the expression of all three genes is mediated by both monovalent (Ag(I) and Cu(I)) and divalent (Zn(II) and Cd(II)) heavy metal ions, a novel property among SmtB/ArsR metal sensors (Liu *et al.*, 2004). An additional cyanobacterial zinc-responsive transcriptional repressor is AztR from *Anabaena sp. PCC7120*. It regulates the expression of aztR and aztA, which is an additional member of the P_{1B}-type ATPase from subgroup IB-2 (Liu and Giedroc manuscript in preparation). A nickel/cobalt-responsive repressor NmtR from *Mycobacterium tuberculosis* is a member of this family as well (Cavet *et al.*, 2002). The nmt operon encodes divergently transcribed *nmtR* and *nmtA*, the latter of which is a P_{1B}-type ATPase from subgroup IB-4, which are considered Co(II)-specific proteins because of a known and characterized Co(II) ATPase exporter, CoaT, from the same subgroup IB-4 (Arguello, 2003; Rutherford *et al.*, 1999). An additional characterized member from *M. tuberculosis* is CmtR, a cadmium- and lead-detecting transcriptional repressor that regulates the expression of *cmtR* and *cmtA*, another P_{1B}-type ATPase (Arguello, 2003; Cavet *et al.*, 2003). *Staphylococcus aureus* contains members from SmtB/ArsR family as well, which include CadC, whose gene is located on the bacterial chromosome as well as on the multiple-resistance plasmid pI258 (Yoon *et al.*, 1991; Yoon and Silver, 1991). CadC from pI258 has been the more studied of the two variants and was determined to sense toxic metal ions Cd(II), Pb(II), Bi(III), and to a lesser degree the essential metal ion zinc (Busenlehner *et al.*, 2001; Sun *et al.*, 2001; Yoon *et al.*, 1991; Yoon and Silver, 1991). The cad operon is regulated by CadC, and contains *cadC* and *cadA*, another member of the membrane bound P_{1B}-type subgroup IB-2 ATPase family that was aforementioned. Staphylococcus aureus CzrA is a chromosomally-encoded

Zn(II)/Co(II)-specific transcriptional repressor of the *czr* operon which encodes a membrane-bound Zn(II) transporter of the cation diffusion family, CzrB, which is homologous to the known zinc transporter of E. coli, ZitB (Kuroda *et al.*, 1999; Singh *et al.*, 1999; Xiong and Jayaswal, 1998).

METAL BINDING SITES OF SmtB/ArsR PROTEINS

Ten years of molecular genetic, biochemical, biophysical, and structural studies revealed that this family of metal-sensing transcriptional repressors generally possesses two well-characterized metal binding sites (Busenlehner *et al.*, 2003). They are termed the α3N site and the α5 site (see Figure 1.5B). The α3N site is composed of cysteine residues from the N-terminal portion of the protein and a highly conserved ELCVCD motif (located at the α3 helix), initially termed the 'metal binding box' (Busenlehner *et al.*, 2003). The α5 site is composed of histidines and carboxylate residues, and is found in the C-terminal portion of the protein. Not all members of this family contain both metal binding sites. Some possess α3N only and others α5 only, some have both sites, and a few have neither site (these proteins appear to possess a new, as yet to be characterized site) (Busenlehner *et al.*, 2003; Cavet *et al.*, 2003). The α5 site interacts site preferentially binds larger thiophilic metal ions such as Cd(II), Pb(II), and Bi(III). SmtB/ArsR proteins that possess both metal binding sites have been shown to utilize only one site for regulation, not both sites (this is not clear for BxmR, which has not been completely characterized and may utilize both sites to regulate different metal

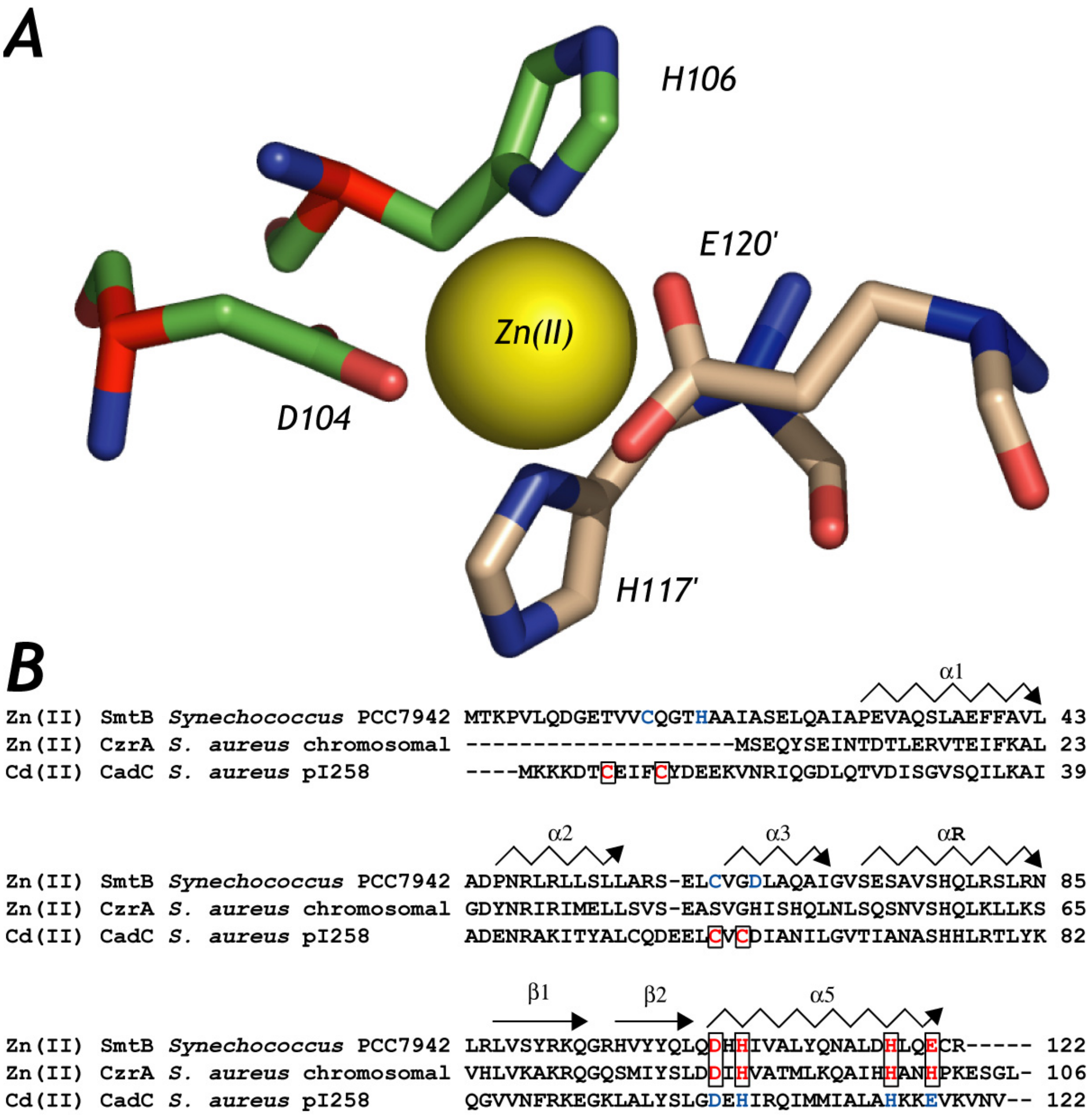
A
H106
E120'
Zn(II)
D104
H117'
B
α1
Zn(II) SmtB Synechococcus PCC7942 MTKPVLQDGETVVCQGTHAAIASELQAIAPEVAQSLAEFFAVL 43
Zn(II) CzrA S. aureus chromosomal --------------------MSEQYSEINTDTLERVTEIFKAL 23
Cd(II) CadC S. aureus pI258 ----MKKKDTCEIFCYDEEKVNRIQGDLQTVDISGVSQILKAI 39
α2
α3
αR
Zn(II) SmtB Synechococcus PCC7942 ADPNRLRLLSLLARS-ELCVGDLAQAIGVSESAVSHQLRSLRN 85
Zn(II) CzrA S. aureus chromosomal GDYNRIRIMELLSVS-EASVGHISHQLNLSQSNVSHQLKLLKS 65
Cd(II) CadC S. aureus pI258 ADENRAKITYALCQDEELCVCDIANILGVTIANASHHLRTLYK 82
β1
β2
α5
Zn(II) SmtB Synechococcus PCC7942 LRLVSYRKQGRHVYYQLQDHHIVALYQNALDHLQECR----- 122
Zn(II) CzrA S. aureus chromosomal VHLVKAKRQGQSMIYSLDDIHVATMLKQAIHHANHPKESGL- 106
Cd(II) CadC S. aureus pI258 QGVVNFRKEGKLALYSLGDEHIRQIMMIALAHKKEVKVNV-- 122

Figure 1.5. Coordination chelate of Zn_2 SmtB and a sequence alignment of three representative members from the SmtB/ArsR family. **(A.)** Close-up of the metal binding domain of SmtB. Zinc ion shown is represented as a yellow colored sphere. Two zinc ligating residues derived from one protomer (D104 and H106) and two (H117' and E120') from the other protomer coordinate the zinc ion in a tetrahedral coordination geometry. **(B.)** Multiple sequence alignment of *Synechococcus* SmtB, *S. aureus* CzrA, and *S. aureus* pI258 CadC. Known metal binding residues are boxed (Busenlehner *et al.*, 2003). Residues shown to be involved in negatively regulating DNA binding are colored *red*. *Blue* residues bind metal ions but are *not* involved in metal sensing. α3N amino acids are the boxed and *red* cysteines in CadC. Secondary structure elements are based upon the crystal structure and defined as in Figure 1.1.

preferably with smaller divalent metal ions, *e.g.* Zn(II), Co(II), and Ni(II), while the α3N ions). What factors determine which site is functional in a protein that possesses both sites is still unclear, but it is known that this selectivity of the allosteric response requires determinants outside of the primary metal ligands (Busenlehner *et al.*, 2002b; VanZile *et al.*, 2002a).

α3N SENSORS: CadC

CadC from *S. aureus* pI258 is the metal-responsive transcriptional repressor of the *cad* operon, and responds to mainly Cd(II) and Pb(II) (Yoon *et al.*, 1991). It is the most extensively characterized CadC protein, and contains both the α3N and α5 metal binding sites. CadC contains 5 cysteine residues, four of which have been shown to be ligands for metal binding (i.e. the α3N site, Cys7, Cys 11, Cys 58 and Cys 60) (Sun *et al.*, 2001). CadC also contains two imidazole ligands (H103 and H114) and two carboxylate ligands (D101 and E117), which make up the α5 site (see Figure 1.5B), and also have been shown to bind metal (Busenlehner *et al.*, 2002b). The location of CadC binding to the *cad* operator/promoter has been mapped by DNase I footprinting to a 20-base pair region between the -10 element and the translational start site (Endo and Silver, 1995). This protected area is located around the 12-2-12 imperfect repeat which is somewhat similar to inverted repeats that are recognized by the biologically essential metal ion sensors SmtB, CzrA, and NmtR, but more similar to the repeat recognized by the toxic metal ion sensor, ArsR (see Figure 1.6).

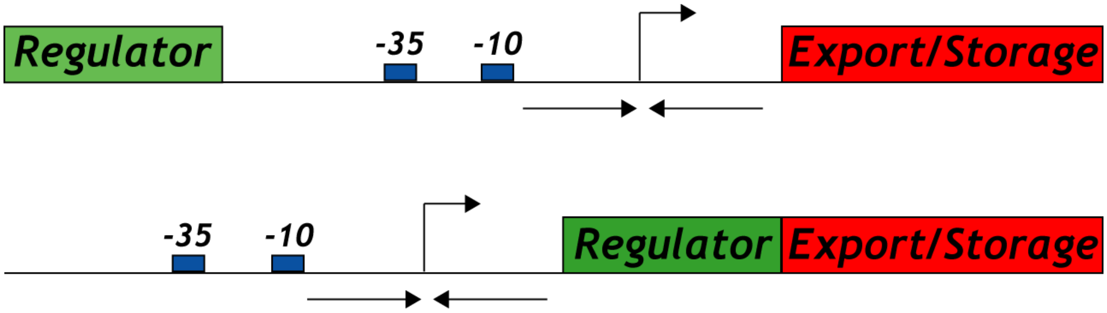

α5 core motif:aAtAxxTGAacaxxtatTCAxaTxtt

α3N core motif:TAxAxTCAAAtaxxtaTTTGaxTxTA

Figure 1.6. The general operon structure regulated by SmtB/ArsR Family transcriptional repressors and the core 12-2-12 inverted repeat motifs of the SmtB/ArsR-regulated O/Ps. The green boxes represent genes that encode the metal-responsive transcriptional repressor which binds to O/P region to block RNA polymerase from carrying out transcription of the corresponding operon. The red boxes represent genes that encode Heavy-metal P_{1B}-type ATPases, Cation Diffusion Facilitator transporters, metal reductases, or metal-sequestering metallothioneins. The blue boxes represent the -10 and -35 elements. The bent arrows represent transcription start sites of the promoter and the straight arrows represent the imperfect 12-2-12 inverted repeats that are recognized by the regulators for binding. An alignment of the imperfect, hyphenated 12-2-12 inverted repeats from the *smt* O/P, *zia* O/P, *czr* O/P, *nmt* O/P are summarized by the core motif for α5 sensors. The capital letters in purple are strictly conserved nucleotides while the small letters in purple represent semi-conserved nucleotides. The x's represent non-conserved nucleotides.

Fluorescence anisotropy experiments reveal one high affinity apo-CadC dimer binds a fluorescein-labeled oligonucleotide containing the O/P region of the cad operon, and that Cd(II), Pb(II), and Bi(III)-saturated CadC proteins are effective in strongly decreasing the DNA binding affinity of CadC for this oligonucleotide (Busenlehner *et al.*, 2001). Substitution of Cys60 and Cys7 with non-ligating residues specifically abrogates metal-dependent negative regulation of *cad* O/P binding, despite the fact that C60G and C7G CadCs maintain high affinity for metals in altered coordination complexes (Busenlehner *et al.*, 2002b). These findings reveal that formation of metal coordination bonds to Cys7 and Cys60 play primary roles in transducing the allosteric response in CadC (Busenlehner *et al.*, 2002b). This indicates that metal sensing in this protein occurs exclusively at the α3N site and not at the intact α5 site (Busenlehner *et al.*, 2002b).

α5 SENSORS: SmtB, NmtR, and CzrA

SmtB, from the cyanobacterium *Synechococcus PCC 7942*, was determined via reporter gene assays to be a trans-acting transcriptional repressor of the *smt* operon (Morby *et al.*, 1993). This operon was shown to encode two divergent genes involved in homeostasis and resistance, *smtA* and *smtB*. SmtA is a class II metallothionein involved in metal ion sequestration. The transcription of *smtA* is repressed in the absence of metal ions but is enhanced in the presence of Zn(II), Cd(II), Cu(II), and Co(II) in *Synechococcus* cells (Huckle *et al.*, 1993). The x-ray crystallographic structure of dimeric apo-SmtB revealed that SmtB is an elongated dimer with a two fold axis of symmetry made up of five α-helices and a β-hairpin arranged into an ααααββα fold with the dimerization interface formed between the two N-terminal α1 helices and the C-terminal α5 helices (see Table 1.1) (Cook *et al.*, 1998). The helix-turn-helix-wing motif (α3-turn-αR-β1-β2) is determined to be the putative DNA binding domain and possesses structural resemblance to another metal-responsive transcriptional regulators, DtxR (diphtheria toxin repressor) (Pohl *et al.*, 1999). Mutational analysis reveals that none of the three cysteine residues (Cys14, Cys61, and Cys121), which are known to be involved in metal coordination, are required for metal-induced de-repression *in vivo*, however, His105/106 in the C-terminus are critical for Zn(II)-responsive de-repression from the *smt* O/P (Turner *et al.*, 1996). In fact, SmtB contains a partial α3N site which includes Cys14, His18, Cys61, and Asp64, and a full α5 site (D104, H106, H117, and E120). Residues from both sites have been shown to bind metal (VanZile *et al.*, 2002b). DNA binding experiments indicate that two high affinity SmtB dimers bind to an oligonucleotide containing a 12-2-12 imperfect repeat, and that Zn(II), Co(II), and Cd(II) are equally effective in decreasing the DNA binding affinity of SmtB for the DNA (VanZile *et al.*, 2002a). Cysteine mutations have no effect on Zn(II)-responsive transcriptional regulation in vitro as well, and there is no effect on metal-mediated SmtB dissociation from the smt O/P in vitro suggesting that these proteins behave as wild-type in terms of DNA binding characteristics (VanZile *et al.*, 2002a). Mutation of the α5 ligand H106 to glutamine abolishes Co(II) binding to this site and also leads to loss of metal-mediated dissociation from DNA, thus revealing that the α5 site and not the α3N site is necessary for zinc sensing by SmtB (VanZile *et al.*, 2002a).

Mycobacterium tuberculosis NmtR regulates the expression of *nmtR* and *nmtA* in Ni(II)/Co(II) dependent fashion, where NmtA is a member of the metal efflux P_{1B}-type ATPases (Arguello, 2003; Cavet *et al.*, 2002). The *nmt* operon contains two divergently transcribed genes which encode the NmtR and NmtA proteins (Cavet *et al.*, 2002). *In vivo*, NmtR repression from the *nmt* O/P could be alleviated by the addition of Ni(II) and Co(II) to the growth media (Cavet *et al.*, 2002). NmtR shares 35% identity with SmtB, but does not contain cysteines, and therefore does not possess an α3N site. However, NmtR does possess the four ligands required for an α5 site (Asp91, His93, His104, and His107), and in addition, has been shown that it may require two more histidine ligands which are located C-terminal to the α5 metal binding site (His109 and His116). Thus, the inclusion of the C-terminal histidines gives rise to name of NmtR's metal binding site as α5C. These two additional ligands were shown to be necessary for an *in vivo* response by single site mutational (His to Arg) analysis assayed by B-galactosidase reporter experiments (Cavet *et al.*, 2002). No footprinting or extensive DNA binding analysis has been reported to map the DNA binding site, but visual inspection of the DNA sequence reveals semi-conserved 12-2-12 imperfect repeat which is similar to inverted repeats that are recognized by the metal ion sensor proteins SmtB, ZiaR, and CzrA (see Figure 1.6).

CzrA from *Staphylococcus aureus* has been shown to be a Zn(II)/Co(II) specific transcriptional repressor of the *czr* operon *in vivo* (Kuroda *et al.*, 1999; Singh *et al.*, 1999; Xiong and Jayaswal, 1998). The czr operon contains two co-transcribed genes which encode the CzrA and CzrB proteins (Kuroda *et al.*, 1999; Xiong and Jayaswal, 1998). Gel-shift analysis reveals that CzrA repression from the czr O/P could be alleviated by the addition of Zn(II) or Co(II) (Singh *et al.*, 1999). However, it was shown that more cobalt was needed to alleviate repression suggesting that the main ligand for metal-mediated repression is zinc (Kuroda *et al.*, 1999; Singh *et al.*, 1999). CzrA, similar to NmtR, does not possess any cysteine ligands, and hence does not contain an α3N metal binding site. It does, however, possess the four residues necessary to make an α5 metal binding site (Asp84, His86, His97, and His100). The location of CzrA binding to the *czr* operator/promoter has been mapped by DNaseI footprinting to a 49-base pair region between the -10 element and the translational start site (Singh *et al.*, 1999). Within this protected are is located a 12-2-12 imperfect repeat which is similar to inverted repeats recognized by SmtB, ZiaR, and NmtR (Cavet *et al.*, 2002; Kuroda *et al.*, 1999; Singh *et al.*, 1999; VanZile *et al.*, 2002a).

SCOPE OF THE RESEARCH

The aims of the experiments presented in this dissertation are two-fold: 1) gain insight into the determinants of metal ion specificity and selectivity of prokaryotic metalloregulatory transcriptional repressors from the SmtB/ArsR family, and 2) determine how metal binding is allosterically linked to specific DNA binding. Comparative studies of two systems, *S. aureus* CzrA (Kuroda *et al.*, 1999; Singh *et al.*, 1999; Xiong and Jayaswal, 1998) and *M. tuberculosis* NmtR (Cavet *et al.*, 2002), that have well-established *in vivo* metal ion selectivity profiles in their respective native hosts, have been chosen for detailed investigation. Previous β-galactosidase, gel-shift, and *in vitro* transcription assays reveal that CzrA and NmtR specifically associate with the *czr* and *nmt* operator/promoter DNA, respectively. Metal ion binding to CzrA and NmtR weakens the affinity of the protein-DNA complex and leads to de-repression of their respective operons (Cavet *et al.*, 2002; Singh *et al.*, 1999). The factors that govern this partially overlapping metal selectivity are not well-understood.

The experiments presented in Chapter II show that CzrA and NmtR are homodimeric proteins that associate to their respective O/Ps with high affinity. Tetrahedral coordination complexes of Zn(II) and Co(II) in CzrA are formed by D84 and H86 from one protomer and H97' and H100' from the other protomer. In contrast, five- or six-coordinate Ni(II) or Co(II) complexes are formed in NmtR, lowering the affinity of these proteins for their respective O/Ps. This finding suggests coordination geometry dictates metal ion selectivity (Zn(II) vs. Ni(II)) for these two proteins. The structural studies presented in Chapter III propose that a key histidine ligand (H97) in the metal coordination complex of CzrA is critical to mediating an inter-subunit hydrogen bonding network that stabilizes a low-affinity DNA-binding conformation. The experiments presented in Chapter IV elucidate functional roles played by each of the four coordinating ligands in CzrA. Mutagenesis studies show that 2/4 ligands (D84 and H97') are absolutely required for maintenance of tetrahedral metal coordination and zinc-mediated negative regulation of DNA binding, thus providing support for the intersubunit hydrogen bonding network model. In contrast, H86 and H100’ are far more tolerant of substitution and are able to regulate DNA binding in the presence of saturating zinc as a result of lowered metal binding affinities.

CHAPTER II

STRUCTURAL ELEMENTS OF METAL SELECTIVITY IN METAL SENSOR PROTEINS[*]

INTRODUCTION

About a third of all proteins exploit specific metal ions to assist in macromolecular folding and/or function at the active site of metalloenzymes (Rosenzweig, 2002). All cells restrict the number of bio-available metal atoms to avoid any excess that would otherwise compete with native metal ion sites that do not support biological activity (O'Halloran, 1993). Essentially all cell types contain intracellular metal sensors that detect surplus metal ions and control the expression of genes encoding proteins that expel or sequester the extra ions (Nies and Brown, 1998). For some metals and some cell types, a complementary set of sensors detect deficiency and regulate genes encoding proteins that acquire more of the required ions (Brocklehurst *et al.*, 1999; Hantke, 2001b). It is currently poorly understood how such metal-sensing metalloregulators accurately discriminate between various metal ions.

SmtB/ArsR-family regulators are ubiquitous in bacterial genomes and bind to the operator/promoter regions of gene(s) encoding proteins involved in metal export or sequestration, repressing transcription (Busenlehner *et al.*, 2003). As the concentration of metal ion increases, the effector-binding sites of the regulators become occupied eliciting a conformational change that weakens the affinity for the operator/promoter region, allowing transcription to proceed. Members of the SmtB/ArsR family include: As(III), Sb(III), Bi(III)-responsive ArsR (Xu *et al.*, 1998), Zn(II)-responsive SmtB (Huckle *et al.*, 1993), Cd(II), Pb(II), Bi(III)-responsive CadC (Rensing *et al.*, 1998; Sun *et al.*, 2001), Zn(II)-responsive ZiaR (Thelwell *et al.*, 1998), Co(II), Zn(II)-responsive CzrA (13,14) and most recently Ni(II), Co(II)-responsive NmtR (Cavet *et al.*, 2002) (see Figure 2.1).

---

[*] Reprinted with permission from Pennella, M.A., Shokes, J.E., Cosper, N.J., Scott, R.A., and Giedroc, D.P. Structural elements of metal selectivity in metal sensor proteins *Proc. Nat. Acad. Sci., U.S.A.* **100**: 3713-3718. Copyright 2003 National Academy of Sciences, U.S.A. (http://www.pnas.org).

Comparative structural and spectroscopic studies of six SmtB/ArsR family members reveal that individual members are characterized by one or both of two structurally distinct metal coordination sites (Busenlehner *et al.*, 2001; Busenlehner *et al.*, 2002a; Busenlehner *et al.*, 2002b; Busenlehner *et al.*, 2003; Cavet *et al.*, 2002; VanZile *et al.*, 2000; VanZile *et al.*, 2002a, b). These two metal sites are designated α3N (or α3) and α5 (or α5C), named for the location of the metal binding ligands within the known or predicted secondary structure of individual family members. The coordination environment and precise ligand set of the α3, α3N and/or α5, α5C sites in the different SmtB/ArsR proteins differ and are presumed to contribute toward metal selectivity. A sequence comparison for proteins discussed herein is shown in Fig. 2.1 and highlights these sites. Here we report insights gained from the study of two additional family members, *S. aureus* CzrA and *M. tuberculosis* NmtR. CzrA and NmtR share 30% sequence identity and a high degree of similarity (60%) yet respond to

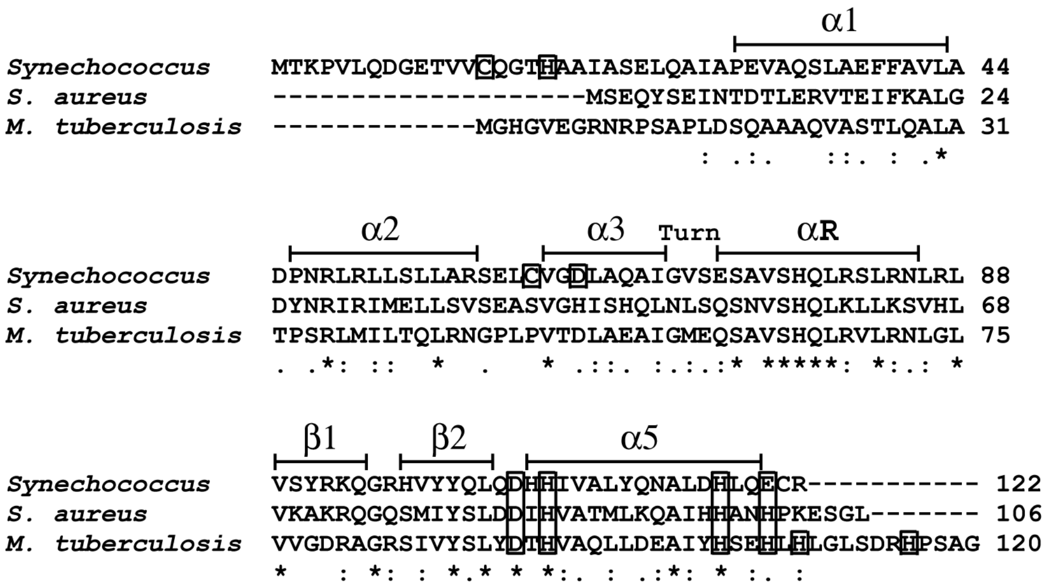
α1
Synechococcus MTKPVLQDGETVVCQGTHAAIASELQAIAPEVAQSLAEFFAVLA 44
S. aureus --------------------MSEQYSEINTDTLERVTEIFKALG 24
M. tuberculosis -------------MGHGVEGRNRPSAPLDSQAAAQVASTLQALA 31
: .:.   ::. : .*
α2
α3
Turn
αR
Synechococcus DPNRLRLLSLLARSELCVGDLAQAIGVSESAVSHQLRSLRNLRL 88
S. aureus DYNRIRIMELLSVSEASVGHISHQLNLSQSNVSHQLKLLKSVHL 68
M. tuberculosis TPSRLMILTQLRNGPLPVTDLAEAIGMEQSAVSHQLRVLRNLGL 75
. .*: :: * .   * .::. :.:.:* *****: *:.: *
β1
β2
α5
Synechococcus VSYRKQGRHVYYQLQDHHIVALYQNALDHLQECR----------- 122
S. aureus VKAKRQGQSMIYSLDDIHVATMLKQAIHHANHPKESGL------- 106
M. tuberculosis VVGDRAGRSIVYSLYDTHVAQLLDEAIYHSEHLHLGLSDRHPSAG 120
*   : *: : *.* * *:. : .:*: * :. :

Figure 2.1. Multiple sequence alignment SmtB, CzrA, and NmtR from the SmtB/ArsR family. A multiple sequence alignment of *Synechococcus* PCC 7942 SmtB (P30340), *Staphylococcus aureus* CzrA (O85142), and *Mycobacterium tuberculosis* NmtR (A70799) generated by ClustalW (Thompson *et al.*, 1997)(Swiss-Prot/TrEMBL accession numbers for CzrA, NmtR, and SmtB are in parentheses). Residues which are identical (*), residues that are strongly similar (:), and residues that are weakly similar (.) are denoted below the alignment. Secondary structure elements are denoted above the alignment and based on the crystal structure of apo-SmtB (Cook *et al.*, 1998) and chemical shift indexing for CzrA (Busenlehner *et al.*, 2003). Conserved metal binding residues located in the α5 site are boxed as are proposed ligands to the α3N site in SmtB (C14, H18, C61, C64) (VanZile *et al.*, 2002a, b).

distinct, but partially overlapping metal profiles *in vivo*. *S. aureus* CzrA is a Co(II)/Zn(II)-specific sensor that regulates the expression of the *czr* operon which encodes a Co(II)/Zn(II)-facilitated pump, CzrB, that effluxes metal out of the cell (Kuroda *et al.*, 1999; Singh *et al.*, 1999). Electromobility shift assays and *in vivo* expression studies indicate that Zn(II) is the strongest inducer of CzrA regulation with Co(II) also capable of regulation but only at higher concentrations than Zn(II). Other metals, including Ni(II) have little to no effect on de-repression of the *czr* operon (Kuroda *et al.*, 1999; Singh *et al.*, 1999). The situation is precisely opposite for *M. tuberculosis* NmtR, with Ni(II) the strongest inducer of NmtR-dependent regulation of the *nmt* operon, which encodes a P-type ATPase metal efflux pump, NmtA (Cavet *et al.*, 2002). Co(II) is an intermediate inducer, while Zn(II) has no effect *in vivo* on de-repression (Cavet *et al.*, 2002). We make the striking finding here that CzrA and NmtR achieve their distinct metal selectivities of negative regulation of DNA binding *in vivo* and *in vitro* largely on the basis of different coordination numbers and geometries, with CzrA forming functional 4-coordinate metal complexes, while NmtR requires formation of 5- or 6-coordinate complexes to effect metalloregulation.

MATERIALS AND METHODS

*Chemicals***.** All buffers were prepared using Milli-Q deionized water. MES, HEPES, and Tris buffer salts and ammonium sulfate were obtained from Sigma. All chromatography materials were obtained from Pharmacia Biotech. Ultrapure cobalt(II) chloride, nickel(II) chloride, and zinc(II) sulfate were obtained from Johnson Matthey.

*Purification of CzrA and NmtR***.** Recombinant CzrA and NmtR were expressed from pET-CzrA and pET-NmtR, respectively, in *E. coli* BL21(DE3)/*pLysS* and grown on 1.5% LB agar plates containing 0.1 mg/mL ampicillin and 34 μg/mL chloramphenicol at 37°C. The growth, expression, and purification of NmtR and CzrA were carried out using the procedure described previously for SmtB (VanZile *et al.*, 2000), except that DTT was excluded from the purification because CzrA and NmtR do not contain cysteine residues. After purification, purified CzrA or NmtR was dialyzed against 6 L of Buffer S (10 mM HEPES, 0.1 M NaCl, pH 7.0) with changes every 4 h for a total of 24 h at 4 °C. Inspection of overloaded Coomassie-stained Tris-glycine SDS gels was used to estimate the purity to be >95%. N-terminal sequencing of CzrA and NmtR (5 cycles) revealed that both proteins do not possess the expected N-terminal methionine residue. The first five cycles do match the expected N-terminal sequences of CzrA and NmtR after the methionine residue. The concentration of purified of CzrA or NmtR was determined using the calculated molar extinction coefficient at 280 nm of 4470 M^{-1} cm^{-1} (Pace *et al.*, 1995).

Atomic Absorption Spectroscopy. The residual metal content of CzrA and NmtR was determined using a Perkin-Elmer AAnalyst 700 atomic absorption spectrophotometer operating in flame mode. The total metal content of purified, "metal-free" proteins was no more than 0.1 mol metal ion per mol protein monomer. For the determination of the concentration of metals used as titrants for optical titrations, each metal was detected using Zn(II)-, Co(II)-, or Ni(II)-specific hollow cathode lamps. Zn(II) was detected at 213.9 nm (slit-width of 0.7 nm), Co(II) at 240.7 nm (slit-width 0.2 nm), and Ni(II) at 232.0 nm (slit-width 0.2 nm).

Analytical Sedimentation Equilibrium Ultracentrifugation. All experiments were run using a Beckman Optima XL-A analytical ultracentrifuge equipped with an An60 Ti rotor and two-channel, 12-mm path length, charcoal-filled Epon Centerpieces and quartz windows at 235 nm with a rotor speed of 30,000 rpm at 25°C. Apo-CzrA and apo-NmtR samples (5 μM) were prepared by dilution into 10 mM HEPES, 0.4 M NaCl, 0.05 mM EDTA, pH 7.0. Co(II), Ni(II), and Zn(II) protein samples were prepared by addition of 1 mol equiv of Co(II), Ni(II), or Zn(II) to the apoprotein in the absence of EDTA. The partial specific volumes (ν) of CzrA and NmtR were calculated to be 0.740 mL g^{-1} and 0.736 mL g^{-1}, respectively, using the Sednterp program (Laue *et al.*, 1991). Sedimentation equilibrium data were fit (using Microcal Origin) to a single, ideal species model, and a self-association model of a single ideal species, assuming a monomer-dimer equilibrium characterized by the association constant K_{dimer}, as described (Busenlehner *et al.*, 2001). The association constant was converted from absorbance to units of M^{-1} using the calculated extinction coefficients ε_{235} = 22543 M^{-1} cm^{-1} and ε_{235} = 25246 M^{-1} cm^{-1} for CzrA and NmtR, respectively, and a path length l = 1.2 cm.

Fluorescence Anisotropy-based DNA binding experiments. All fluorescence anisotropy experiments were carried out with an SLM 4800 spectrofluorometer operating in the steady-state mode fitted with Glan-Thompson polarizers in the L format (Busenlehner *et al.*, 2002b). The 57-mer, double-stranded *czr* O/P oligonucleotide

(Operon Technologies) used was fluorescein-labeled on one 5'-end with the sequence given below:

F-5′-TTAAATTAATATATGAACAAATATTCAGATGAAAGGATTGTCATATAATGTCAGAAC-3′

3′-AATTTAATTATATACTTGTTTATAAGTCTACTTTCCTAACAGTATATTACAGTCTTG-5′

The 48-mer, double stranded *nmt* O/P oligonucleotide (Operon Technologies) used was also fluorescein-labeled on one 5'-end with the sequence given below:

F-5′-AGAAATAAATGAACAGTTGATCCTATATTCTGATATGTTGGCCGGGTG-3′

3′-TCTTTATTTACTTGTCAACTAGGATATAAGACTATACAACCGGCCCAC-5′

All experiments were carried out with 40 nM dsDNA in 10 mM HEPES and 0.4 M NaCl (pH 7.0) in a volume of 1.8 mL. Up to 650 µL of ~25-35 µM apo-, Co(II)$_1$-, Ni(II)$_1$-, or Zn(II)$_1$-protein stocks were added in known aliquots up to a total concentration of ~6 µM protein. DNA binding experiments were performed in the presence and absence of 50 µM EDTA for metal-free apo-protein and metal-complexed proteins, respectively. The binding equilibria of metal-complexed CzrA and NmtR were determined for protein titrants prepared 1:1 with metal (i.e., 1 molar equiv of metal per monomer of protein or 2 molar equiv per dimer).

Binding isotherms for CzrA were fit using DynaFit (Kuzmic, 1996) utilizing a model involving the sequential binding of five CzrA dimers (P_2) to the DNA oligonucleotide (D), each defined by the indicated K_i, linked to the monomer-dimer equilibrium established for CzrA (VanZile *et al.*, 2002a).

$$P + P \Leftrightarrow P_2;\ K_{dimer}$$

$$P_2 + D \Leftrightarrow P_2{\bullet}D;\ K_2$$

$$P_2 + P_2{\bullet}D \Leftrightarrow (P_2)_2{\bullet}D;\ K_3$$

$$P_2 + (P_2)_2{\bullet}D \Leftrightarrow (P_2)_3{\bullet}D;\ K_4$$

$$P_2 + (P_2)_3{\bullet}D \Leftrightarrow (P_2)_4{\bullet}D;\ K_5$$

$$P_2 + (P_2)_4{\bullet}D \Leftrightarrow (P_2)_5{\bullet}D;\ K_6$$

In these fits, K_{dimer} was fixed at the value determined by analytical equilibrium ultracentrifugation under identical solution conditions (Table 2.1). The characteristic anisotropies, r_i, for each $(P_2)_n{\bullet}D$ complex, i.e., $r_{P2{\bullet}D}$, $r_{(P2)2{\bullet}D}$, $r_{(P2)3{\bullet}D}$, and $r_{(P2)4{\bullet}D}$, were determined from stoichiometric additions of wild-type CzrA to 10 μM dsDNA. These were found to be $r_{P2{\bullet}D} = 0.121$, $r_{(P2)2{\bullet}D} = 0.128$, $r_{(P2)3{\bullet}D} = 0.135$, and $r_{(P2)4{\bullet}D} = 0.146$ relative to a measured anisotropy value for the uncomplexed DNA (r_D) of 0.117 and were treated as fixed parameters in resolution of K_i from all fits. If r_D in a particular experiment was smaller or larger than $r_D = 0.117$, then the fixed values of r_i were adjusted accordingly. The value for $r_{(P2)5{\bullet}D}$ was set to 0.15 in all fits when it was necessary to include it.

Anisotropy data for NmtR were also fit using the program Dynafit (Kuzmic, 1996) to a dissociable dimer model with a 1:1 binding stoichiometry (NmtR dimer to *nmt* O/P oligonucleotide) linked to a monomer-dimer equilibrium. The binding isotherms (raw r_{obs} vs $[\text{NmtR}]_{\text{total}}$) were fit using a fixed K_{dimer} derived from sedimentation equilibrium ultracentrifugation experiments (see Table 2.1).

Co(II) Binding Experiments. All metal binding experiments were carried out in buffer S at ambient temperature using a Hewlett-Packard model 8452A spectrophotometer. Apo-protein (0.8 mL of 150 μM) was prepared by dilution with

Table 2.1 Sedimentation Equilibrium Ultracentrifugation Analysis of CzrA and NmtR

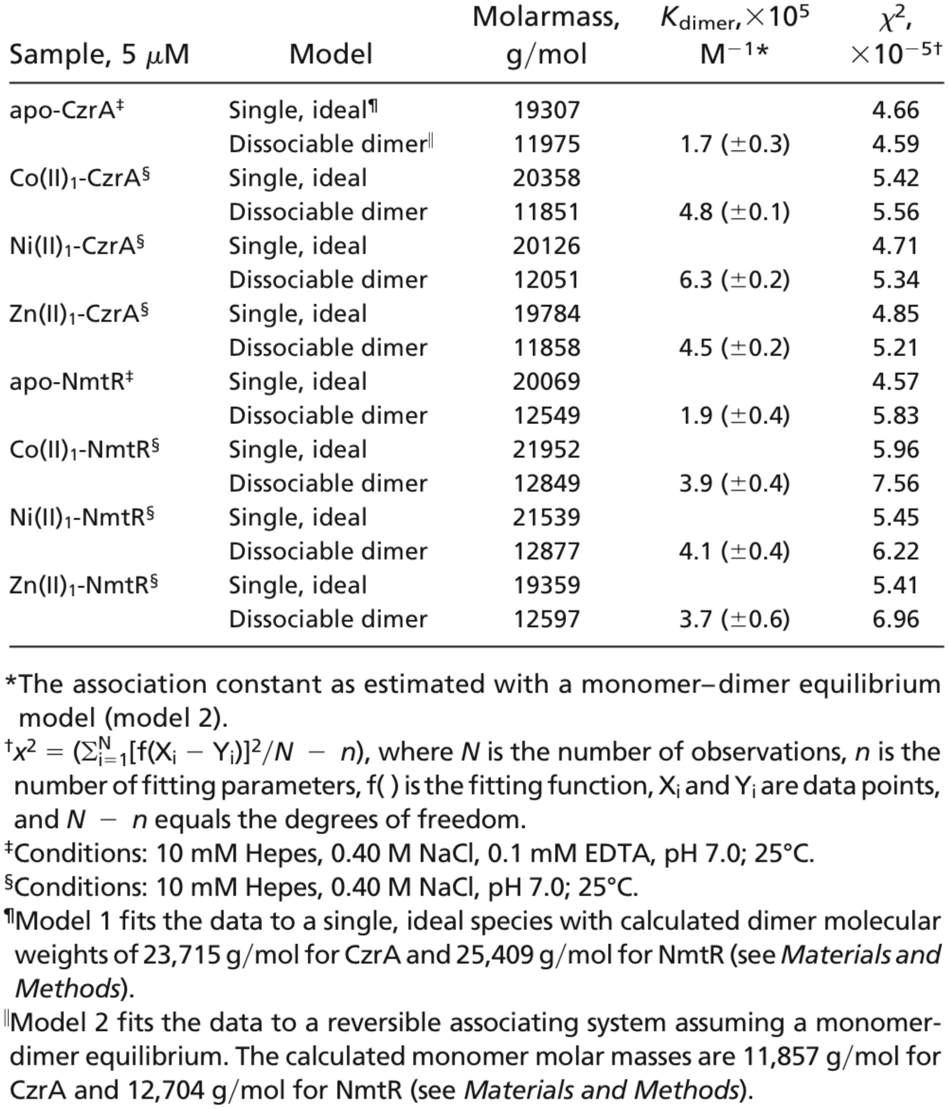

Sample, 5 μM	Model	Molarmass, g/mol	K_{dimer}, $\times 10^5$ M^{-1}*	χ^2, $\times 10^{-5}$†
apo-CzrA‡	Single, ideal¶	19307		4.66
	Dissociable dimer‖	11975	1.7 (±0.3)	4.59
$Co(II)_1$-CzrA§	Single, ideal	20358		5.42
	Dissociable dimer	11851	4.8 (±0.1)	5.56
$Ni(II)_1$-CzrA§	Single, ideal	20126		4.71
	Dissociable dimer	12051	6.3 (±0.2)	5.34
$Zn(II)_1$-CzrA§	Single, ideal	19784		4.85
	Dissociable dimer	11858	4.5 (±0.2)	5.21
apo-NmtR‡	Single, ideal	20069		4.57
	Dissociable dimer	12549	1.9 (±0.4)	5.83
$Co(II)_1$-NmtR§	Single, ideal	21952		5.96
	Dissociable dimer	12849	3.9 (±0.4)	7.56
$Ni(II)_1$-NmtR§	Single, ideal	21539		5.45
	Dissociable dimer	12877	4.1 (±0.4)	6.22
$Zn(II)_1$-NmtR§	Single, ideal	19359		5.41
	Dissociable dimer	12597	3.7 (±0.6)	6.96

*The association constant as estimated with a monomer–dimer equilibrium model (model 2).

†$x^2 = (\Sigma_{i=1}^{N}[f(X_i - Y_i)]^2/N - n)$, where N is the number of observations, n is the number of fitting parameters, f( ) is the fitting function, X_i and Y_i are data points, and $N - n$ equals the degrees of freedom.

‡Conditions: 10 mM Hepes, 0.40 M NaCl, 0.1 mM EDTA, pH 7.0; 25°C.

§Conditions: 10 mM Hepes, 0.40 M NaCl, pH 7.0; 25°C.

¶Model 1 fits the data to a single, ideal species with calculated dimer molecular weights of 23,715 g/mol for CzrA and 25,409 g/mol for NmtR (see *Materials and Methods*).

‖Model 2 fits the data to a reversible associating system assuming a monomer-dimer equilibrium. The calculated monomer molar masses are 11,857 g/mol for CzrA and 12,704 g/mol for NmtR (see *Materials and Methods*).

buffer S. Experiments were performed and data was analyzed essentially as described (VanZile *et al.*, 2000).

X-ray Absorption Spectroscopy. Ni and Zn XAS data were collected at 10 K at Stanford Synchrotron Radiation Laboratory, beamline 9-3, with the SPEAR storage ring operating at 3.0 GeV. The beamline used focusing optics and a fully tuned monochromator containing a Si[220] crystal. A 30-element Ge solid-state X-ray fluorescence detector was employed for data collection. All data collection parameters were as described previously (VanZile *et al.*, 2000). EXAFS analysis was performed with EXAFSPAK software (www-ssrl.slac.stanford.edu/exafspak.html) according to standard procedures (Scott, 1985). Multiple scattering models, calculated using FEFF version 8.2 (Poiarkova and Rehr, 1999; Zabinski *et al.*, 1995), were based on bis(aceto)-bis(imidazole)zinc(II) (Horrocks *et al.*, 1980), tetra(imidazole)zinc(II) (Bear *et al.*, 1975), hexakis(imidazole)nickel(II) chloride tetrahydrate (Konopelski *et al.*, 1976), as described previously (Yamaguchi *et al.*, 1999).

RESULTS

Assembly state of CzrA and NmtR. CzrA and NmtR were subjected to analytical equilibrium sedimentation ultracentrifugation at 30,000 rpm at 5 μM protein monomer at pH 7.0, 25°C, and 0.4 M NaCl, solution conditions identical to those used to monitor DNA binding (below). The results of these experiments are presented in Table 2.1. The data reveal that both CzrA and NmtR are well described as dissociable homodimers under these conditions, with the magnitude of K_{dimer} generally in the 10^5 M^{-1} range for both apo-CzrA and apo-NmtR. This value is comparable to that previously found for apo-zinc sensor, SmtB, but about 10-fold less than that for apo-CadC (Busenlehner *et al.*, 2001). The magnitude of K_{dimer} in the presence of bound metal is consistently larger than that determined for the apo-proteins, but the effect is relatively small (within a factor of 2-3). This magnitude of K_{dimer} reveals that the homodimer is not strongly stabilized by metal binding in these proteins.

Allosteric Regulation of czr O/P and nmt O/P Binding of CzrA and NmtR, respectively, by Co(II), Ni(II), and Zn(II). Previously published gel mobility shift experiments suggested that the addition of exogenously added Co(II) and Zn(II) to pre-formed apo-CzrA DNA complexes resulted in dissociation of the DNA-bound CzrA, but that addition of Ni(II) did not (Singh *et al.*, 1999). In contrast, for NmtR, gel mobility shift data suggested that the addition of Ni(II) and Co(II) to pre-formed apo-NmtR DNA complexes resulted in dissociation of the DNA-bound NmtR, but that Zn(II) had little affect at the same concentrations (Cavet *et al.*, 2002). However, the stoichiometry and affinity of CzrA and NmtR for their specific binding sites, as well as the mode of metalloregulation could not be determined from those experiments.

Figure 2.2A shows representative binding experiments carried out with apo-CzrA and a fluorescein-labeled 57-bp DNA oligonucleotide that contains the entire region of the *czr* operator/promoter (O/P) region footprinted by CzrA (Singh *et al.*, 1999), under solution conditions of relatively high monovalent salt concentration (pH 7.0, 0.40 M NaCl, 25.0 $^{\circ}$C). The solid lines through each set of experimental data in Figure 2.2A are

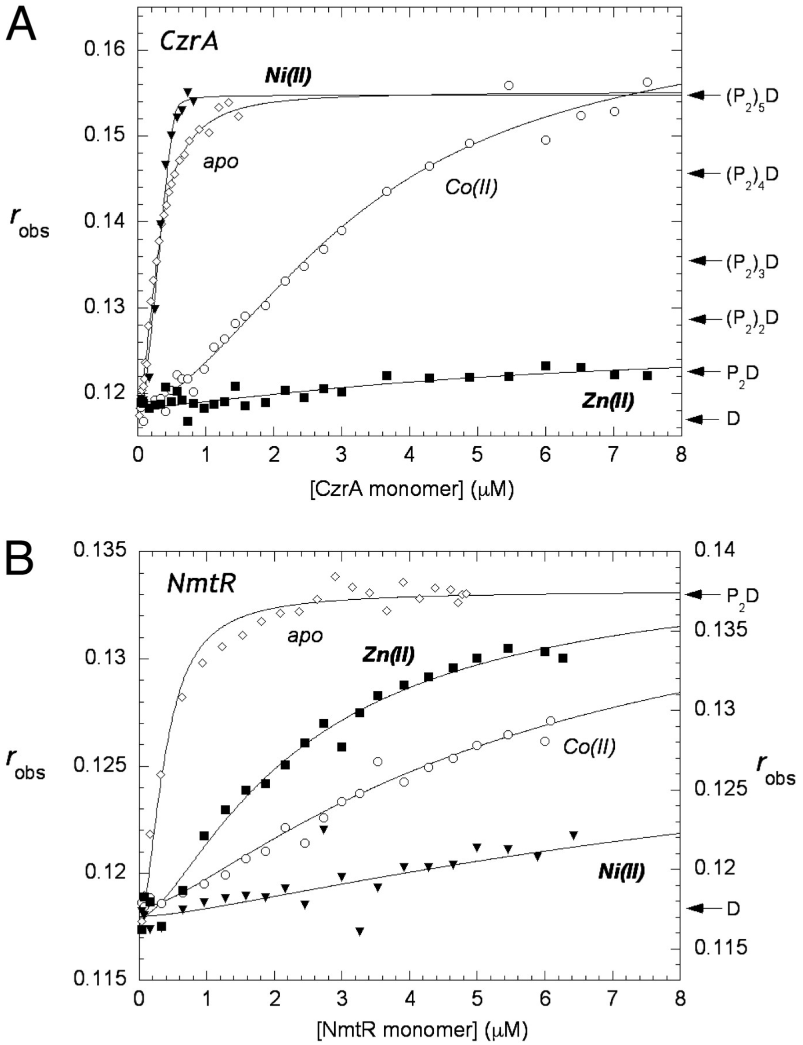

Figure 2.2. CzrA and NmtR DNA binding experiments. **(A.)** Fluorescence anisotropy of CzrA binding to the 57-base pair fluorescein labeled oligonucleotide containing the *czr* O/P region in the absence (◊) and presence of Co(II) (○), Ni(II) (▼), and Zn(II) (■). **(B.)** NmtR binding to the 48-base pair fluroescein labeled oligonucleotide containing the *nmt* O/P region in the absence (◊) and presence of Co(II) (○), Ni(II) (▼), and Zn(II) (■). (Filled symbols use left and open symbols use right axes.) All experiments were performed at 25°C in 10 mM HEPES, 0.4 M NaCl, 0.1 mM EDTA (EDTA is not present in the metal-protein titrations), pH 7.0. The anisotropy, r_{obs}, is plotted as a function of total protein concentration in monomer. The solid lines through the data represent nonlinear least-squares fits to the binding models described in the text for CzrA and NmtR. For $Co(II)_1$ CzrA, $K_2 = 6.8\ (\pm 0.8) \times 10^6\ M^{-1}$, $K_3 = 3.6\ (\pm 0.6) \times 10^6\ M^{-1}$, $K_4 = 1.3\ (\pm 0.3) \times 10^6\ M^{-1}$, $K_5 = 1.1\ (\pm 0.2) \times 10^6\ M^{-1}$; all other K_i are given in the text.

nonlinear least squares fits to the sequential dimer binding model described in Materials and Methods with K_{dimer} constrained to a value of 1.67×10^{5} M^{-1} (Table 2.1). The large change in the anisotropy upon CzrA binding suggests that CzrA oligomerizes or assembles on the DNA, forming complexes characterized by stoichiometries beyond that of a dimer binding to a single site on the DNA. This finding is consistent with the extensive footprint observed on the czr O/P (Singh *et al.*, 1999). The same features characterize the binding of apo-SmtB to its operator-promotor DNA (VanZile *et al.*, 2002a). The binding affinity of the first three dimers of CzrA onto the DNA is essentially stoichiometric under these conditions and hence only a lower limit of 5×10^{9} M^{-1} can be obtained for K_2, K_3 and K_4. The binding affinity of the fourth dimer was found to be $K_5 = 3.4\ (\pm 0.5) \times 10^{8}$ M^{-1}, while that of the fifth dimer was significantly weaker, $K_6 = 2.4\ (\pm 0.4) \times 10^{7}$ M^{-1}.

To test the effect of regulatory metal ions on the association of CzrA for the fluorescein-labeled *czr* O/P region, metal:protein complexes were pre-formed and titrated into free DNA (Cavet *et al.*, 2002; Kuroda *et al.*, 1999; Thelwell *et al.*, 1998). Figure 2.2A shows representative binding isotherms obtained for Co(II), Ni(II), and Zn(II) CzrA. Ni(II) CzrA has little effect on the association of CzrA with the DNA, as the data for apo-CzrA and Ni(II) CzrA superimpose on one another. However, titration of Co(II) CzrA results in a reduced affinity of CzrA for DNA. The data were satisfactorily fit with the binding of four dimers, with the affinities of all four in the 10^{6} M^{-1} range, or ~1000-fold reduced relative to apo-CzrA (Fig. 2.2A). Zn(II) CzrA results in even weaker association with the DNA as only one Zn_2 homodimer associates with an affinity of $K_2 = 4.7\ (\pm 0.3) \times 10^5\ M^{-1}$ or 10^5-fold lower affinity than apo-CzrA. These findings are in full agreement with previous studies that indicate that Zn(II) and Co(II) specifically and strongly negatively regulate *czr* O/P binding, with Zn(II) being the strongest inducer *in vivo* (Kuroda *et al.*, 1999; Singh *et al.*, 1999).

Figure 2.2B shows representative binding isotherms obtained for Co(II), Ni(II), and Zn(II) NmtR. The solid line through each set of experimental data represents a fit to a model that describes the binding of a fully dissociable NmtR homodimer to a *single* site on a 48-bp fluorescein-labeled DNA oligonucleotide encompassing the *nmt* operator/promoter (O/P) region (see (Busenlehner *et al.*, 2001; Busenlehner *et al.*, 2002b) for CadC):

$$2\ \mathrm{NmtR} \overset{K_{\mathrm{dimer}}}{\Leftrightarrow} (\mathrm{NmtR})_2 + \mathrm{D} \overset{K_2}{\Leftrightarrow} (\mathrm{NmtR})_2\bullet\mathrm{D}$$

K_{dimer} for apo-NmtR was constrained to an average value determined by analytical ultracentrifugation, with the fits optimized for K_2 and the value for the anisotropy (r_{max}) of the $(\mathrm{NmtR})_2$-DNA complex. Dimeric NmtR forms a complex with its DNA binding site with $K_2 = 5.6\ (\pm 0.7) \times 10^7\ M^{-1}$, again indicating strong linkage to the monomer-dimer equilibrium under these conditions. In striking contrast, the addition of a single equivalent of bound Ni(II) or Co(II) (Fig. 2.2B) results in negative regulation of *nmt* O/P binding, with $K_2 = 1.9\ (\pm 0.4) \times 10^5\ M^{-1}$ and $K_2 = 4.9\ (\pm 0.1) \times 10^5\ M^{-1}$, respectively, or about 200- and 100-fold reduced, respectively, relative to apo-NmtR. Relative to Ni(II) and Co(II), Zn(II) is the weakest negative regulator of *nmt* operator/promoter binding, but still induces some negative regulation of DNA binding $K_2 = 1.6\ (\pm 0.2) \times 10^6\ M^{-1}$, a result in qualitative agreement with previous gel mobility shift assays (Cavet *et al.*, 2002).

Thus, the ability of metals to allosterically regulate specific operator/promoter binding by CzrA and NmtR is precisely opposite one another with Zn(II)>Co(II)>>Ni(II) for CzrA, while for NmtR, Ni(II)>Co(II)>Zn(II) *in vivo* (Singh *et al.*, 1999; Thelwell *et al.*, 1998) and *in vitro*. UV-Visible electronic and X-ray absorption spectroscopies were used to determine the structural nature of the metal-sensing coordination complexes in each protein.

UV-Visible Absorption Spectroscopy of Co(II) CzrA and NmtR. Shown in Figure 2.3 are UV-visible absorption spectra that result upon aerobic titration of metal-free apo-CzrA or apo-NmtR with Co(II) (pH 7.0, 0.1 M NaCl, 25 °C). CzrA binds one mole equivalent of Co(II) per monomer with a spectrum characterized by intense d-d ligand field transitions at 570 nm, with $\varepsilon_{570} \approx 450$ (±20) M^{-1} cm^{-1}, clearly indicative of tetrahedral or distorted tetrahedral coordination geometry (VanZile *et al.*, 2000). The spectra of Co(II) SmtB, in which metal is restricted to bind to the $\alpha5$ sites (VanZile *et al.*, 2002b) is essentially identical to that of CzrA although less intense, also indicative of tetrahedral or distorted tetrahedral coordination geometries. In contrast, the low molar absorptivities of both the 1:1 and 2:1 Co(II):NmtR dimer complexes (Cavet *et al.*, 2002) are suggestive of five- or six-coordinate Co(II), rather than four (Corwin *et al.*, 1987). The saturated UV-visible absorption spectrum of Ni(II)-NmtR (Figure 2.4A) recorded at a 1:1 Ni(II)-NmtR monomer ratio reveals three very weak ($\varepsilon \leq 80$ M^{-1} cm^{-1})and very broad ligand field absorption transitions diagnostic (Rosa *et al.*, 2001) of six-coordinate

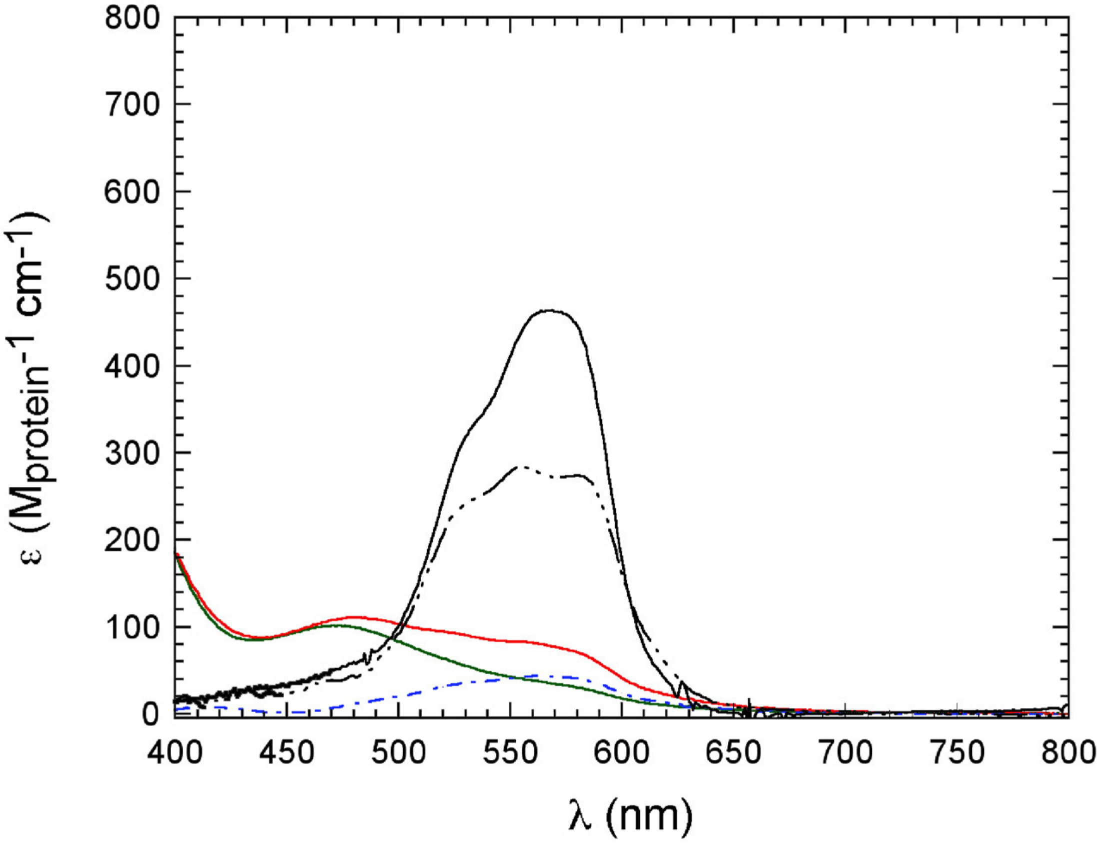

Figure 2.3. Optical spectroscopy of CzrA, NmtR, and SmtB. Electronic absorption spectrum of 150µM Co(II) CzrA (solid), along with 150 µM Co(II)$^{\alpha 5}$ SmtB (black — •••), the 1:1 and 2:1 Co(II):dimer complexes of 500 µM Co(II) NmtR (green and red solid, respectively), and the difference spectrum characteristic of the binding of the second Co(II) to the NmtR dimer (blue dash-dot). Conditions: pH 7.0, 10 mM Hepes with 0.1 M NaCl (for CzrA and SmtB) or 0.4 M NaCl (for NmtR).

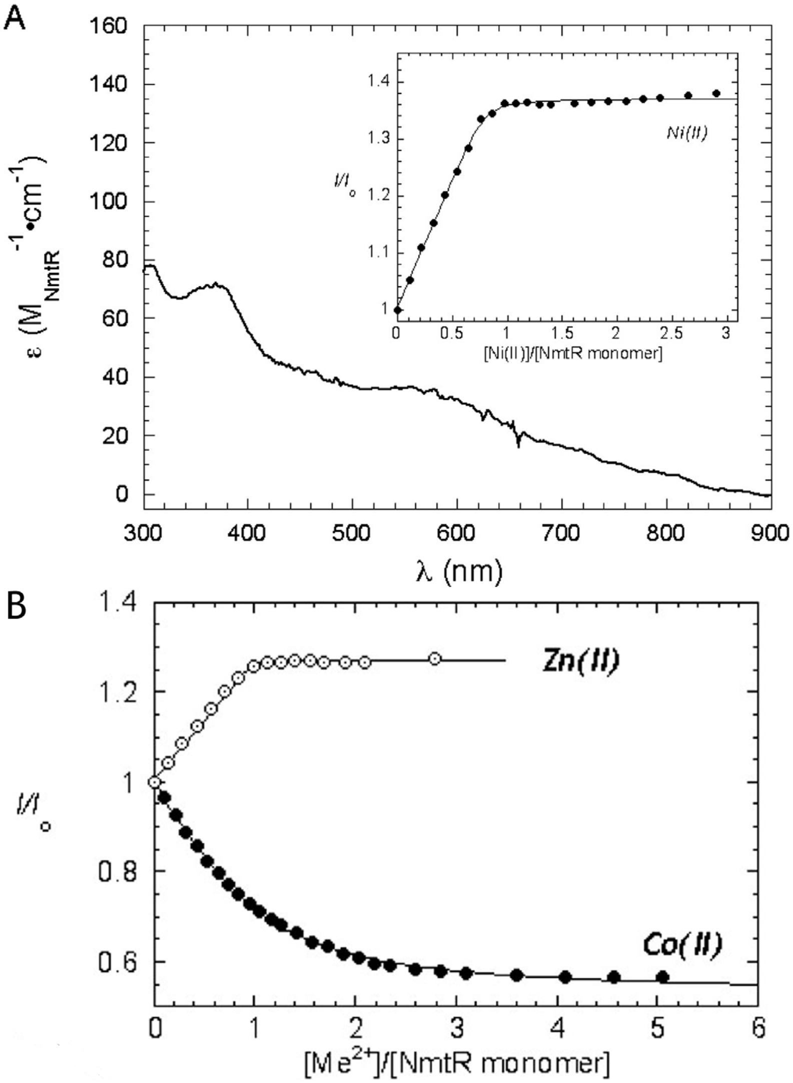

Figure 2.4. Spectroscopic analysis of metallated NmtR. **(A.)** Electronic molar absorptivity spectrum of Ni(II)-NmtR (1:1 molar ratio of Ni(II):NmtR monomer or two per dimer). *Inset*, Ni(II) binding isotherm as monitored by tyrosine fluorescence (λ_{ex} = 280 nm; λ_{em} = 305 nm) with the *solid line* representing a fit to a 1:1 (metal:monomer) binding model (n = 0.8, K_{Ni} = 2.6 (±0.7) × 10^7 M^{-1}). **(B.)** Co(II) and Zn(II) binding isotherms as monitored by tyrosine fluorescence with the *solid lines* representing fits to a 1:1 binding model for Co(II) (K_{Co} = 7.1 (±0.3) × 10^5 M^{-1}) and Zn(II) (K_{Zn} = 1.5 (±2.3) × 10^8 M^{-1}). K_{Ni} and K_{Zn} are too tight to measure under these conditions and represent only lower limits. Conditions: 10 mM HEPES, 0.4 M NaCl (pH 7.0), 22 °C.

d^8 Ni(II). The *inset* (Figure 2.4A) reveals that the stoichiometry of Ni(II) binding to NmtR is 1 Ni(II) per monomer or 2 per dimer with a lower limit of the affinity for Ni(II), $K_{\mathrm{Ni}} \geq 2 \times 10^7$ M^{-1}. For SmtB, $K_{\mathrm{Ni}} = 1.7\ (\pm)0.4 \times 10^5$ M^{-1} (VanZile *et al.*, 2000). Consistent with the competitive metal binding experiments described above, Co(II) binds to NmtR with an affinity ≥40-fold weaker than Ni(II) and at least 500-fold weaker than Zn(II) (Figure 2.4B) again implying that for NmtR, $K_{\mathrm{Zn}} \geq K_{\mathrm{Ni}} > K_{\mathrm{Co}}$. Remarkably, K_{Co} for NmtR is ≈1500-fold smaller for NmtR relative to CzrA under similar solution conditions.

X-ray Absorption Spectroscopy. Comparison of the extended x-ray absorption fine structure (EXAFS) and Fourier transforms (FTs) for Ni(II)- or Zn(II)-bound forms of NmtR, CzrA, and SmtB [the last published previously (VanZile *et al.*, 2000) and reproduced here for comparison] reveals a distinction between the metal binding sites of SmtB and those of NmtR and CzrA (Fig. 2.5). Noticeable differences in the EXAFS arise in the region near $k \approx 4$ Å^{-1}. This region is sensitive to variations in high-frequency oscillations that are commonly associated with the multiple-scattering contribution from the outer-shell atoms of the imidazole ring of histidine. An increase in the number of histidine ligands causes splitting of the main peak in this region, also visualized as increased intensity in the high-R region of the FT plot, specifically at ca. 3 and 4 Å, which is diagnostic for histidine ligation. The absence of a 3-Å peak, in the presence of a 4-Å peak in the FT, has been assigned previously as the result of destructive interference between the outer-shell contributions from carboxylate and histidine ligands (Cosper *et al.*, 1999; VanZile *et al.*, 2000). This is most clearly observed in the Zn FTs

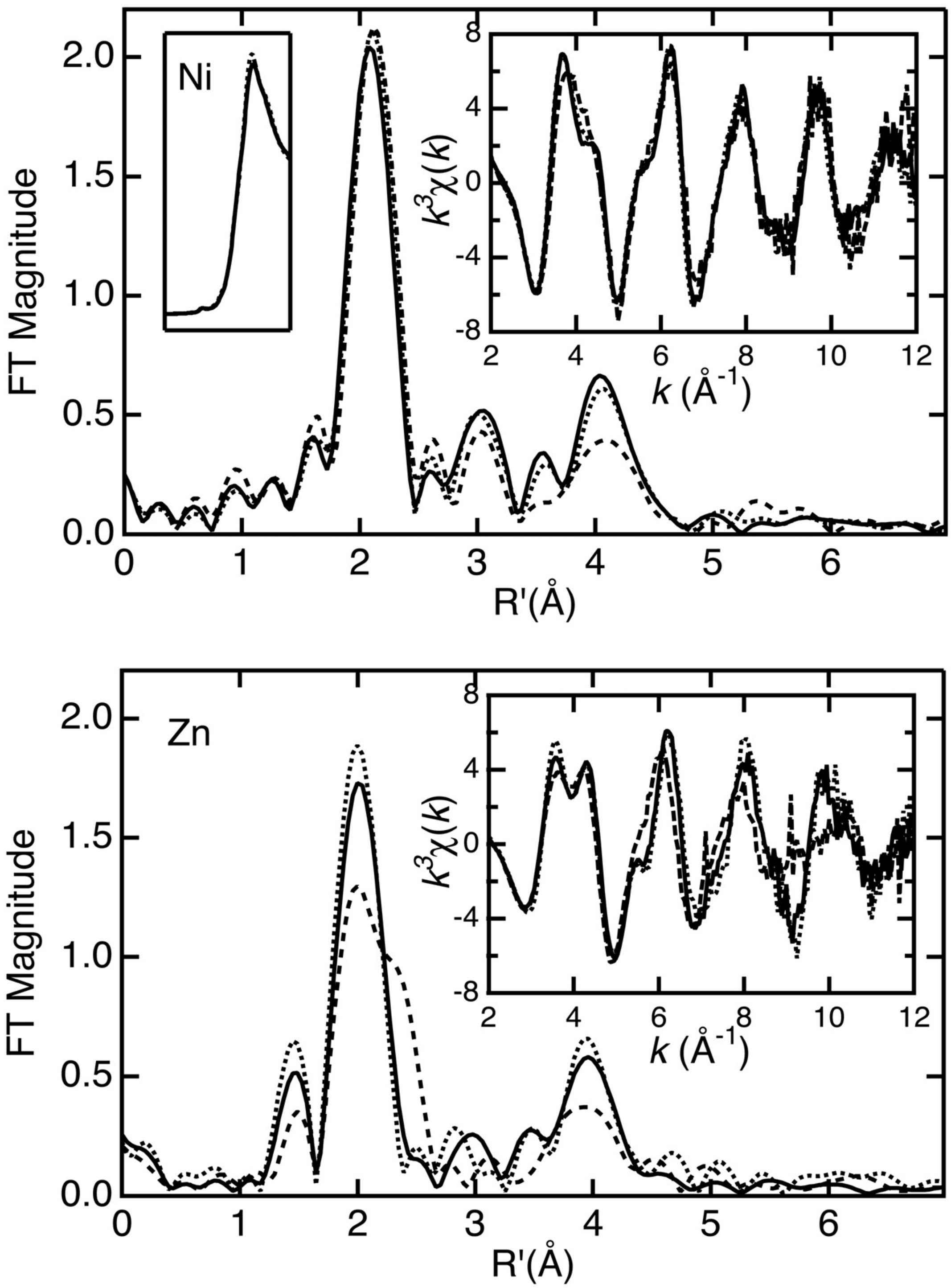

Figure 2.5. EXAFS of CzrA, NmtR, and SmtB. Ni (*Upper*) and Zn (*Lower*) k^3-weighted EXAFS (*Right Inset*) and Fourier transforms (k = 2-12 Å^{-1}) for NmtR (*solid*), CzrA (*dotted*), and SmtB (*dashed* (VanZile *et al.*, 2000)). (*Upper Left Inset*) Comparison of the Ni K-edge spectra NmtR (solid) and CzrA (*dotted*).

(Fig. 2.5) and supports the binding of a carboxylate-containing residue to the metal. The EXAFS are consistent with an increase in imidazole ligation in NmtR and CzrA, relative to SmtB. Another key difference between SmtB and NmtR/CzrA is the ~2.3-Å shoulder in the main FT peak that appears in Zn(II) SmtB (Fig. 2.5). This shoulder arises from the contribution of a first-shell sulfur ligand contributed by cysteine (VanZile *et al.*, 2000).

The results of extensive curve-fitting analysis of these samples are consistent with the observation that NmtR and CzrA have increased contribution from imidazole-containing ligands and no contribution from sulfur-containing ligands, consistent with the fact that neither CzrA nor NmtR have cysteine residues (Fig. 2.1). Best fits for both Ni(II) NmtR and Ni(II) CzrA indicate a coordination environment containing three histidine ligands and three other oxygen- or nitrogen-containing ligands (Fits 1, 2; Table 2.2). Similarly, Zn(II) NmtR and Zn(II) CzrA are best fit with three histidine ligands, although in striking contrast to the Ni(II) complexes, the coordination geometry of the Zn(II)-binding site is most likely tetrahedral rather than octahedral (Fits 3, 4; Table 2.2). This would be consistent with the tetrahedral coordination geometry associated with the Co(II) complex of CzrA, but in contrast to Co(II) NmtR, which clearly adopts a higher coordination number (Fig. 2.3) than Zn(II) NmtR.

Table 2.2. Curve Fitting Results for EXAFS[a]

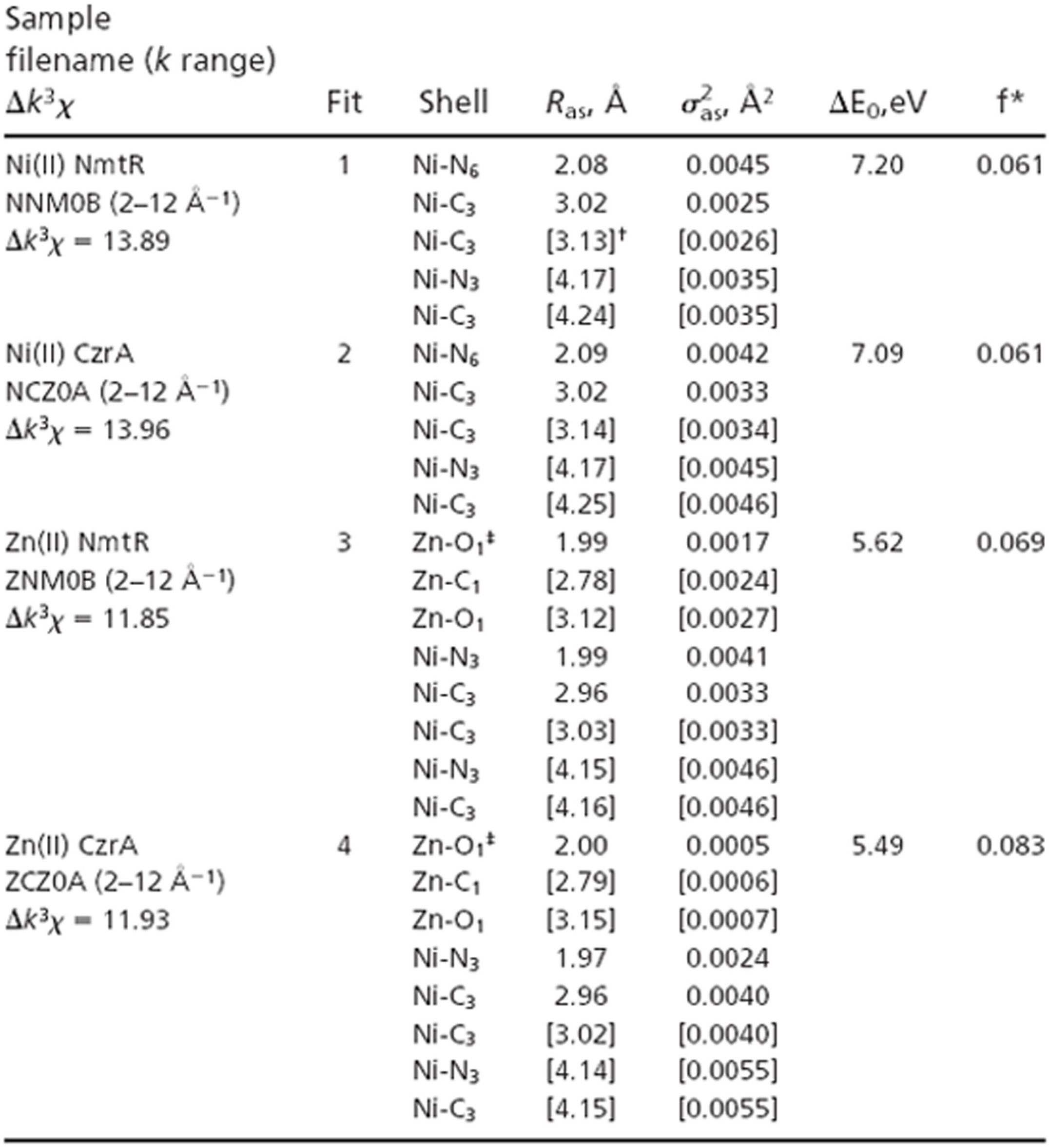

Sample filename (k range) $\Delta k^3\chi$	Fit	Shell	R_{as}, Å	σ^2_{as}, Å^2	ΔE_0,eV	f*
Ni(II) NmtR	1	Ni-N_6	2.08	0.0045	7.20	0.061
NNM0B (2–12 Å^{-1})		Ni-C_3	3.02	0.0025		
$\Delta k^3\chi$ = 13.89		Ni-C_3	[3.13]†	[0.0026]		
		Ni-N_3	[4.17]	[0.0035]		
		Ni-C_3	[4.24]	[0.0035]		
Ni(II) CzrA	2	Ni-N_6	2.09	0.0042	7.09	0.061
NCZ0A (2–12 Å^{-1})		Ni-C_3	3.02	0.0033		
$\Delta k^3\chi$ = 13.96		Ni-C_3	[3.14]	[0.0034]		
		Ni-N_3	[4.17]	[0.0045]		
		Ni-C_3	[4.25]	[0.0046]		
Zn(II) NmtR	3	Zn-O_1‡	1.99	0.0017	5.62	0.069
ZNM0B (2–12 Å^{-1})		Zn-C_1	[2.78]	[0.0024]		
$\Delta k^3\chi$ = 11.85		Zn-O_1	[3.12]	[0.0027]		
		Ni-N_3	1.99	0.0041		
		Ni-C_3	2.96	0.0033		
		Ni-C_3	[3.03]	[0.0033]		
		Ni-N_3	[4.15]	[0.0046]		
		Ni-C_3	[4.16]	[0.0046]		
Zn(II) CzrA	4	Zn-O_1‡	2.00	0.0005	5.49	0.083
ZCZ0A (2–12 Å^{-1})		Zn-C_1	[2.79]	[0.0006]		
$\Delta k^3\chi$ = 11.93		Zn-O_1	[3.15]	[0.0007]		
		Ni-N_3	1.97	0.0024		
		Ni-C_3	2.96	0.0040		
		Ni-C_3	[3.02]	[0.0040]		
		Ni-N_3	[4.14]	[0.0055]		
		Ni-C_3	[4.15]	[0.0055]		

---

[a] Shell defines the absorber-scatterer pair (the subscript is N_s, the number of scatterers). R_{as} is the metal-scatterer distance. σ_{as}^2 is a mean square deviation in R_{as}. ΔE_0 is the shift in E_0 for the theoretical scattering functions.

[b] f' is a normalized error (chi-squared):

$$f' = \frac{\left\{ \sum_i \left[k^3 \left(\chi_i^{obs} - \chi_i^{calc} \right) \right]^2 \Big/ N \right\}^{1/2}}{\left[\left(k^3 \chi^{obs} \right)_{max} - \left(k^3 \chi^{obs} \right)_{min} \right]}$$

[c] Numbers in square brackets were constrained to be either a multiple of the above value (σ_{as}^2) or to maintain a constant difference from the above value (R_{as}, ΔE_0).

DISCUSSION

The SmtB/ArsR family of metalloregulators is uniquely characterized by the presence of two metal-binding sites, neither of which is absolutely conserved across the family (Busenlehner *et al.*, 2003). Some SmtB/ArsR members possess only the α3N site, others just the α5 site, while some, including cyanobacterial zinc sensors SmtB and ZiaR, appear to possess both. Recent work from our laboratory has defined the coordination environments of the α3N and α5 metal-binding sites of SmtB (VanZile *et al.*, 2002a, b) (Fig. 2.1). These studies reveal that the histidine/carboxylate-containing α5 site is responsible for binding Zn(II) in a tetrahedral coordination complex and allosterically regulating binding of SmtB to the *smt* operon (VanZile *et al.*, 2002a). The α3N site, which contains at least one cysteine thiolate ligand (Cys14), not present in CzrA or NmtR (VanZile *et al.*, 2002a) (*cf.* Fig. 2.1), plays some other role. These findings are fully compatible with characterization of mutant SmtBs *in vivo* (Turner *et al.*, 1996). The α3N metal site possesses a higher affinity for Zn(II) in the free protein at equilibrium; this is the Zn(II) complex characterized in previous EXAFS studies and reproduced here for comparison (VanZile *et al.*, 2000) (Fig. 2.5).

The protein determinants of metal ion specificity are not currently well defined. An attractive hypothesis is that proteins simply follow the trends predicted by traditional inorganic chemistry. Unfortunately, those trends have not provided a complete explanation for why certain metal ions are preferred by certain proteins. Sometimes the metal ion that binds with the highest affinity to the protein is not the metal ion that provides *in vivo* functionality, complicating the study of metal ion specificity (Cavet *et al.*, 2002). Our results provide a basis for bridging the gap between inorganic and biological chemistry that can be applied to the understanding of nature's selection process.

SmtB and CzrA which favor Zn(II) coordination at the α5 site, utilize carboxylate and imidazole ligands to bind harder Lewis acids, such as Co(II), Ni(II), and Zn(II). NmtR, which discriminates toward Ni(II) and Co(II), also uses imidazoles. CadC and ArsR possess α3N and α3 metal sites that have all-cysteinyl coordination spheres that prefer softer Lewis acids, such as Cd(II), Pb(II), and Bi(III) (Busenlehner *et al.*, 2001; Busenlehner *et al.*, 2002a; Busenlehner *et al.*, 2002b). Interestingly, *S. aureus* pI258 CadC contains an intact α5 metal site that has been shown to bind Zn(II) and Co(II) directly; however, the binding of metal here is not regulatory for DNA binding *in vitro* (Busenlehner *et al.*, 2002b) or *in vivo* (Wong *et al.*, 2002).

Here, we provide spectroscopic evidence for the coordination environment of the metalloregulatory sites of *S. aureus* CzrA and *M. tuberculosis* NmtR in an attempt to determine how these proteins functionally discriminate between different transition metals. The spectroscopic properties of both CzrA and NmtR lend support to the model in which ligands located in the α5 site of the proteins contribute to binding Co(II), Ni(II), or Zn(II) (Fig. 2.1). The optical absorption spectra of Co(II)-substituted CzrA are consistent with a tetrahedral coordination model that utilizes three histidines and one carboxylate-containing residue to ligate the metal ion. Preliminary Co(II) XAS data support this coordination. XAS data for Zn(II) CzrA and Zn(II) NmtR also indicate a coordination model in which three histidines and one carboxylate residue donate ligands to the Zn(II) ion. By contrast, XAS data for Ni(II) NmtR and Ni(II) CzrA indicate a six-coordinate environment containing at least three histidine ligands and three other oxygen or nitrogen-containing ligands.

CzrA is selective for Co(II)/Zn(II), discriminating between Ni(II) and Co(II)/Zn(II) by creating a coordination environment in which the Ni(II) forms an octahedral complex, while Co(II)/Zn(II) binding is clearly tetrahedral. The XAS data are fully compatible with the $\alpha 5$ site schematized in the sequence alignment (Fig, 2.1), with Asp84, His86, His97, and His100 providing ligands to the metal. It seems likely that each pair of ligands is drawn from opposite monomers of the homodimer, as originally hypothesized from the crystal structure of apo-SmtB (Cook *et al.*, 1998). The DNA binding data (Fig. 2.2) indicate that a tetrahedral coordination environment is required to effect negative allosteric regulation *in vivo* and *in vitro*. Thus, CzrA appears to discriminate between Co(II)/Zn(II) and Ni(II) strictly on the basis of the coordination geometry of the metal complex. How this complex expands to increase its coordination number in the Ni(II) complex is not known, but presumably reflects the addition of solvent molecules. The binding of Ni(II) to the zinc sensor SmtB at low Ni(II):monomer stoichiometries can also be described by a similar mechanism. It has already been shown that Ni(II) binds weakly to SmtB [about 10^4 weaker than Co(II)] (VanZile *et al.*, 2000).

Conversely, NmtR appears to employ an octahedral coordination environment to negatively regulate DNA binding with Co(II)/Ni(II) versus Zn(II), despite the fact that

Zn(II) and Ni(II) bind with comparable affinities to the protein (Figure 2.4) (Cavet *et al.*, 2002). The distinguishing feature of NmtR relative to CzrA is the presence of a short C-terminal extension which contains up to three additional potential hard Lewis base donors beyond the four ligands conserved between CzrA and NmtR (Asp91, His93, His104, and His107 in NmtR), including His109, Asp114, and His116 (Fig. 2.1). Functional studies with substitution mutants reveal that His109 and His116, as well as the four ligands in common with CzrA, are essential to effect Ni(II)-mediated de-repression *in vivo* (Cavet *et al.*, 2002). This suggests a model that Ni(II) and Co(II) are uniquely capable of recruiting one or two of these His residues into the coordination shell to create the six-coordinate species compatible with the optical absorption [Fig. 2.3;(Cavet *et al.*, 2002)] and XAS experiments presented here (Fig. 2.5). The Ni EXAFS FT peaks at 3 and 4 Å for NmtR and CzrA are very similar (Fig. 2.5), suggesting a similar histidine ligand count, although the precision of this determination can be affected by imidazole geometry or disorder (Ferreira *et al.*, 2002).

NmtR requires hexacoordinate metal binding (as observed for Ni(II) and Co(II)) to affect allosteric de-repression of transcription, while CzrA requires tetrahedral metal binding (as observed for Co(II) and Zn(II)) to achieve the same biological function. Thus Zn(II) NmtR adopts a less effective (tetrahedral) coordination, while Ni(II) CzrA is hexacoordinate and similarly ineffective. Nature has adapted the allosteric coupling of metal coordination (in the α5 helices) to DNA binding (to the α3-turn-αR region (Busenlehner *et al.*, 2003); Fig. 2.1) to take advantage of inorganic coordination preferences. The exact mechanism of this allosteric coupling, and how the coupling must differ for CzrA and NmtR, is still under investigation. However, the evidence presented here indicates that metal coordination number and geometry play a dominant role in determining which metal ions negatively allosterically regulate operator/promoter binding *in vitro*.

CHAPTER III

A METAL-LIGAND MEDIATED INTERSUBUNIT ALLOSTERIC SWITCH IN RELATED SmtB/ArsR ZINC SENSOR PROTEINS*

INTRODUCTION

Zinc and other transition metal ions play essential roles in the diverse array of cellular processes, either as structural components in proteins or as obligate cofactors in metalloenzymes (Berg and Shi, 1996; McCall *et al.*, 2000). All metal ions, however, become toxic at high concentrations. This has led to the evolution of homeostatic mechanisms that maintain the intracellular concentrations of biologically required metal ions, e.g., Zn, Fe, Cu, Mn, Co, and Ni, in a range that is compatible for cell viability through the involvement of specific metallochaperones that traffic metals inside cells and/or the coordinate regulation of specific uptake and efflux systems (Finney and O'Halloran, 2003; O'Halloran, 1993). Heavy metal pollutants, e.g., Cd, Pb, Bi, and Hg, are efficiently removed from cells using the same general mechanisms. Although the specific details differ, gene regulatory systems required for the efficient detoxification and resistance of high concentrations of transition metal ions are ubiquitous in nature.

In prokaryotes, the SmtB/ArsR (Busenlehner *et al.*, 2003) and MerR

---

*Reprinted from *Journal of Molecular Biology*, **333**, Eicken, C., Pennella, M.A., Chen, X., Koshlap, K.M., VanZile, M.L., Sacchettini, J.C., and Giedroc, D.P. A metal-ligand-mediated intersubunit allosteric switch in related SmtB/ArsR zinc sensor, 683-695. Copyright 2003with permission from Elsevier. (http://www.sciencedirect.com/science/journal/00222836).

(Brown *et al.*, 2003) family of metal sensor proteins represent two general classes of metalloregulatory proteins. MerR proteins are transcriptional repressors in the absence of inducing metal ions and become potent activators when bound to their metal-ion coactivator (Ansari *et al.*, 1992); metal binding drives an underwinding of the promoter DNA which repositions the –10 and –35 sequences to allow for a favorable interaction with RNA polymerase (Ansari *et al.*, 1995). Other non-metal regulated MerR family members include *E. coli* SoxR (Ding and Demple, 1996), which senses oxidative stress via a 2Fe-2S redox center, and *B. subtilis* BmrR (Heldwein and Brennan, 2001), which binds toxic drugs and regulates the expression of a multidrug efflux transporter. Although metal-sensing MerR proteins have been characterized that respond to a wide range of divalent transition metals (Brown *et al.*, 2003), how individual MerR regulators discriminate among distinct metal ions and couple metal-binding to DNA conformational changes is unknown.

The SmtB/ArsR family of homodimeric helix-turn-helix (HTH) proteins represses the expression of operons associated with metal ion sequestration or efflux in both Gram-positive and Gram-negative bacteria, allowing these organisms to survive when challenged with toxic concentrations of heavy metal ions (Shi *et al.*, 1994). Human pathogenic bacteria, including virulent hospital strains of *S. aureus* and *Mycobacterium tuberculosis* (Cavet *et al.*, 2002) sometimes encode many such metal resistance systems, potentially providing a selective advantage for survival in the human host. Comparative biochemical and spectroscopic studies of six SmtB/ArsR proteins reveal that these proteins harbor one or both of two structurally distinct metal coordination sites, denoted α3N or α5 (Busenlehner *et al.*, 2002b; Busenlehner *et al.*, 2003), named for the location of the metal sites in the known or predicted secondary structure of individual family members. The α3N site is cysteine thiolate-rich, forming S_3 or S_4 complexes with large, thiophilic metals including Cd, Pb and Bi, as found in the cadmium sensor *S. aureus* CadC (Busenlehner *et al.*, 2001; Busenlehner *et al.*, 2002a; Busenlehner *et al.*, 2002b). Site-directed mutagenesis and amino acid sequence comparisons suggested that the α5 site is composed of a combination of carboxylate and imidazole ligands, preferentially interacting with harder transition metals ions including Zn, Co and Ni (Cavet *et al.*, 2002; Pennella *et al.*, 2003; VanZile *et al.*, 2002b). Spectroscopic studies of a zinc sensor encoded by *S. aureus*, CzrA, and a Ni-sensor from *M. tuberculosis*, NmtR, suggest that a change in the coordination number from four in CzrA to six in NmtR in the α5 metal sites is sufficient to switch the metal selectivity from Zn/Co in CzrA to Ni/Co in NmtR (Pennella *et al.*, 2003). Metal binding to both sites is known to strongly negatively allosterically regulate operator-promoter binding, reducing the affinity of the repressor for DNA by ≥300-fold, depending on the system (Busenlehner *et al.*, 2001; Pennella *et al.*, 2003; VanZile *et al.*, 2002a).

Synechococcus SmtB regulates the expression of the divergently transcribed *smt* operon nearly exclusively in response to Zn(II) (Cavet *et al.*, 2002; Turner *et al.*, 1996). In addition to the *smtB* gene, this operon encodes SmtA, a prokaryotic metallothionein that sequesters toxic metals (Huckle *et al.*, 1993). *S. aureus* CzrA regulates the expression on the *czr* operon, the expression of which is induced by Zn and Co (Kuroda *et al.*, 1999; Xiong and Jayaswal, 1998). The *czr* operon encodes CzrB, a predicted cation diffusion facilitator (CDF) antiporter efflux pump (Guffanti *et al.*, 2002) that appears structurally homologous to *E. coli* ZitB (Grass *et al.*, 2001). SmtB and CzrA share 35% identity in overlapping regions, including proposed ligands to the α5 metal ion; however, CzrA lacks an N-terminal extension as well as other amino acids ligands thought to comprise the α3N metal binding site in SmtB (Cys14, His18, Cys61' and Asp64') (see Fig. 3.1A) (VanZile *et al.*, 2002b). The 2.3 Å structure of apo-SmtB previously reported (Cook *et al.*, 1998) reveals that homodimeric SmtB is a highly elongated winged helix-turn-helix protein, with each subunit adopting an ααααββα structure. This structure provided little direct insight into the regulatory mechanism since the structure of the zinc-bound protein was not reported.

MATERIALS AND METHODS

Protein expression, purification and crystallization. Wild-type *Synechococcus* PCC7942 SmtB (VanZile *et al.*, 2000) and *S. aureus* CzrA (Pennella *et al.*, 2003) were overexpressed in *E. coli* BL21(DE3) and purified to homogeneity as described. The expression plasmid encoding the triple substitution mutant α5 SmtB (C14S/C61S/C121S SmtB) was prepared using PCR-based mutagenesis of the C14S/C61S overexpression plasmid as template and C121S mutagenic primers (VanZile *et al.*, 2002b). The integrity of the nucleotide sequence of both strands of the plasmid was confirmed by DNA sequencing. α5 SmtB was purified to homogeneity using a methods essentially

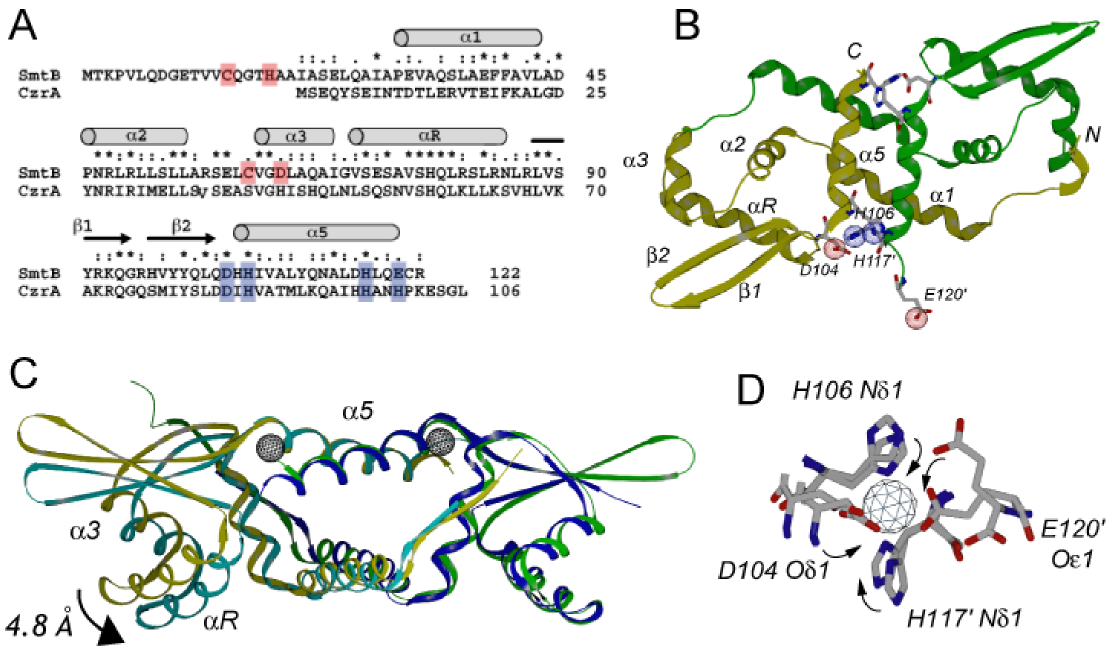
A
α1
SmtB MTKPVLQDGETVVCQGTHAAIASELQAIAPEVAQSLAEFFAVLAD 45
CzrA MSEQYSEINTDTLERVTEIFKALGD 25
α2
α3
αR
SmtB PNRLRLLSLLARSELCVGDLAQAIGVSESAVSHQLRSLRNLRLVS 90
CzrA YNRIRIMELLSvSEASVGHISHQLNLSQSNVSHQLKLLKSVHLVK 70
β1
β2
α5
SmtB YRKQGRHVYYQLQDHHIVALYQNALDHLQECR 122
CzrA AKRQGQSMIYSLDDIHVATMLKQAIHHANHPKESGL 106
B
C
N
α3
α2
α5
α1
αR
H106
β2
D104
H117'
β1
E120'
C
α5
α3
4.8 Å
αR
D
H106 Nδ1
E120' Oε1
D104 Oδ1
H117' Nδ1

Figure 3.1. Structure of cyanobacterial SmtB. **(A.)** Sequence alignment of *Synechococcus* SmtB and *S. aureus* CzrA pointing out the location of the proposed ligands to the α3N and α5 metal binding sites(VanZile *et al.*, 2002b). **(B.)** Ribbon representation of the structure of homodimeric apo-SmtB solved to 1.7 Å resolution, with the side chains of the proposed ligands of one of the α5 metal sites indicated (see Fig. 3.1a). Secondary structural units (N-α1-α2-α3-αR(α4)-β1-β2-α5-C) are indicted for the *gold-shaded* protomer. In the *gold*-shaded subunit, C-terminal residues 119-121, including zinc ligand Glu120, are not visible in the electron density maps, indicative of significant disorder in the absence of zinc. **(C.)** Superposition of apo-SmtB (*green* and *gold*-colored protomers) with Zn_2 α5-SmtB (*blue* and *cyan*-colored subunits), the later solved to 2.3 Å resolution. The polypeptide chain could not be traced from residues 92-97 in the *blue-colored* Zn_2 α5-SmtB subunit. The figure was generated by performing a superposition of the C^{α} atoms of the α5 helices of the *green*- and *blue*-shaded subunits of apo- and Zn_2 α5-SmtB, respectively. This illustrates the large movement of the HTH and β-wings of one subunit relative to the other, represented by a movement of the Ser74 C^{α} atoms positioned toward the N-terminus of the αR helix by 4.8 Å. **(D.)** Superposition of the metal binding residues in the apo- and Zn_2 forms of SmtB derived from the superposition shown in Fig. 3.1c. Figures were created using SPOCK: http://mackerel.tamu.edu (Christopher, 1998).

identical to wild-type SmtB. All preparations of SmtB, α5 SmtB and CzrA were devoid of bound zinc by atomic absorption spectroscopy (≤0.05 mol•equiv metal) and thus were designated apoproteins; Zn_2 complexes were obtained upon the addition of 1.1 monomer-equivalents of $ZnSO_4$ to apoproteins.

Initial crystallization conditions were obtained using the hanging drop method employing Crystal Screens from Hampton Research and Wizard Screens from Emerald Biostructures. Crystallization conditions were as follows: apo-SmtB: 1.6 M Na/K phosphate, 0.1 M Hepes pH 7.0; Zn_2 α5 SmtB: 1.6 M Na/K phosphate, 0.1 M Hepes, pH 7.5; apo-CzrA: 2.5 M NaCl, 0.1 M Na/K phosphate pH 6.2; Zn_2-CzrA: 10% PEG 8000, 0.1 M CHES pH 9.5, 0.2 M NaCl. Crystals of Zn_1 SmtB were obtained from stoichiometric mixtures of Zn(II) and apo-wild-type SmtB obtained under the same conditions of apo-SmtB. Cell parameters, symmetry and monomers per asymmetric unit of all crystals are listed in Table 3.1. All crystals were soaked in paraffin oil for a few seconds before flash cooling to 100 K and subjected to x-ray diffraction.

*Data collection, structure determination and refinement***.** Diffraction data were collected at beamline 14-BM-C and D (MAD) at the Advanced Photon Source (APS), Argonne National Laboratory on a charge-coupled-device area detector (ADSC Q4). Apo-CzrA data were collected with a rotating anode and a Rigaku IPDS IV++ system. Data collection parameter and statistics are listed in Table 3.1. Reflection data were processed and scaled using DENZO and SCALEPACK (Otwinowski, 1993). Initial phases were determined by molecular replacement using the search models based on the

Table 3.1 Data Collection and Refinement Statistics

Data collection[a]

Data set	apo-SmtB	Zn_2 α5-SmtB remote	(Zn MAD) Peak	Inflection	Zn_2 α5-SmtB (refinement)	Zn_1 SmtB	apo-CzrA	Zn_2 CzrA
Beam line	APS 14C	APS 14D	APS 14D	APS 14D	APS 14D	APS 14C	In house	APS 14C
Unit cell parameters								
a (Å)	37.24	64.48	64.47	64.50	64.45	37.00	50.12	54.44
b (Å)	69.72	125.72	125.00	125.47	124.68	70.37	50.12	75.37
c (Å)	43.22	26.00	26.00	26.00	25.91	42.68	153.55	50.63
β (deg.)	95.84					95.50		
Space group	$P2(1)$	$P2(1)2(1)2$	$P2(1)2(1)2$	$P2(1)2(1)2$	$P2(1)2(1)2$	$P2(1)$	$P31$	$P2(1)2(1)2$
Monomers/ASU	2	2	2	2	2	2	4	2
Wavelength (Å)	1.00	1.2398	1.2828	1.2833	1. 2828	1.00	1.54	1.00
Resolution (Å)	60–1.7	62–2.8	62–2.8	62–2.8	50–2.3	60–2.0	18.9–2.0	60–2.3
Redundancy	4.3	5.8	5.8	6.0	6.0	3.3	3.0	5.7
Completeness (%)	92.5 (58.3)	98.5 (94.5)	96.3 (87.2)	98.1 (92.5)	94.4 (85.8)	96.8 (85.7)	96.7 (74.1)	97.4 (91.4)
$I/\sigma(I)$	19.9	18.8	22.6	20.8	12.6	27.4	13.6	15.4
R_{sym} (%)[b]	2.9 (18.5)	5.8 (12.8)	4.5 (10.1)	4.8 (11.5)	6.9 (27.1)	3.0 (7.4)	3.5 (13.7)	4.9 (12.2)

Refinement statistics

Data set	apo-SmtB	Zn_2 α5-SmtB	Zn_1 SmtB	Apo-CzrA	Zn_2 CzrA
Resolution (Å)	60–1.7	60–2.3	60–2.0	18.9–2.0	60–2.3
No. reflections used	21,874	8841	14,328	20,625	9215
Test set	2163	442	1458	2355	949
R_{cryst} (%)[c]	21.6	22.9	20.4	20.2	19.5
R_{free} (%)[c]	24.9	29.0	23.6	25.6	24.9
Average B-factor (Å^2)	66.3	35.5	53.7	33.8	37.6
No. of non-hydrogen atoms	1640	1569	1712	3216	1638
rmsd. bond length (Å)	0.004	0.028	0.005	0.022	0.005
rmsd. bond angle (deg.)	1.038	2.175	1.056	1.818	1.017

[a] Values in parentheses are for the highest-resolution shell.

[b] $R_{sym} = \Sigma_h \Sigma_i |I(h)I - \langle I(h) \rangle| / \Sigma_h \Sigma_i \langle I(h)_i \rangle$, where I is the observed intensity, and $\langle I \rangle$ is the average intensity of multiple observations of symmetry-related reflections.

[c] $R = \Sigma||F_o| - |F_c||/\Sigma|F_o|$. R_{cryst} and R_{free} were calculated using the working and the test reflection sets, respectively.

previously published structure of apo-SmtB (Cook *et al.*, 1998). Molecular replacement solutions were found using CNS (Brunger *et al.*, 1998) or programs from the CCP4 suite (Idea, 1994). Multi-wavelength anomalous dispersion (MAD) (Hendrickson *et al.*, 1990) using the Zn-edge of the derivative was used to solve the phase problem for Zn_2 α5-SmtB (see Table 3.1). The program SOLVE (Terwilliger and Berendzen, 1999) was used to locate the metal ion sites in the asymmetric unit. Refinement was carried out against the peak data set. Initial phases of all forms were improved by solvent flattening as implemented in DM (Cowtan, 1994), RESOLVE (Terwilliger, 2000) and CNS (Brunger *et al.*, 1998). The molecular coordinates were constructed using the computer program O (Jones *et al.*, 1991) and refined with CNS (Brunger *et al.*, 1998) or REFMAC (Murshudov *et al.*, 1999). Shake&wARP (Kantardjieff *et al.*, 2002) was used to minimize model bias.

NMR Spectroscopy. All NMR spectra were acquired on Varian Unity Inova 500- and 600-MHz spectrometers in the Biomolecular NMR Laboratory at Texas A&M University. Typical solution conditions were 0.6-2 mM ^{15}N- or ^{15}N/^{13}C-labeled protein, pH 6.0, 10 mM d_{18}-Hepes, 100 mM NaCl and 10% (v/v) D_2O, 40 ºC. Samples in >99.9% (v/v) D_2O were obtained by buffer exchange over a G-25 column (Sigma). Chemical shift referencing is relative to 2,2-dimethyl-2-silapentane-5-sulfonic acid (DSS) (Wishart *et al.*, 1995). All spectra were processed and analyzed using NMRPipe (Delaglio *et al.*, 1995) and Sparky 3 (Goddard and Kneller). ^{1}H-^{15}N HSQC spectra (Kay *et al.*, 1992) were recorded as 128* x 512* two-dimensional matrices in the t_1 and t_2 dimensions, respectively. The three-dimensional ^{15}N-separated NOESY spectrum

(Marion *et al.*, 1989) (τ_m=100 ms) was recorded as a 12* x 256* x 741* three-dimensional matrix with acquisition times of 49.4 ms (t_1, ^{15}N), 21.3 ms (t_2, ^1H), and 61.8 ms (t_3, $^1H^N$), at a decoupler offset positioned at 168 ppm. The 2D ^1H-^{15}N HMBC (Huyghues-Despointes *et al.*, 2003) spectrum of Zn_2 CzrA was acquired in ^2H_2O with the ^{15}N spectral width set to 70 ppm, centered at 195 ppm. The 2D [^{13}C,^1H]-TROSY-H(CDCG)CB experiment (Lohr *et al.*, 2002 Feb) was acquired in ^1H_2O at 40°C with a ^{13}C spectral width of 32.5 ppm centered on C^β resonances. Complete resonance assignments of apo- and Zn_2 CzrA will be reported elsewhere.

Samples for hydrogen-deuterium (H-D) exchange were prepared by exchanging protein samples into D_2O in 10 mM d_{18} Hepes, pH 6.0, 100 mM NaCl using a G-25 spin column equilibrated in the final NMR buffer in D_2O (Huyghues-Despointes *et al.*, 1999). The sample was placed immediately into the NMR spectrometer and ^{15}N-^1H HSQC spectra acquired continuously every 20-30 minutes over 11 h immediately following exchange and then at various exchange times (t_{ex}) for 5-6 weeks thereafter (apo-CzrA: t_{ex}=456 h and 575 h; Zn_2 CzrA: t_{ex}=35 h, 45 h, 100 h, 113 h, and 912 h). Cross-peak intensities of the ^{15}N-^1H HSQC spectra for each non-overlapping peak of apo- and Zn(II) CzrA were measured by volume integration using Sparky 3. Peak intensities were then fit to a single-exponential function, $A = A_0[e^{(-kt)}] + C$, where C is baseline noise of a particular sample (Huyghues-Despointes *et al.*, 1999; Huyghues-Despointes *et al.*, 2001).

Coordinates. The atomic coordinates for apo-SmtB, Zn_2 $\alpha5$ SmtB, apo-CzrA, Zn_2 CzrA and Zn_1 SmtB have been deposited in the Protein Data Bank, Research

Collaboratory for Structural Bioinformatics, Rutgers University, New Brunswick, NJ (http://www.rcsb.org/) under accession codes 1R1T, 1R22, 1R1U, 1R1V AND 1R23 respectively.

RESULTS

A metal-induced quaternary structural conformational change in Synechococcus SmtB. A ribbon representation of the structure of apo wild-type SmtB solved to higher resolution than previously (1.7 Å; see Table 3.1 for structure statistics) is shown in Fig. 3.1B. As expected (Cook *et al.*, 1998), the structure conforms to the "winged helix" class of homodimeric helix-turn-helix (α3-turn-αR) DNA binding proteins (Gajiwala and Burley, 2000). As previously found (Cook *et al.*, 1998), the first 20 or so N-terminal amino acids of both subunits, denoted the N-terminal "arm", are missing from the electron density maps, presumably because they are disordered. However, it is clear from this structure that the N-terminal arm of one subunit is close to the α3 helix of the other, suggesting that the previously characterized α3N Zn(II) in SmtB (Fig. 3.1A) (VanZile *et al.*, 2002b) site employs ligands drawn from both subunits.

Previous biochemical studies showed that apo-SmtB contained both α3N and α5 metal binding sites and that the occupancy and precise coordination environment of each depended on the nature of the metal ion (VanZile *et al.*, 2002b). Therefore, a triple-substitution mutant of SmtB was prepared in which all three cysteines (Cys14 in the N-terminal arm, Cys61 in the α3 helix, and Cys121 near the C-terminus; Fig. 3.1A) were converted to nonliganding serines, to create α5-SmtB. This mutant, like *S*-methylated SmtB (VanZile *et al.*, 2002a, b), retains the high binding affinity of the α5 metal ion, and strong negative regulation of *smt*O/P binding *in vitro*, but blocks metal binding to the α3N site (VanZile *et al.*, 2002b). Fig. 3.1C shows the global structural differences between apo-SmtB and fully zinc-liganded α5-SmtB, determined to 2.3 Å resolution, as depicted by a superposition of the α5 helices of one of the two protomers (the subunits on the *right*) within each dimer. Strikingly, the overall structural change induced by metal binding is exclusively quaternary structural in nature, well-described as a rigid-body rotation/translation of one subunit relative to the other. For example, in this superposition (Fig. 3.1C), the Ser74 Cα atom in the αR helix of the subunit shown on the *left* moves by 4.8 Å, or an average of ≈2.4 Å in each subunit within the dimer; this reduces the point-to-point distance between Ser74 Cα atoms on opposite subunits by 3.6 Å, from 51.7 to 48.1 Å. Thus, the homodimer becomes more globally compact on Zn(II) binding in qualitative agreement with previous sedimentation equilibrium experiments (Kar *et al.*, 1997); this results in significant movements of both the HTH motif and β-hairpin wings in opposite subunits relative to one another.

The two zinc ions are bound to the homodimer across the dimer interface in a symmetry-related pair of interhelical α5 metal binding sites that straddle the α5 helices, fully compatible with predictions made from the primary structure (Fig. 3.1D) (VanZile *et al.*, 2002b) as well as a preliminary analysis of a heavy atom derivative of apo-SmtB obtained from mercuric acetate soaks (Cook *et al.*, 1998). Both zinc chelates in Zn_2 α5-SmtB adopt distorted tetrahedral coordination geometries (ligand-Zn-ligand bond angles ranging from 89-124° with 109.5° perfect tetrahedral symmetry; averaged Zn-ligand bond lengths of 2.05-2.14 Å), with ligands donated by Asp104 Oδ1 and the His 106 Nδ1 atoms of one protomer, and His117' Nδ1 and Glu120' Oδ1 of the other. The metal chelate is largely pre-organized, with the exception of Glu120, which is in an "open" conformation in the absence of metal (in one protomer, electron density could not be traced beyond L118) and swings in to "close the gate" on the metal complex (Fig. 3.1D). Mutagenesis of His106 to a non-liganding Gln abolishes negative regulation of DNA-binding *in vitro* (VanZile *et al.*, 2002a) and when replaced by Arg, abrogates zinc-sensing *in vivo* (Turner *et al.*, 1996), revealing that this is in fact the functional zinc-sensing site in SmtB.

Crystallographic studies of S. aureus CzrA. A ribbon representation of the dimer of dimers of the related zinc sensor apo-CzrA found in the crystallographic asymmetric unit, solved to 2.0 Å resolution, is shown in Fig. 3.2A. The first 8 N-terminal residues and C-terminal 3-5 amino acids are not visible in the electron density maps. Chemical shift indexing (Busenlehner *et al.*, 2003) reveal that these N-terminal and C-terminal regions are disordered in solution as well. In contrast to the extensive interface formed by the N-terminal α1 and C-terminal α5 helices on opposite subunits within the dimer, the interdimer interface is filled with H_2O molecules with contacts largely limited to the turn connecting the α3 and α4 helices and the N-terminal end of the α4 helix (primarily residues Asn50, Ser54 and Gln55) in the HTH motif. This is likely a crystal packing interface since sedimentation equilibrium experiments show no evidence of self-

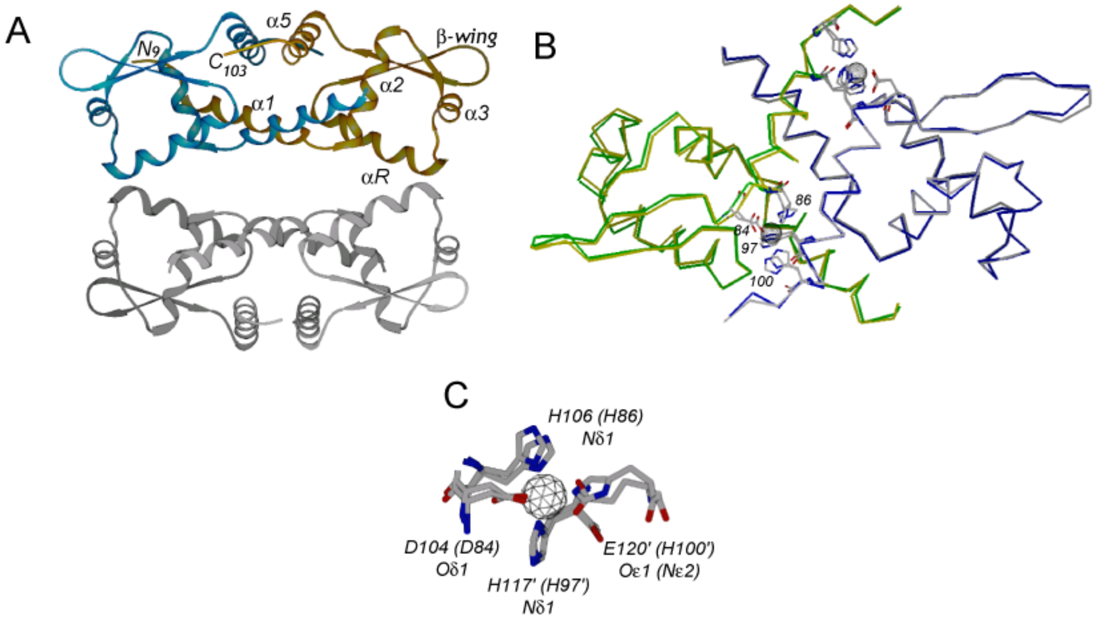
A
N9
C103
α5
β-wing
α1
α2
α3
αR
B
86
84
97
100
C
H106 (H86)
Nδ1
D104 (D84)
Oδ1
H117' (H97')
Nδ1
E120' (H100')
Oε1 (Nε2)

Figure 3.2. Structure of *S. aureus* CzrA. **(A.)** Ribbon representation of the structure of apo-CzrA solved to 2.0 Å resolution with all four subunits of the asymmetric unit shown. The secondary structural units for the *orange* subunit are shown. **(B.)** Global C^{α} trace subunit-based superposition of apo-CzrA with Zn_2 CzrA, the latter solved to 2.3 Å resolution. **(C.)** Representative structure of the zinc coordination chelate of Zn_2 α5-SmtB superimposed on that derived from Zn_2 CzrA.

association beyond the dimer (Pennella *et al.*, 2003). As expected from previous NMR studies the secondary $\alpha\alpha\alpha\alpha\beta\beta\alpha$ and tertiary structures of apo-CzrA are identical to that of apo-SmtB (Fig. 3.1B and 3.2A) (Busenlehner *et al.*, 2003). The major difference between the crystallographic dimeric structures of apo-SmtB and apo-CzrA is that apo-CzrA is more compact than either apo- or Zn_2 $\alpha5$-SmtB. For example, the point-to-point distance between Ser54 C^{α} atoms in the αR helices on opposite subunits in apo-CzrA (Ser54 is analogous to Ser74 in SmtB; see Fig. 3.1A) is 43.8 Å, nearly 8 Å smaller than in apo-SmtB.

A global superposition of the structures of apo- and Zn_2 CzrA, the latter solved to 2.3 Å resolution, shown as a protomer C^{α} superposition (Fig. 3.2B), reveals that in contrast to SmtB (Fig. 3.1C), the global quaternary structural change upon metal binding in CzrA is small, with the intersubunit Ser54 C^{α} distance decreasing by only 0.5 Å. This may be due in part to crystal packing forces since both Zn_2 vs. apo-CzrA crystal lattices (*vide supra*) are stabilized by a similar set of interdimer interactions mediated by the $\alpha3$-turn-$\alpha4$ HTH motif. In apo-CzrA these interdimer contacts may significantly alter the relative orientation of one subunit relative to the other in this dissociable homodimer (K_{dimer}=1.7x10^5 M^{-1}) (Pennella *et al.*, 2003). In the case of Zn_2 CzrA, a zinc ion is bound between Ser52 (3.7-3.8 Å) and Asn55 (3.3 Å) bridging two molecules related by crystallographic symmetry (data not shown). In addition, a second metal ion appears to bridge the *bona fide* $\alpha5$-metal binding sites mediating a second interdimer contact via a distorted square pyramidal coordination sphere, the base of which is formed by His86 $N^{\varepsilon2}$, His96 $N^{\varepsilon2}$, His96'' $N^{\varepsilon2}$ (from another dimer), and a water molecule, with the apical position of the pyramid donated by His86'' $N^{\varepsilon 2}$. Since there is no evidence for additional metal ion binding beyond two per dimeric CzrA in solution (Pennella *et al.*, 2003), these additional metal ions bound by the $\alpha 4$ and $\alpha 5$ helices of Zn_2 CzrA are likely crystallographic artifacts that play no role *in vivo* and may have been facilitated by the high pH of these particular crystals (Table 3.1).

Despite these additional interdimer contacts, the coordination structure of the $\alpha 5$ chelate in CzrA is virtually superimposable on that of SmtB (Fig. 3.2C), with the $N^{\varepsilon 2}$ atom of His100 donating the fourth ligand in CzrA, rather than the carboxylate oxygen of Glu120 in SmtB, as anticipated from the sequence alignment (Fig. 3.1A). In Zn_2 CzrA, Zn(II)-ligand coordination bond lengths range from 1.8-2.1 Å, typical for tetrahedral Zn coordination to N/O atoms. The coordination geometry is less distorted than in Zn_2 $\alpha 5$-SmtB since ligand-Zn-ligand bond angles cluster more closely around 109.5° (the range is 102-112°), with the exception of the H86 $N^{\delta 1}$-Zn(II)-H97 $N^{\delta 1}$ angle which is 128°.

A metal-ligand mediated cross-subunit hydrogen bonding network links the metal and DNA-binding sites. A detailed analysis of the crystallographic structures of apo- and Zn_2 SmtB suggests that His117 plays a critical role in establishing an intersubunit hydrogen bonding network that may be important for allostery (Fig. 3.3). This network originates with the non-liganding $N^{\varepsilon 2}$ atom of this His, and extends, via just two hydrogen bonds, the full distance to the DNA-binding αR helix via the αR-$\beta 1$ loop (Fig. 3.3A). In Zn_2 SmtB, but not in the apoprotein, this His forms a short, linear $N^{\varepsilon 2}$-$H^{\varepsilon 2}$•••O=C Arg87' side-chain to main-chain hydrogen bond ($d_{N\text{-}O}$=2.67 Å vs. 3.6 Å in

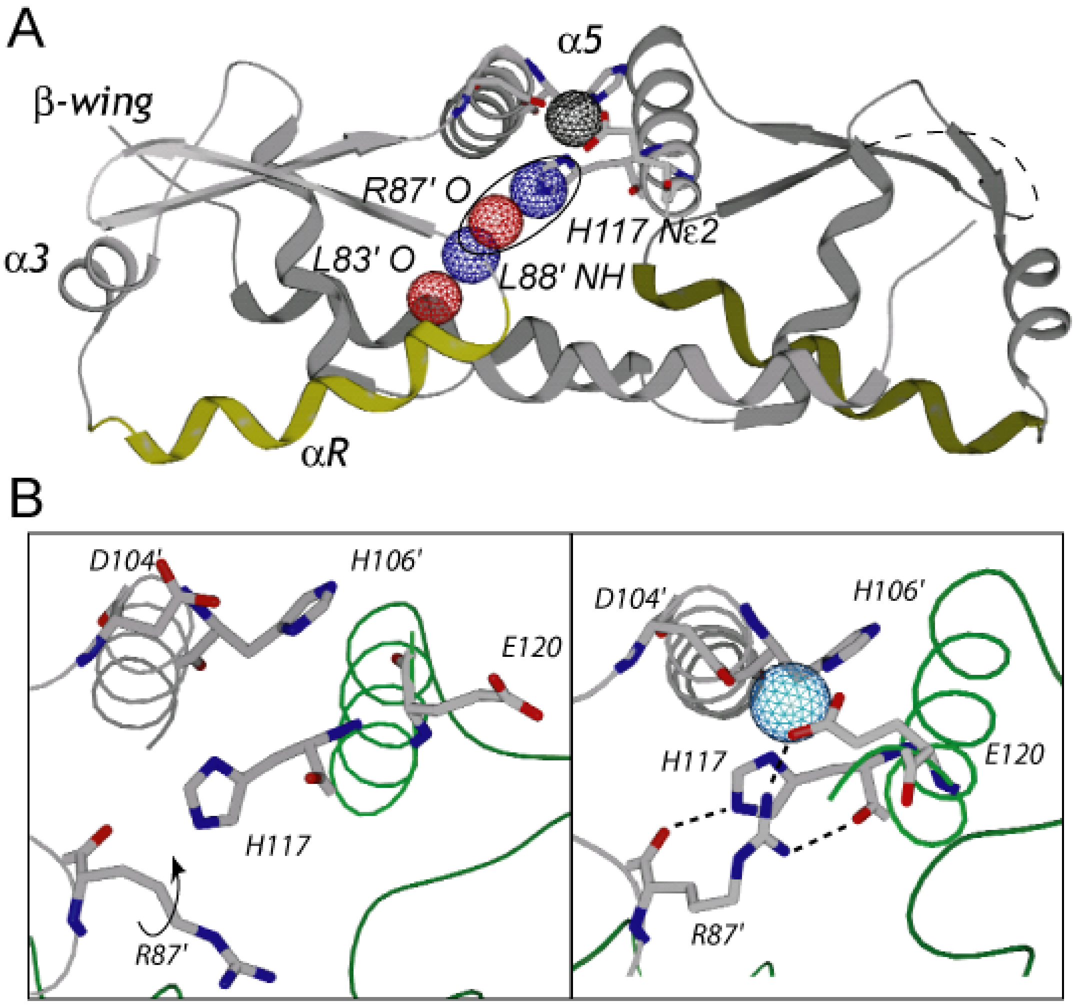
A
α5
β-wing
R87' O
α3
L83' O
H117 Nε2
L88' NH
αR
B
D104'
H106'
E120
H117
R87'
D104'
H106'
H117
E120
R87'

Figure 3.3. An intersubunit hydrogen-bonding network in $\mathrm{Zn_2}$ α5-SmtB involved in allosteric coupling of Zn and DNA binding sites. **(A.)** Schematic of the intersubunit hydrogen-bonding network that links the allosteric α5 zinc binding sites to the DNA-binding αR helices (shaded *yellow*) in $\mathrm{Zn_2}$ α5-SmtB. Only one of the coordination chelates is shown (the zinc ion is indicated as a *black* sphere). The critical intersubunit His117 Nε2-Hε2•••O=C Arg87' hydrogen bond is encircled. **(B.)** Another view of structural changes that occur upon Zn(II) binding to the α5 metal sites of SmtB. *Left* panel, apo-SmtB; *right* panel, $\mathrm{Zn_2}$ α5-SmtB. Only one of the two metal chelates is shown.

the apo-SmtB structure) across the subunit interface of both protomers. The immediately adjacent amide group of Leu88' then forms a short backbone N-H•••O=C Leu63' hydrogen bond ($d_{\text{N-O}}$=2.95 Å) to the carbonyl oxygen of Leu83', an unsatisfied α-helical hydrogen bond acceptor near the C-terminus of the DNA binding αR helix. Furthermore, on at least one side of the homodimer, the side chain of Arg87' interacts intimately with the metal chelate, with the guanidino group moving into hydrogen-bonding distance of both the backbone carbonyl oxygen of His117 and the nonliganding $O^{\varepsilon 2}$ atom of Glu120 upon formation of the zinc complex (Fig. 3.3B). A comprehensive sequence alignment reveals that only α5 zinc sensors like SmtB and CzrA universally conserve a basic Arg/Lys/His residue in the position corresponding to Arg87 in the αR-β1 loop of SmtB (Busenlehner *et al.*, 2003). We hypothesize that these reciprocal main-chain and side-chain hydrogen bonding interactions functionally link the α5 and αR helices of opposite protomers and play a significant role in allosteric coupling of the metal and DNA binding sites in SmtB.

Since the crystallographic structures of apo- and Zn_2 CzrA are more similar than different (the average N-O distance for the analogous His97 $N^{\varepsilon 2}$-$H^{\varepsilon 2}$•••O=C His67' interaction in CzrA decreases by just 0.1 Å on zinc binding, from 2.9 to 2.8 Å) (Fig. 3.2B), insight into changes in conformation and dynamics induced upon Zn(II) binding to apo-CzrA in solution was sought. A high resolution NMR perturbation map, in which changes in backbone ^{1}HN and ^{15}N amide frequencies that occur upon Zn(II) binding to apo-CzrA are color-coded on the ribbon representation of the structure, with the thickness of the worm also scaling with increased perturbation (Fig. 3.4A). Large

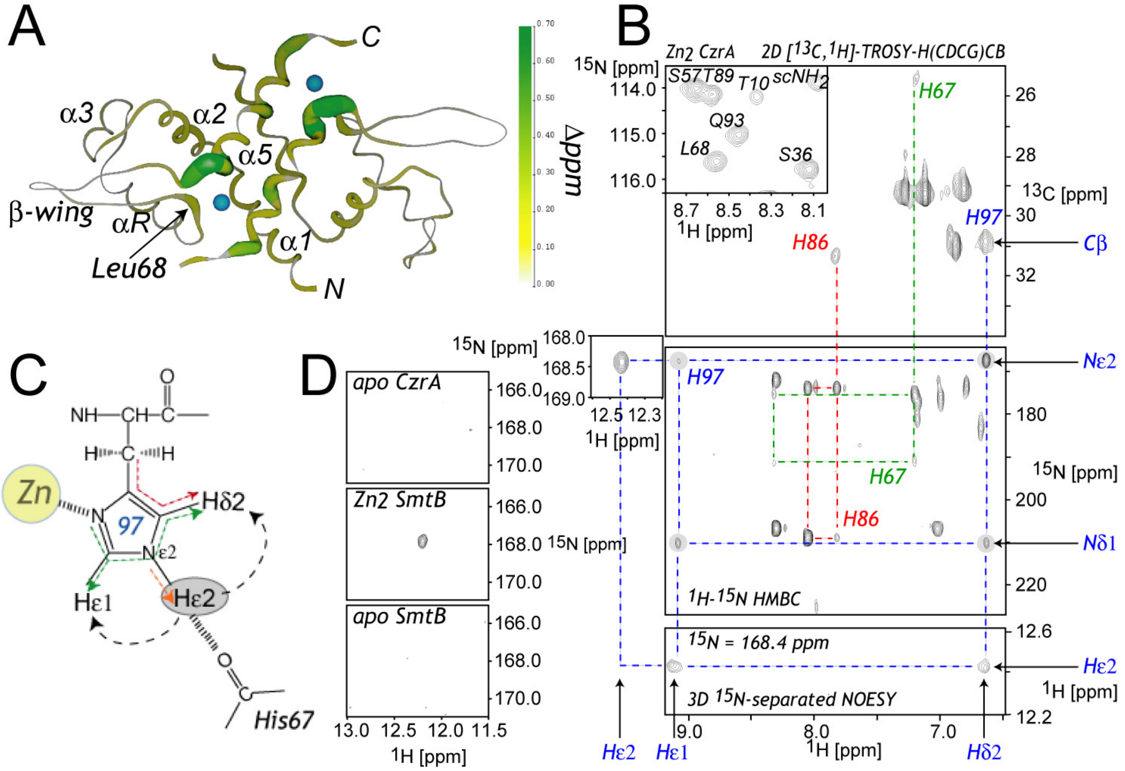

Figure 3.4. NMR evidence in support of a metal-ligand mediated hydrogen-bonding network in Zn_2 CzrA in solution. **(A.)** Structural representation of the NMR chemical shift perturbation map of CzrA which reflects changes in ^{1}H and ^{15}N chemical shift induced upon zinc binding to the α5 metal sites in solution, where $\Delta ppm=\sqrt{(\Delta\delta_H{}^2 + (\Delta\delta_N/7)^2)}$(Wishart and Sykes, 1994). In each case, the ribbon is color-coded and ramped from white (0.00), through yellow to green (0.70) according to the magnitude of Δppm, with yellow set at the mean perturbation value for all amide groups (Δppm=0.127), and green reflecting large changes (Δppm≥0.35) in chemical shift of amide ^{1}H and ^{15}N resonances (see Materials and Methods). The worm diameter thickness also reflects these changes, going from thin to thick, indicative of small to large values in Δppm. **(B.)** Complete side chain assignment for His97 in Zn_2 CzrA, revealing an unambiguous assignment of the $N^{\varepsilon2}$-$H^{\varepsilon2}$ correlation of His97 observed in ^{1}H-^{15}N HSQC spectrum (*far left*), obtained by linking the 2D [^{13}C,^{1}H]-TROSY-H(CDCG)CB (Lohr *et al.*, 2002 Feb) ^{13}Cβ-$^1H^{\delta2}$ correlation (*top*) to the remainder of the His97 side chain via an ^{1}H-^{15}N HMBC (*middle*) and 3D ^{15}N-separated NOESY spectra (^{15}N=168.4 ppm) (*bottom*). A portion of the full ^{1}H-^{15}N HSQC spectrum is also shown (*inset, top panel*). **(C.)** Chemical structure of His97, showing the scalar correlations indicated in *panel B*. The dashed *red* line links the $^{13}C^{\beta}$ and $^1H^{\delta2}$ nuclei in the 2D [^{13}C,^{1}H]-TROSY-H(CDCG)CB spectrum, the dashed *green* lines link the non-exchangeable ^{1}H and ^{15}N nuclei identified in the ^{1}H-^{15}N HMBC spectrum, the *orange* dashed line identifies the nuclei correlated in the ^{1}H-^{15}N HSQC spectrum, while the *black* dashed lines correspond to the crosspeaks observed in the 3D ^{15}N-separated NOESY spectrum. **(D.)** The same His97 $N^{\varepsilon2}$-$H^{\varepsilon2}$ correlation is *not* observed in ^{1}H-^{15}N HSQC spectrum of apo CzrA acquired under the same solution conditions (*top* panel) or apo-SmtB (*bottom* panel), but is present in Zn_2 α5-SmtB (*middle* panel).

perturbations (Δppm$\geq$0.35 ppm) are generally localized to the immediate vicinity of the bound metal ion in the N- and C-termini of both α5 helices, with a notable exception being the amide group of Leu68 in the αR-β1 loop, analogous to Leu88 in SmtB (*vide supra*). Formation of a hydrogen bonding network in CzrA structurally analogous to that determined for SmtB (Fig. 3.3) makes the prediction that in solution, the His97 $H^{\varepsilon 2}$ proton of CzrA would exchange slowly with solvent and therefore should be visible in an ^{1}H-^{15}N HSQC spectrum. This is indeed the case under our standard NMR solution conditions (40 ºC, pH 6.0) (Fig. 3.4B-C), but *only* in the Zn_2 conformation ($^{1}H^{\varepsilon 2}$ δ=12.4 ppm; $^{15}N^{\varepsilon 2}$ δ=168.4 ppm) (Fig. 3.4D). The same is true of the corresponding His117 $H^{\varepsilon 2}$ proton in Zn_2 α5-SmtB ($^{1}H^{\varepsilon 2}$ δ=12.2 ppm; $^{15}N^{\varepsilon 2}$ δ=167.9 ppm) (Fig. 3.4D).

In addition, if the amide group of Leu68 in the αR-β1 loop in CzrA donates a hydrogen bond propagating this hydrogen-bonding network in solution, the main-chain amide hydrogen-deuterium (H-D) exchange rates of both Leu68 and Leu63 would be expected to be among the slowest in the CzrA, but again, only in the Zn_2 form. Although the exchange rate of Leu63 in the Zn_2 conformation could not be obtained due to spectral overlap, the k_{ex} for Leu68 NH is reduced by 30-fold (0.77 to 0.024 h^{-1}) on zinc binding. Strikingly, the H-D exchange rates of not only Leu68 in the αR-β1 loop, but nearly all of the buried hydrogen-bonding amide protons in the core of α-helices α1, α2, αR and α5, as well as those at the base of the β-hairpin wing, uniformly decrease substantially ($\geq$20-fold) in the Zn_2 vs. apo forms of the homodimer (Fig. 3.5). A striking exception to this is the β-hairpin wings, whose exchange rates remain rapid in both

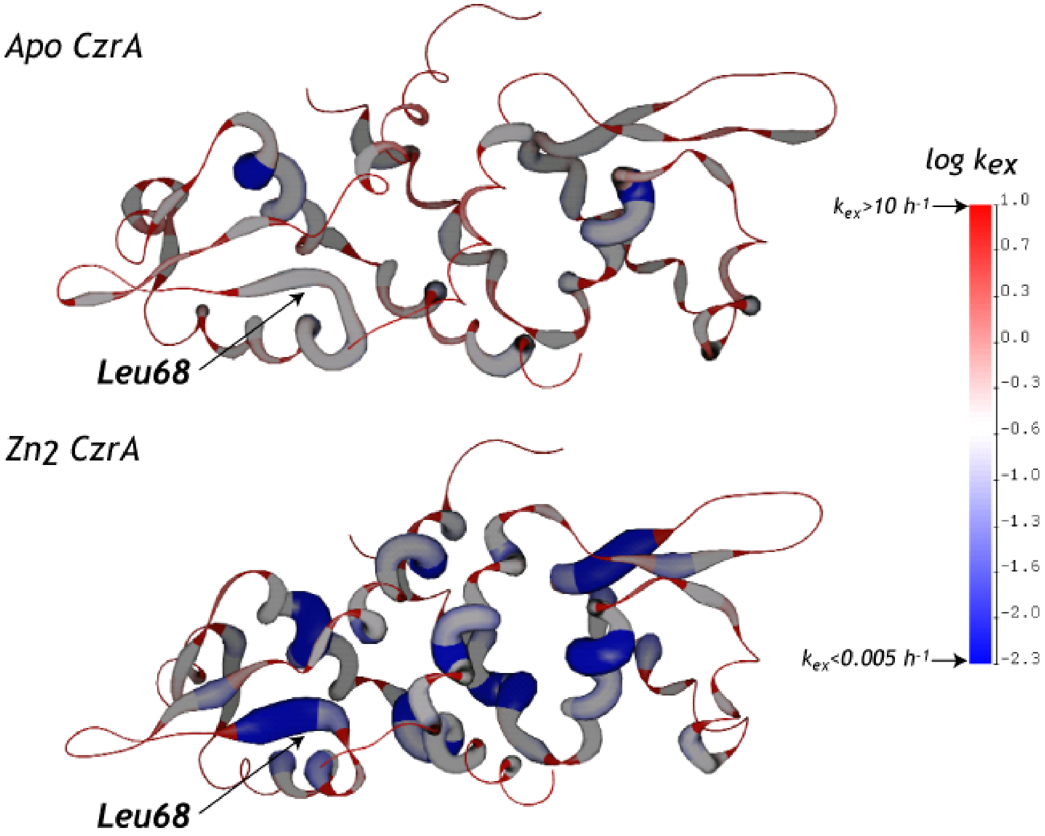
Apo CzrA
Leu68
Zn2 CzrA
Leu68
log kex
kex>10 h-1
kex<0.005 h-1
1.0
0.7
0.3
0.0
-0.3
-0.6
-1.0
-1.3
-1.6
-2.0
-2.3

Figure 3.5. Main-chain amide hydrogen-deuterium exchange rates of apoCzrA and Zn_2 CzrA. Zinc binding induces a dramatic dampening of the internal dynamics of CzrA. Ribbon representation of the raw H-D exchange rates (k_{ex}) of all resolvable amide protons in apo (*top*) vs. Zn_2 (*bottom*) CzrA (pH 6.0, 0.1 M NaCl, 40 ºC). Those amide groups for which $k_{ex} \geq 10\ h^{-1}$ or $\leq 0.005\ h^{-1}$ were assigned the lower and upper limits of 10 h^{-1} or 0.005 h^{-1} for illustration purposes. The ribbon is color-coded from red to blue, with *red* indicative of fast exchange (no protection from exchange with solvent) and *blue* indicative of slow exchange (see scale, *right*). The width of the ribbon is also made to reflect the absolute exchange rate, with fast exchange thin and slow exchange, thick.

conformations. These same trends in internal dynamics in solution mirror the crystallographic temperature factors for both forms of CzrA, with mobilities within the core of Zn$_2$ CzrA strongly dampened, again with the exception of the β-wings, which become even more highly mobile on Zn(II) binding (data not shown). Note that in the structure of Zn$_2$ α5-SmtB (Fig. 3.1C), the polypeptide chain of one of the β-hairpin wings within the homodimer could not be traced, indicative of considerable disorder in the crystal in this region.

Both α5 Zn(II) sites in SmtB must be filled to drive the quaternary structural switch. The crystallographic structure of Zn$_1$ wild-type SmtB, solved to 2.0 Å resolution, where just one of the α5 zinc binding sites was occupied by metal ion, was also obtained (Fig. 3.6A). The empty site on the homodimer is easily distinguished from the filled site in this structure due to the distinct conformations of the Glu120 "gating" residue (Fig. 3.6B). Strikingly, the quaternary structure of Zn$_1$ SmtB is essentially superimposable on that of apo-SmtB, with the aforementioned hydrogen-bonding network clearly not established on *either* side of the homodimer. Consistent with this, the intersubunit distance between the αR Ser74 C$^{\alpha}$ atoms is 51.3 Å, very close to the 51.7 Å found for apo-SmtB. Interestingly, the metal chelate appears only partially formed, with very long coordination bonds to both His106 (2.55 Å) and His117' (2.57 Å) in this complex (Fig. 3.6B), relative to Zn$_2$ SmtB ($d_{\text{Zn-H106}\delta 1}$=2.08 Å; $d_{\text{Zn-H117'N}\delta 1}$=2.05 Å). These results suggest that both α5 metal binding sites must be loaded in order to drive a concerted quaternary structural conformational transition. This finding makes the prediction that zinc binding to the α5 metal sites of the CzrA or SmtB homodimer

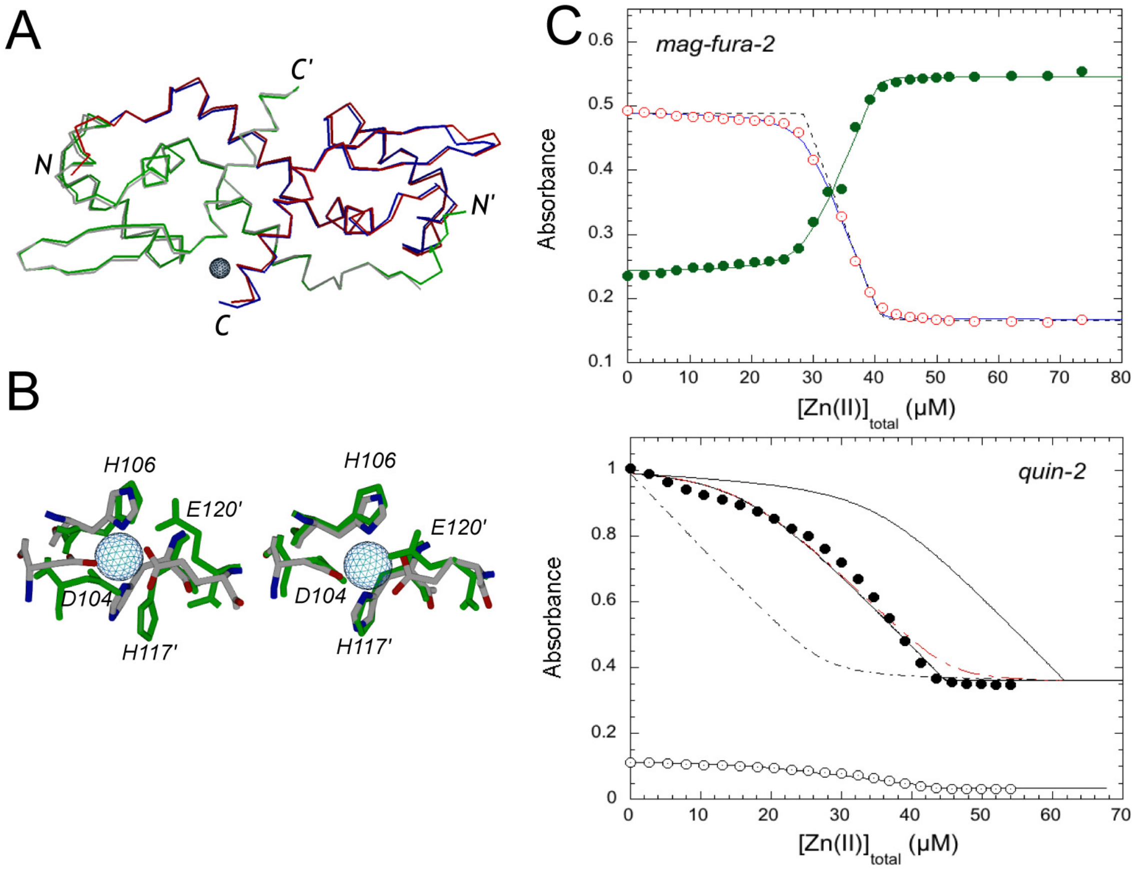

Figure 3.6. Structure of Zn$_1$ SmtB and zinc binding properties of CzrA. **(A.)** Monomer superposition of the structures of Zn$_1$ SmtB with apo-SmtB, depicted as a C$^\alpha$ trace; the position of the single metal ion is shown as a blue sphere. **(B.)** Superposition of the empty (*left*) and filled (*right*) zinc sites in Zn$_1$ SmtB (shaded *green*) compared to that of the two filled sites in Zn$_2$ α5-SmtB. Note that the coordination bond lengths to His106 and His117 are significantly longer in the Zn$_1$ SmtB structure (see text). **(C.)** Binding of Zn(II) to apo-CzrA as monitored by chelator competition assays with mag-fura-2(VanZile *et al.*, 2000) (*top*) and quin-2(VanZile *et al.*, 2002b) (*bottom*). *Top panel*: The solid line is a simultaneous nonlinear least squares fit of the changes in absorbance measured at 365 nm (○) and 325 nm (●) to an independent site metal binding model, and where K=4.2 (±0.9) x10^9 M^{-1}. The dashed curved is a simulation with K=5.1x10^{12} M^{-1} (see below), shown for comparison. [Mag-fura-2]=12.3 μM; [apo-CzrA]=28 μM monomer. *Bottom panel*: The solid line represents a simultaneous nonlinear least squares fit of the changes in absorbance measured at 366 nm (○) and 265 nm (●) to a two-step metal binding-nondissociable dimer model, where K_1 and K_2 are the step-wise zinc binding affinities and $K_1 >> K_2$. Here, K_1=5.1 (±2.1) x10^{12} M^{-1}, and $K_2 \leq 10^9$ M^{-1}. Other simulated curves are shown for comparison: *solid curve to right*, $K_1 = K_2$ = 5.1 (±2.1) x10^{12} M^{-1}; *red dashed* curve, K_1=5.1 (±2.1) x10^{12} M^{-1}, K_2=4.2 x10^9 M^{-1} (K derived from the mag-fura-2 titration, *top panel*); *black dot-dashed* curve, $K_1 = K_2$ = 4.2 x10^9 M^{-1}. [Quin-2]=28 μM ; [apo-CzrA]=17 μM dimer (34 μM monomer). The data reveal that the apo-CzrA homodimer binds two Zn(II) ions with strong negative cooperativity since $K_1 >> K_2$ (see text for details).

might be negatively cooperative (stepwise metal association equilibrium constants, K_i, where $K_1 > K_2$), since some of the free energy of binding to the second site (ΔG_2) must be used to drive the quaternary structural change in conformation and/or dynamics. This is what is found for apo-CzrA (Fig. 3.6C). A quantitative analysis of metal binding affinities using two fluorescent-chelator competition assays (VanZile *et al.*, 2000; VanZile *et al.*, 2002b) reveals that Zn(II) binding to apo-CzrA is extremely tight at equilibrium (25 ºC, 0.1 M NaCl, pH 7.0), and strongly negatively cooperative, with $K_1 = 5.1 \times 10^{12}$ M^{-1}, with upper and lower limits only obtainable for K_2 (10^9 $M^{-1} \leq K_2 \leq 10^{10}$ M^{-1} (Fig. 3.6C)).

DISCUSSION

The x-ray crystallographic and NMR studies reported here provide new molecular level insight into the mechanism of negative allosteric regulation of operator/promoter binding by evolutionarily related zinc-sensing metalloregulatory transcriptional repressors. Utilization of both $N^{\delta 1}$ and $N^{\varepsilon 2}$ faces of a critical liganding histidine residue (His97 in CzrA; His117 in SmtB) drive a quaternary structural switch in the global conformation and/or internal dynamics of the repressor thereby stabilizing a low-DNA binding affinity conformation. In the case of SmtB, Zn(II) induces a quaternary structural compaction of the homodimer which spatially alters the positions of the putative DNA recognition (αR) helices relative to one another (Fig. 3.1C). In the case of CzrA, Zn(II) binding simply functions to globally "freeze out" the internal dynamics of the dimer (Fig. 3.5), such that the high-affinity operator/promoter-binding conformation is not energetically accessible to the repressor. In contrast, both apoproteins maintain a substantial degree of global quaternary structural flexibility that may help maximize the affinity of the repressor for various specific DNA binding sites.

Utilization of both sides of a key imidazole metal ligand ensures that formation of the α5 metal-sensing coordination chelate is directly coupled to formation of the hydrogen-bonding network that links the allosteric inducer site to the DNA-binding αR helices some 15 Å away. Characterization of CzrA substitution mutants in which His97 is replaced with either a non-liganding but hydrogen bonding asparagine (H97N CzrA) vs. a potentially metal liganding but poorly hydrogen bond donating carboxylate group (H97D) will provide a critical test of the proposed allosteric model. Consistent with our expectations, H97N CzrA maintains high affinity, wild-type operator/promoter binding activity *in vitro*, but is completely unresponsive to metal ions (M. Pennella and D. Giedroc, unpublished observations). Efforts are currently underway to determine how this coupling network has been modified to require six metal coordination bonds in the specific Ni-sensing site in *M. tuberculosis* NmtR (Cavet *et al.*, 2002), rather than four in CzrA/SmtB, since the same set of four α5 metal ligands are proposed to be common to both CzrA and NmtR metal chelates (Cavet *et al.*, 2002; Pennella *et al.*, 2003). In addition, Cd and Pb binding to *S. aureus* CadC results in negative regulation of DNA binding via the α3N site in that sensor (Busenlehner *et al.*, 2002b), despite maintaining a high affinity α5 Zn site. This requires either a key interruption in the flow of communication from the α5 metal sensing sites to the DNA binding helices beyond the first shell of the metal ligands, and/or evolution of another pathway(s) of allosteric coupling in these homologous SmtB/ArsR sensors.

CHAPTER IV

FUNCTIONAL ROLES OF INDIVIDUAL ZINC LIGANDS IN MEDIATING ALLOSTERIC REGULATION OF DNA BINDING IN *S. aureus* CzrA

INTRODUCTION

Bacteria respond to stress by inducing the expression of resistant genes that encode proteins that mediate the response to a change in their environment. In some cases, proteins play roles in protecting bacteria from chemical toxicity of antibiotics or thermal stress (Mager and De Kruijff, 1995). The cellular response to metal toxicity in bacteria is mediated by the expression of genes that encode proteins specifically in metal export and/or storage (Finney and O'Halloran, 2003; O'Halloran, 1993). Although numerous metal ions play essential roles in biology, even these metal ions can adversely affect viability if the intracellular concentration rises above some physiological level. The expression of these metal resistance systems is regulated at the level of transcription by metal-sensing proteins (Brown *et al.*, 2003; Busenlehner *et al.*, 2003; Hantke, 2001b, 2002; van Vliet *et al.*, 2004). For example, the ArsR/SmtB family of prokaryotic metal-responsive transcriptional repressors, regulates the expression of genes involved with metal ion efflux and sequestration (Busenlehner *et al.*, 2003; Morby *et al.*, 1993; Shi *et al.*, 1994; Wu and Rosen, 1993).

Staphylococcus aureus CzrA is a member of the ArsR/SmtB family of homodimeric helix-turn-helix proteins. CzrA regulates the expression of the *czr* operon, which is involved in the resistance of *S. aureus* to zinc toxicity (Chapter II) (Kuroda *et al.*, 1999; Pennella *et al.*, 2003; Singh *et al.*, 1999; Xiong and Jayaswal, 1998). The *czr* operon encodes two convergently transcribed genes, *czrA* and *czr*B. CzrB is a member of the cation diffusion facilitator family of antiporters (Anton *et al.*, 2004; Grass *et al.*, 2001) that effluxes zinc ions from the cytoplasm. CzrA represses the transcription of *czrA* and *czrB* in the absence of metals and *czrAB* gene expression in the presence of zinc is de-repressed (Kuroda *et al.*, 1999; Singh *et al.*, 1999; Xiong and Jayaswal, 1998).

Previous studies reveal that three pairs of structurally distinct metal-sensing sites have evolved in this family of transcriptional repressors. These sites are named for the known or proposed secondary structures that provide ligands to the metal ion. The α3N site is predominantly composed of cysteines that preferentially coordinate larger, thiophilic metals including Bi(III), Cd(II), and Pb(II), as well as Zn(II) and Cu(I) in some cases, with the paradigm CadC, encoded on the plasmid pI258 in *S. aureus* (Busenlehner *et al.*, 2003; Liu *et al.*, 2004; Yoon *et al.*, 1991). The α4R site is also a cysteine rich site that preferentially binds Cd(II) and Pb(II). The α5 site contains imidazole- and carboxylate-containing ligands found near the C-terminus of certain members of this protein family and preferentially coordinates smaller, harder metals including Co(II), Ni(II), and Zn(II) (See Figure 4.1) (Chapter II) (Pennella *et al.*, 2003; VanZile *et al.*, 2002a, b). Previous studies on the zinc sensor CzrA and the nickel sensor NmtR from *M. tuberculosis* revealed that a difference in the coordination number in the α5 metal binding site is a primary determinant for metal selectivity between these two proteins (four ligands – Zn(II)/Co(II) CzrA; six ligands Ni(II)/Co(II)-NmtR (Chapter II)

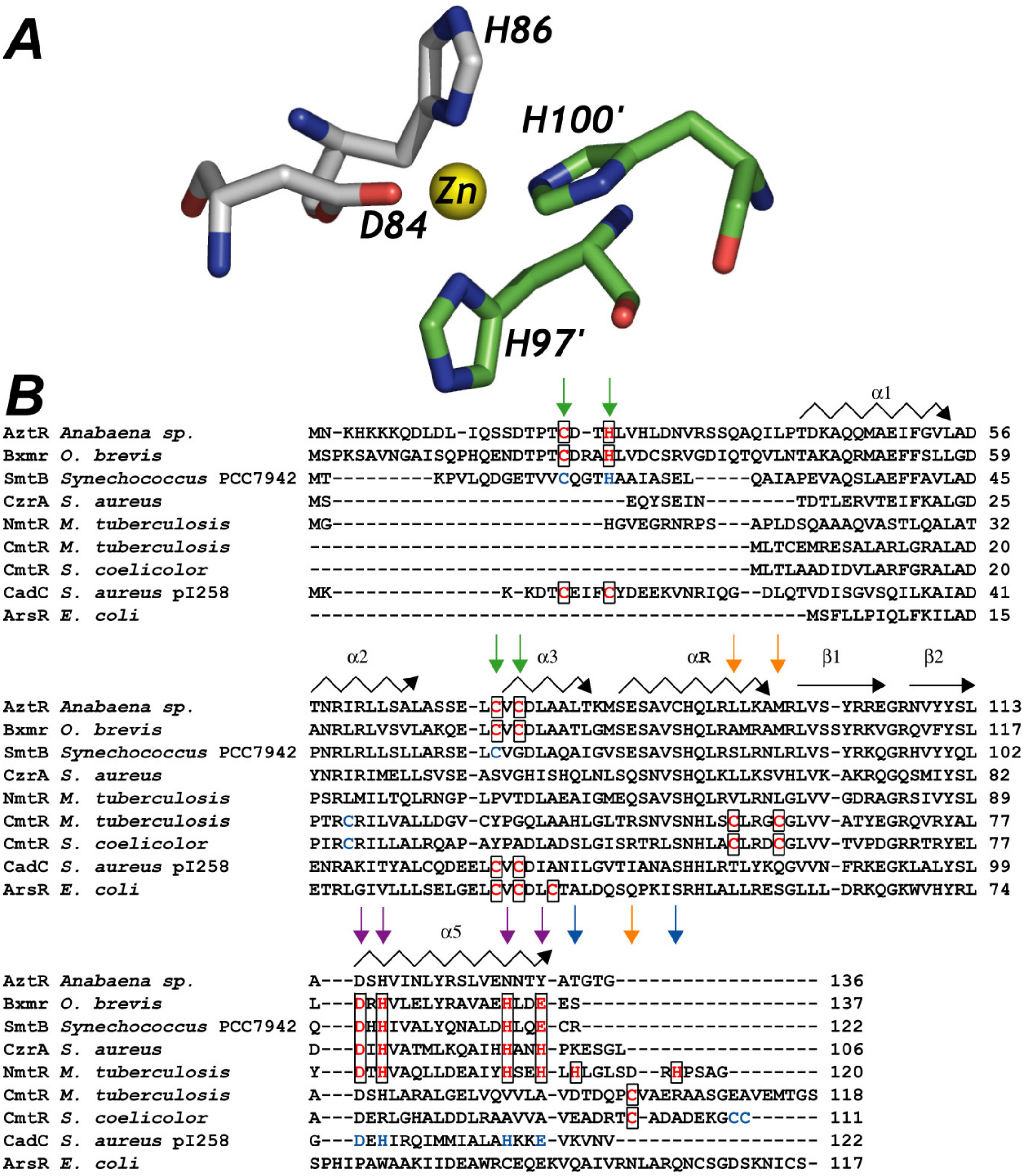

```
AztR Anabaena sp.            MN-KHKKKQDLDL-IQSSDTPTCD-THLVHLDNVRSSQAQILPTDKAQQMAEIFGVLAD 56
Bxmr O. brevis               MSPKSAVNGAISQPHQENDTPTCDRAHLVDCSRVGDIQTQVLNTAKAQRMAEFFSLLGD 59
SmtB Synechococcus PCC7942   MT---------KPVLQDGETVVCQGTHAAIASEL-----QAIAPEVAQSLAEFFAVLAD 45
CzrA S. aureus               MS-------------------------EQYSEIN--------TDTLERVTEIFKALGD 25
NmtR M. tuberculosis          MG-----------------------HGVEGRNRPS---APLDSQAAAQVASTLQALAT 32
CmtR M. tuberculosis         ----------------------------------------MLTCEMRESALARLGRALAD 20
CmtR S. coelicolor           ----------------------------------------MLTLAADIDVLARFGRALAD 20
CadC S. aureus pI258         MK---------------K-KDTCEIFCYDEEKVNRIQG--DLQTVDISGVSQILKAIAD 41
ArsR E. coli                 ---------------------------------------------MSFLLPIQLFKILAD 15

AztR Anabaena sp.            TNRIRLLSALASSE-LCVCDLAALTKMSESAVCHQLRLLKAMRLVS-YRREGRNVYYSL 113
Bxmr O. brevis               ANRLRLVSVLAKQE-LCVCDLAATLGMSESAVSHQLRAMRAMRLVSSYRKVGRQVFYSL 117
SmtB Synechococcus PCC7942   PNRLRLLSLLARSE-LCVGDLAQAIGVSESAVSHQLRSLRNLRLVS-YRKQGRHVYYQL 102
CzrA S. aureus               YNRIRIMELLSVSE-ASVGHISHQLNLSQSNVSHQLKLLKSVHLVK-AKRQGQSMIYSL 82
NmtR M. tuberculosis          PSRLMILTQLRNGP-LPVTDLAEAIGMEQSAVSHQLRVLRNLGLVV-GDRAGRSIVYSL 89
CmtR M. tuberculosis         PTRCRILVALLDGV-CYPGQLAAHLGLTRSNVSNHLSCLRGCGLVV-ATYEGRQVRYAL 77
CmtR S. coelicolor           PIRCRILLALRQAP-AYPADLADSLGISRTRLSNHLACLRDCGLVV-TVPDGRRTRYEL 77
CadC S. aureus pI258         ENRAKITYALCQDEELCVCDIANILGVTIANASHHLRTLYKQGVVN-FRKEGKLALYSL 99
ArsR E. coli                 ETRLGIVLLLSELGELCVCDLCTALDQSQPKISRHLALLRESGLLL-DRKQGKWVHYRL 74

AztR Anabaena sp.            A---DSHVINLYRSLVENNTY-ATGTG------------------ 136
Bxmr O. brevis               L---DRHVLELYRAVAEHLDE-ES--------------------- 137
SmtB Synechococcus PCC7942   Q---DHHIVALYQNALDHLQE-CR--------------------- 122
CzrA S. aureus               D---DIHVATMLKQAIHHANH-PKESGL----------------- 106
NmtR M. tuberculosis          Y---DTHVAQLLDEAIYHSEH-LHLGLSD--RHPSAG-------- 120
CmtR M. tuberculosis         A---DSHLARALGELVQVVLA-VDTDQPCVAERAASGEAVEMTGS 118
CmtR S. coelicolor           A---DERLGHALDDLRAAVVA-VEADRTC-ADADEKGCC------ 111
CadC S. aureus pI258         G---DEHIRQIMMIALAHKKE-VKVNV------------------ 122
ArsR E. coli                 SPHIPAWAAKIIDEAWRCEQEKVQAIVRNLARQNCSGDSKNICS- 117
```

Figure 4.1. Sequence alignment of members from the SmtB/ArsR family. **(A.)** Shows a representation of the coordination chelate of CzrA with carbon atoms from D84 and H86 from one protomer colored in white while from the other protomer carbon atoms from H97' and H100' are colored green. Yellow sphere represents a zinc ion. **(B.)** Multiple sequence alignment of several functionally characterized SmtB/ArsR proteins generated by ClustalW (Thompson *et al.*, 1997): *Anabaena sp.* AztR, *O. brevis* BxmR, *Synechococcus PCC7942* SmtB, *S. aureus* CzrA, *M. tuberculosis* NmtR, *M. tuberculosis* CmtR, *S. coelicolor* CmtR, *S. aureus pI258* CadC, and *E. coli* ArsR. The α3N, α4C, and α5 sites are denoted by green arrows, orange arrows, and purple arrows, respectively. NmtR contains ligands from the α5 site plus 2 additional ligands in the C-terminal region of the protein which are denoted by blue arrows. The secondary structure of Zn_2 SmtB (Chapter III) (Eicken *et al.*, 2003) is indicated above the alignment, with metal binding residues shown to be involved in metal sensing are boxed and colored red. Residues colored blue have been to bind metal but are not involved in metal sensing.

(Pennella *et al.*, 2003). Zinc binding to CzrA and nickel binding to NmtR is known to strongly negatively regulate operator-promoter binding *in vitro* and *in vivo* (Cavet *et al.*, 2002; Kuroda *et al.*, 1999; Pennella *et al.*, 2003).

Structural studies of the apo- and zinc forms of CzrA and SmtB, a well-characterized α5 zinc sensor from *Synechococcus PCC7942*, reveal a metal-ligand mediated inter-protomer hydrogen bonding network that appears to link the metal and DNA binding sites (Chapter III) (Eicken *et al.*, 2003). The Zn_2 forms of CzrA and SmtB reveal an absolutely essential role for His97 of CzrA (H117 in SmtB) in mediating the allosteric response (Chapter III) (Eicken *et al.*, 2003). In fact, the formation of the initial hydrogen bond appears to originate with the non-liganding $N^{\varepsilon 2}$ atom of His97 (Chapter III) (Eicken *et al.*, 2003). However, functional roles played by the metal-binding ligands were not determined from these studies. To elucidate the functional roles played by individual ligands, we introduced single, potentially liganding and non-liganding, amino acid substitutions within the chelate and characterized each protein as to their metal-binding and DNA-binding properties.

Not surprisingly, all non-native substitutions, whether potentially liganding or not, greatly reduce metal binding affinity for both Co(II) and Zn(II) by 3-4 orders of magnitude compared to wild-type CzrA. However, there is a clear “division of labor” within the chelate. D84 and H97 of CzrA play key roles in maintaining the tetrahedral symmetry around the chelate; in contrast, H86 and H100 are much more amenable to substitution with both strongly ligating and poorly ligating amino acid substitutions capable of maintaining tetrahedral coordination geometry around the chelate. In all cases, maintenance of tetrahedral coordination geometry is 100% correlated with the ability to mediate an allosteric response to DNA binding.

MATERIALS AND METHODS

*Chemicals***.** All buffers were prepared using Milli-Q deionized water. MES, HEPES, and Tris buffer salts and ammonium sulfate were obtained from Sigma. All chromatography materials were obtained from Pharmacia Biotech. Ultrapure cobalt(II) chloride and zinc(II) sulfate were obtained from Johnson Matthey.

*Overexpression and Purification of Variant CzrAs***.** All mutants of CzrA were generated using the protocol supplied by the QuikChange from Stratagene. Generation of the single aspartate to asparagine, histidine to asparagine, histidine to aspartate, histidine to glutamate, and histidine to glutamine mutations was carried out using the wild-type expression plasmid (pET-CzrA) (Pennella *et al.*, 2003) as a template for PCR and the appropriate mutagenic primers. Both strands of all expression constructs were completely sequenced to verify the integrity of the plasmids. All mutant CzrA proteins were purified in a manner essentially identical to that of wild-type CzrA (Pennella *et al.*, 2003). The resulting proteins were exhaustively dialyzed against buffer a containing 10 mM HEPES and 0.4 M NaCl (pH 7.0) to remove EDTA used throughout the purification in order to generate apoproteins. All CzrA variants were determined to be zinc-free (≤ 0.1 molar equiv of metal) by atomic absorption spectroscopy. The concentration of the

CzrA monomer was determined for all variants using an ε_{280} of 4470 M^{-1} cm^{-1} (Pace *et al.*, 1995; Pennella *et al.*, 2003).

Co(II) Binding Experiments. All metal binding experiments were carried out as previously described (Chapter II) (Pennella *et al.*, 2003). Under these solution conditions as well as those below, CzrA is largely dimeric as defined by a monomer-dimer equilibrium constant of 1.7×10^5 M^{-1} for apo-CzrA and 3.4×10^5 M^{-1} for Zn(II)-saturated CzrA (Chapter II) (Pennella *et al.*, 2003).

Zn(II) Binding Experiments. Two different zinc chelator indicator dyes were used as apo-CzrA competitors: mag-fura-2 ($K_{Zn} = 5.0 \times 10^7$ M^{-1} at pH 7.0 and 25°C) (Walkup and Imperiali, 1997) and quin-2 ($K_{Zn} = 2.70 \times 10^{11}$ M^{-1}) (Jefferson *et al.*, 1990). Mag-fura-2 competition experiments were carried out as previously described (VanZile *et al.*, 2000; VanZile *et al.*, 2002b). For quin-2 competition assays, a known concentration of quin-2 (10-20 μM) was mixed with a known concentration of apoprotein (20-40 μM) in 0.8 mL of buffer S and the optical spectrum was recorded from 240 to 800 nm. Following each *i*th addition of $ZnSO_4$ (2.5-10 μL), the reaction mixture was allowed to equilibrate for 15-30 minutes before the optical spectrum was recorded. The concentration of the Zn(II)-quin-2 complex was determined by the change in absorption at 265 and 366 nm (absorbance maxima of quin-2) (Jefferson *et al.*, 1990; VanZile *et al.*, 2000; VanZile *et al.*, 2002b) following each addition of Zn(II), thus defining the extent of competition between the protein and the chelator. These data were fit using a competitive binding model in Dyna-Fit (Kuzmic, 1996) to determine the zinc binding affinity, K_{Zn}, of each of the variant CzrAs.

NMR Spectroscopy. NMR spectra were acquired on a Varian Unity Inova 500 MHz spectrometer in the Biomolecular NMR Laboratory at Texas A&M University. The sample contained 0.5 mM uniformly labeled ^{15}N-labeled CzrA in 10 mM d_{18}-HEPES and 100 mM NaCl (pH 6.0). Chemical shift referencing is relative to DSS (Wishart *et al.*, 1995). All spectra were processed and analyzed using NMRPipe (Delaglio *et al.*, 1995) and SPARKY (Goddard and Kneller). The ^{1}H-^{15}N HSQC spectrum was recorded as a 160* × 512* two-dimensional (2D) matrix in the t_1 and t_2 dimensions, respectively, where n* represents n complex points. Acquisition times in each dimension were 88.9 (t_1, ^{15}N) and 85.3 ms (t_2, ^{1}H^{N}) defined by sweep widths of 1800 and 6000 Hz, respectively, for a total measurement time of 1.6 h. The data were apodized along t_1 by using a 90°-shifted sine bell, truncated at 9%, and along t_2 with a 90°-shifted squared sine bell, truncated at 1%. The data were zero-filled to digital resolutions of 5.6 (F_1) and 10 Hz (F_2).

Atomic Absorption Spectroscopy. The residual metal content of variant CzrA proteins was determined using a Perkin-Elmer AAnalyst 700 atomic absorption spectrophotometer operating in flame mode. The total metal content of purified, "metal-free" proteins was no more than 0.1 mol metal ion per mol protein monomer. For the determination of the concentration of metals used as titrants for optical titrations, each metal was detected using Zn(II)-, or Co(II)-specific hollow cathode lamps. Zn(II) was detected at 213.9 nm (slit-width of 0.7 nm) and Co(II) at 240.7 nm (slit-width 0.2 nm).

Preparation of Oligonucleotide Probes. Fluorescein-labeled DNA oligonucleotides were obtained from Operon Technologies. The oligonucleotides were purified using TBE/urea gel electrophoresis followed by an 8 h elution from the gel matrix. The oligonucleotides were then desalted using a C18 column, eluted in 100% methanol, and taken to dryness in a Speed-Vac. The DNA pellets were resuspended in 200 μL of deionized water. dsDNA stocks (100 μM) were prepared in 10 mM HEPES and 0.4 M NaCl (pH 7.0), heated to 95^{o}C, and allowed to anneal at room temperature for 3-4 hr. Subsequent dilutions were prepared via serial 1:10 dilutions with titration buffer.

Fluorescence Anisotropy-based DNA binding experiments. All fluorescence anisotropy experiments were carried out with an ISS PC1 spectrofluorometer operating in the steady-state mode fitted with Glan-Thompson polarizers in the L format. The 57-mer, double-stranded *czr* O/P oligonucleotide (Operon Technologies) used was fluorescein-labeled on one 5'-end as previously reported (Pennella *et al.*, 2003). All experiments were carried out with 40 nM dsDNA in 10 mM HEPES and 0.4 M NaCl (pH 7.0) in a volume of 1.8 mL. Up to 100 μL of ~30 μM apoprotein or Zn(II) saturated CzrA stocks were added in known aliquots up to a total concentration of ~2 μM protein. 50 μM EDTA was present in all binding experiments carried out with metal-free apoprotein. For zinc-complexed CzrA, protein titrants were prepared 1:1 with metal (i.e., 1 molar equivalent of metal per monomer of protein or 2 molar equivalents per dimer) with 2.0 μM zinc present in the binding buffer to help insure saturation of metal binding sites in variants that have low affinity for zinc. Higher concentrations of zinc in the binding buffer could not be used for some variants due to precipitation. Experimental binding isotherms obtained for CzrA variants were fit using DynaFit (Kuzmic, 1996) with a model of the sequential binding of four or five variant CzrA dimers (P_2) to the DNA oligonucleotide (D) as described previously (Chapter II) (Pennella *et al.*, 2003), each defined by the indicated K_i, linked to the monomer-dimer equilibrium established for wild-type CzrA (Chapter II) (Pennella *et al.*, 2003).

RESULTS

The crystallographic structure of Zn(II)-bound CzrA reveals a pair of symmetry-related inter-helical metal sites (Chapter III) (Eicken *et al.*, 2003). The pair of metal sites lie across the α5 helices, with Zn(II) coordinated by the $O^{\delta 1}$ atom of Asp84 and the $N^{\delta 1}$ atom of His86 from one protomer and the $N^{\delta 1}$ atom of His97' and the $N^{\varepsilon 2}$ atom of His100' from the other protomer (see Figure 4.1). In this chapter, we describe spectroscopic characterization of a series of single amino acid non-native metal liganding mutants (asparagine, aspartate, glutamate, and glutamine) introduced into the CzrA chelate in an effort to probe the functional role played by individual ligands. Since H86 and H97 utilize the $N^{\delta 1}$ atom to chelate the metal, aspartate and asparagine substitutions were characterized in order to conserve the metal ligand size. H100 coordinates the metal with the $N^{\varepsilon 2}$ atom, therefore glutamate and glutamine substitution mutants were incorporated.

UV-Visible Absorption Spectra of Co(II)-Substituted Variant CzrAs. Complete corrected UV-vis electronic spectra are shown for a series of substitution (Asp84 → Asn, His86 → Asp/Asn/Gln, His97 → Asp/Asn, and His100 → Glu/Gln) mutants of CzrA in Figure 4.2A and 4.2B. K_{Co} values for each CzrA mutant were determined by

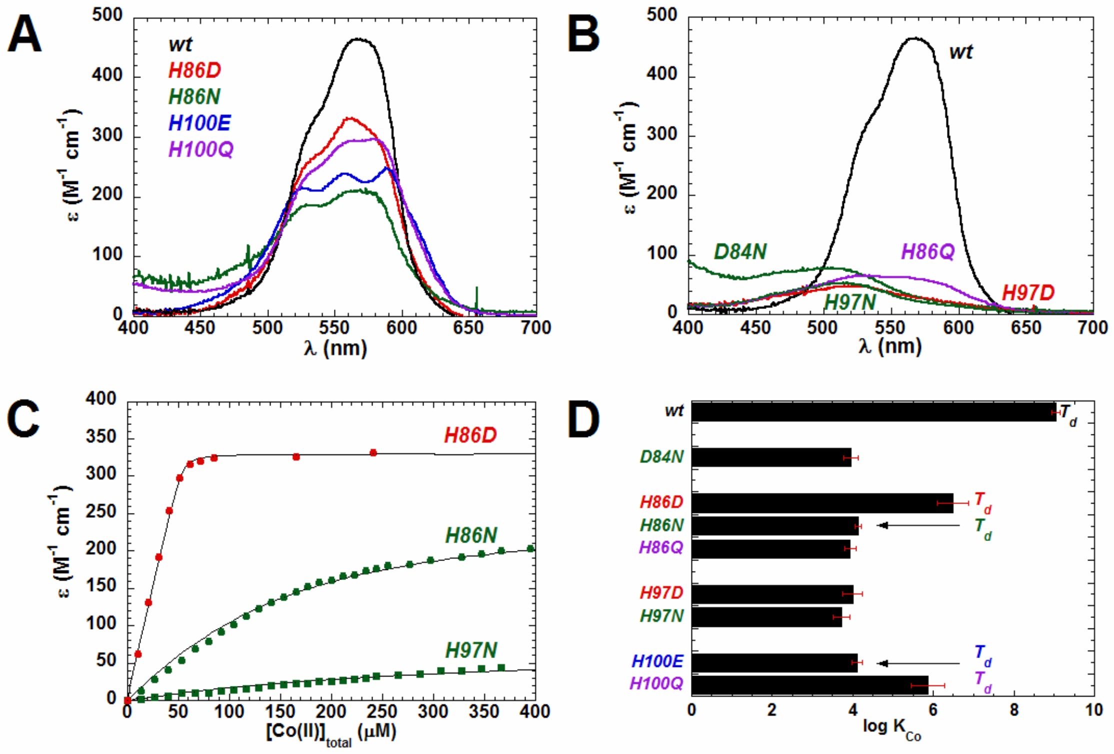

Figure 4.2. Cobalt uv-vis spectroscopy on CzrA variants. **(A.)** Absorption spectra of wild-type (black line), H86D (red line), H86N (green line), H100E (blue line), and H100Q (purple line) CzrAs. **(B.)** Absorption spectra of wild-type (black line), D84N (green line), H97D (red line), and H97N (green line) CzrAs. **(C.)** Representative fitted binding isotherms of H86D (red circles), H86N (green circles), and H97N (green squares) CzrAs. **(D.)** Bar plot of binding affinities of wild-type and variants with K_{Co} on a log scale. Error bars are based on fitted isotherms. T_d represents proteins that coordinate Co(II) with tetrahedral geometry.

fitting the data to a nonlinear least-squares fit to a 1:1 binding model. Figure 4.2C shows representative fitted isotherms for H86D, H86N, and H97N with the compilation of the results of all mutants given in graphical form in Figure 4.2D.

Asp84 mutant CzrAs. The ligand field region of the absorption spectrum of Co(II)-substituted D84N is blue-shifted and much less intense relative to wild-type CzrA (Figure 4.2B). The low molar absorptivity ($\varepsilon < 80$ M^{-1} cm^{-1}) is suggestive of five- or six-coordinate Co(II), rather than four (Chapter II) (Pennella *et al.*, 2003), and its affinity for Co(II) is >10,000-fold lower than wild-type CzrA (see Table 4.1).

His86 mutants CzrAs. H86D and H86N CzrAs are characterized by absorption spectra similar to that of wild-type CzrA (Figure 4.2A). The coordination environment remains tetrahedral, but the spectrum is characterized by an overall diminution in intensity in the ligand field transition region at 563 nm and 570 nm, with $\varepsilon_{563} \approx 325$ (± 5) M^{-1} cm^{-1} for H86D CzrA and $\varepsilon_{570} \approx 210$ (± 10) M^{-1} cm^{-1} for H86N CzrA (Figure 4.2A). The H86N variant appeared capable of donating a ligand to the Co(II) ion while maintaining tetrahedral coordination geometry and moderate metal binding affinity. This provided motivation to investigate the properties of substituting a larger side chain, H86Q CzrA. Surprisingly, the Co(II) binding properties of H86Q CzrA are more similar to D84N CzrA than they are to H86N CzrA. The molar absorptivity is more consistent with five or six-coordinate Co(II), and H86Q CzrA has a low affinity for Co(II); however, the affinities of H86N and H86Q for Co(II) are essentially identical to one another (see Figure 4.2D).

Table 4.1. Equilibrium Association Constants for the Binding of Co(II) (K_{Co}) and Zn(II) (K_{Zn}) to CzrA Variants[a]

Protein	K_{Zn1} (M^{-1})[b]	K_{Zn2} (M-1)[c]	K_{Co} (M^{-1})
Wild-type[d]	5.1 (± 2.1) x 10^{12}	$10^9 \leq 10^{10}$	1.1 (± 0.1) x 10^9
D84N	4.0 (± 0.2) x 10^7	$\leq 10^5$	9.0 (± 0.4) x 10^4
H86D	8.4 (± 1.0) x 10^{10}	$\leq 10^5$	3.1 (± 0.7) x 10^6
H86N	2.0 (± 0.7) x 10^9	$\leq 10^5$	1.4 (± 0.1) x 10^5
H86Q	nd[e]	nd[e]	8.6 (± 0.1) x 10^4
H97D	1.5 (± 0.1) x 10^7	$\leq 10^5$	1.0 (± 0.1) x 10^4
H97N	6.8 (± 0.3) x 10^6	$\leq 10^5$	5.3 (± 0.3) x 10^3
H100E	6.0 (± 1.2) x 10^8	$\leq 10^5$	1.3 (± 0.1) x 10^4
H100Q	3.6 (± 0.5) x 10^{10}	$\leq 10^5$	7.5 (± 0.5) x 10^5

[a] Conditions: pH 7.0, 25 °C, and 0.4 M NaCl.

[b] Resolved from fits to a 1:1 binding model in a mag-fura-2 [Zn(II)] or a quin-2 [Zn(II)] competition assay where K_{Zn2} was fixed to 1 x 10^5 M^{-1}.

[c] All variants showed negative cooperativity when binding zinc. The binding affinity for the second zinc was to low to measure and only a lower limit is given.

[d] Zinc binding affinities reported previously Chapter III (Eicken *et al.*, 2003)

[e] Experiments not yet performed to determine zinc binding affinities.

His97 mutant CzrAs. H97D and H97N CzrAs have very low Co(II) binding affinities compared to wild-type CzrA (see Table 1). However, in this case, the affinities of aspartate and asparagine substitutions for H97 are nearly identical versus H86 substitutions, which are different for H86D and H86N CzrAs. In addition, the molar absorptivities ($\varepsilon < 80\ M^{-1}\ cm^{-1}$) of H97D and H97N CzrAs are similar to D84N and H86Q CzrAs, suggestive of five- or six-coordinate geometry as well (see Figure 4.2B).

His100 CzrAs. H100E and H100Q CzrAs have Co(II) binding properties similar to H86D and H86N CzrAs. H100E and H100Q CzrAs have d-d ligand field transitions at $\varepsilon_{588} \approx 240\ (\pm 20)\ M^{-1}\ cm^{-1}$ and $\varepsilon_{570} \approx 290\ (\pm 5)\ M^{-1}\ cm^{-1}$, respectively (Figure 4.2D). This is a clear indication of tetrahedral or distorted tetrahedral coordination geometry (Chapter II) (Pennella *et al.*, 2003). Interestingly, H100E CzrA has a lower binding affinity for cobalt than H100Q CzrA (Figure 4.2D). This may be explained by the substitution of a basic amino acid (His) with an acidic amino acid (Glu), which perturbs the environment for metal-binding.

Zn(II) binding affinities of CzrA mutants. Two indicator chelators, mag-fura-2 and quin-2 were employed to determine the stoichiometry and affinity of Zn(II) binding to wild-type CzrA (Chapter III) (Eicken *et al.*, 2003). Similar experiments with each of the variant CzrAs were carried out to determine the extent to which substitution of chelating ligands influenced Zn(II) binding affinity.

Figure 4.3A and 4.3B show representative mag-fura-2, Zn(II) titrations of H86D and H97N CzrAs. The titration of H86D CzrA reveals that this mutant binds *one* Zn(II) per dimer far tighter than mag-fura-2 followed by binding of the second Zn(II) with a

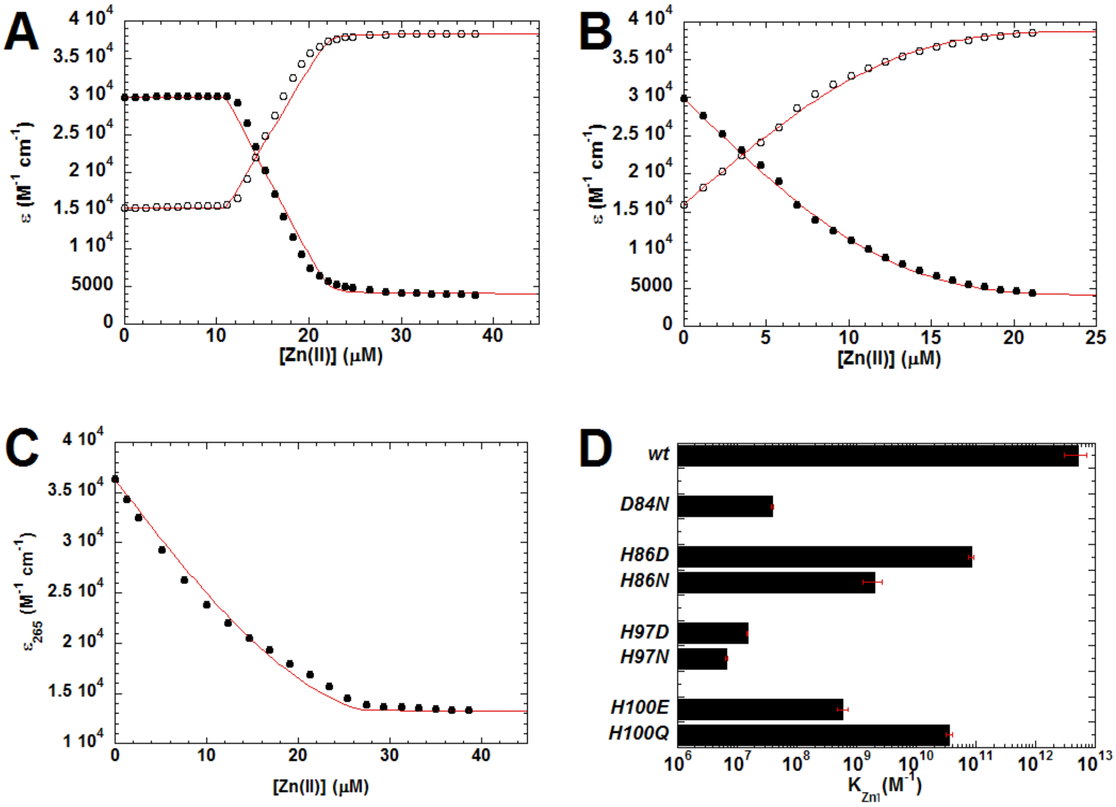

Figure 4.3. Representative titrations of Zn(II) into a mixture of competitor (mag-fura-2 or quin-2) and variant CzrAs with the overall K_{Zn} for each variant CzrA plotted. **(A.)** 20.1 μM H86D CzrA and 11.1 μM mag-fura-2 and **(B.)** 19.7 μM H97N and 10.8 μM mag-fura-2. In both panels, the open circles represent ε_{325} values, which are maximal in the Zn(II)-mag-fura-2 complex, and the filled circles represent ε_{366} values, which are maximal in the uncomplexed mag-fura-2. The solid red lines represent nonlinear least-squares fits to a 2:1 binding model with K_{Zn2} values fixed at 10^4 M^{-1} to account for the low binding affinity of the second zinc. K_{Zn1} values of $\geq 10^9$ and 6.8 (± 0.3) x 10^6 M^{-1} were obtained for H86D CzrA and H97N CzrA, respectively. **(C.)** 20.8 μM H86D CzrA and 16.8 μM quin-2. The filled circles represent ε_{265} values, which are maximal in the uncomplexed quin-2. The solid red line represents a nonlinear least-squares fit to a 2:1 binding model with K_{Zn2} value fixed at 10^4 M^{-1} to account for the low binding affinity of the second zinc binding. A K_{Zn1} value of 8.44 (± 0.99) x 10^{10} M^{-1} was obtained. **(D.)** Bar plot of binding affinities of wild-type and variant CzrAs determined by mag-fura-2 or quin-2 competition assays with K_{Zn} on a log scale. Error bars are based on fitted isotherms.

K_{Zn} less than that of mag-fura-2. This mutant possesses the property of binding two zinc ions with strong negative cooperativity. Not surprisingly, H97N CzrA binds one Zn(II) per dimer with an affinity on the order of mag-fura-2 (K_{Zn1} = 6.8 (±0.3) x 10^6 M^{-1}) followed by binding of the second zinc with a K_{Zn2} less than that of mag-fura-2. H100Q CzrA was the only other variant CzrA with a zinc binding affinity far tighter than mag-fura-2. Since only a lower limit for K_{Zn} for variant CzrAs, H86D and H100Q, could be obtained with the low-affinity indicator dye mag-fura-2, a higher-affinity zinc chelator dye, quin-2, was used. Quin-2 forms a 1:1 complex with Zn(II) with a K_{Zn} of 2.7 × 10^{11} M^{-1} (Jefferson *et al.*, 1990). The remaining variants zinc binding affinities were characterized with the competitor mag-fura-2 and a bar plot in Figure 4.3D shows the relative difference for the variant CzrAs compared with wild-type CzrA.

Although complete equilibration of Zn(II) with quin-2/CzrA mixtures required ≥15 minutes under these conditions, equilibrium titrations could be obtained. Results from a representative experiment are shown with H86D CzrA (Figure 4.3C). K_{Zn} for wild-type CzrA was characterized previously (Chapter III) (Eicken *et al.*, 2003) and was determined to be 5.1 (± 2.1) x 10^{12} M^{-1} (Table 1). K_{Zn1} for H86D and H100Q CzrA is easily determined from this competition assay and is ≥60-fold lower than that of wild-type CzrA but still quite high (on the order of 10^{10} M^{-1}) (Table 1). All variant CzrA proteins maintain the wild-type property of binding two zinc ions with strong negative cooperativity, but with a considerable lower affinity than wild-type CzrA (Table 4.1).

NMR Studies of variant CzrAs. The presence of a cross-peak for H97 $N^{\varepsilon 2}$-$H^{\varepsilon 2}$ in wild-type CzrA (Figure 4.4) was previously suggested to report on the His97 $N^{\varepsilon 2}$-$H^{\varepsilon 2}$ – O=C His67 hydrogen bond important for allosteric regulation of DNA binding (see Chapter III, Figure 3.4C) (Eicken *et al.*, 2003). Thus, uniformly ^{15}N-labeled mutant CzrAs were purified as described previously (see Methods) and ^{15}N-^{1}H HSQC spectra were recorded for each (see Figure 4.4). All proteins exhibit spectra with a majority of backbone amide-proton cross-peaks nearly indistinguishable from wild-type CzrA in the presence and absence of zinc (data not shown). However, only the zinc-saturated spectra of H86D and H100Q CzrAs exhibit the His97 $N^{\varepsilon 2}$-$H^{\varepsilon 2}$ cross-peak; zinc forms of D84, H97D, and H97N CzrAs do not show this resonance. These data suggest that only those mutants that adopt tetrahedral coordination stabilize this putative hydrogen bond.

Zinc-saturated H86N CzrA was expected to exhibit the His97 $N^{\varepsilon 2}$-$H^{\varepsilon 2}$ cross-peak, since it adopts a tetrahedral coordination of Co(II). Unexpectedly, it did not. The amide-proton backbone resonances of H86N CzrA were shifted to wild-type resonances in the presence of zinc, suggestive of Zn(II) binding. However, the cross-peaks previously to residues that shift significantly upon zinc binding were found to have low intensities and appear exchange broadened (data not shown). This suggests a zinc-saturated form of H86N CzrA may be chemical exchange broadened due to weak metal binding affinity. H100E CzrA might be expected to behave similarly to H86N CzrA since they have similar binding affinities for zinc (see Table 4.1).

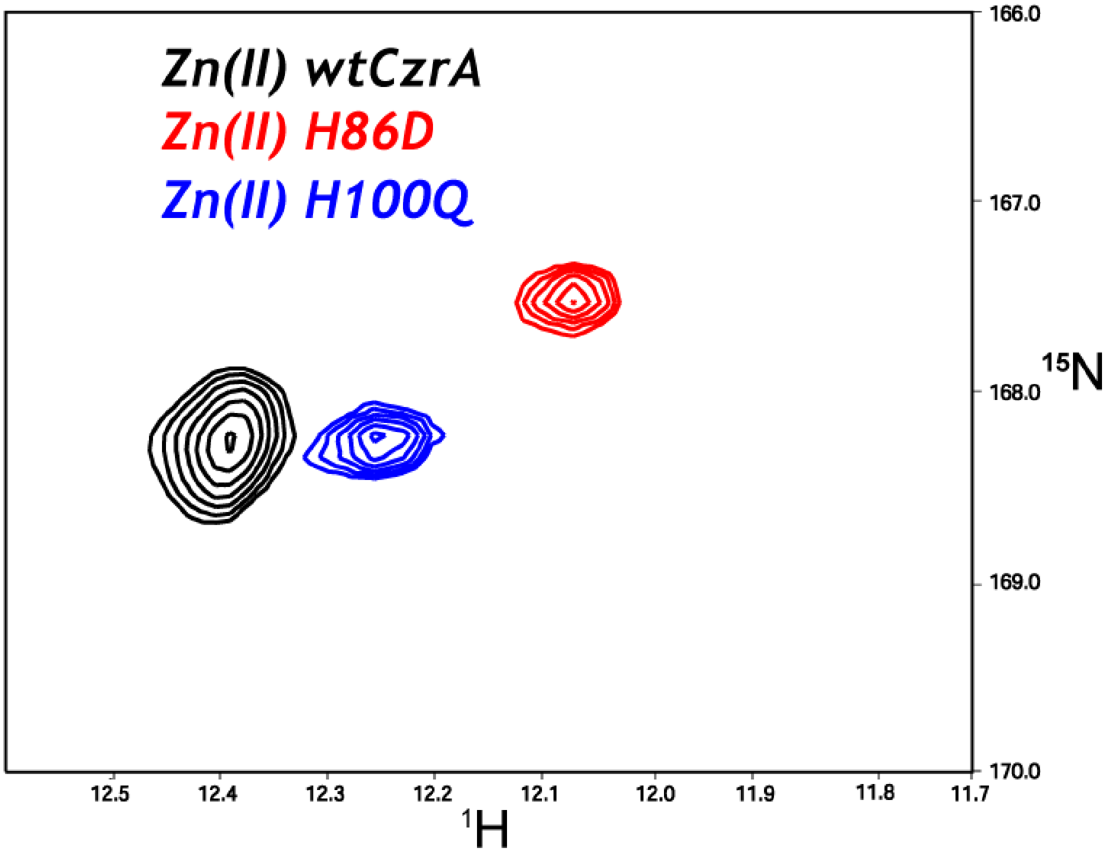

Figure 4.4. NMR Spectroscopy of wild-type and variant CzrAs. Portion of ^{15}N-^{1}H HSQC spectra, which were acquired with the ^{15}N carrier frequency at 168 ppm. Red peak represents His97 $N^{\varepsilon2}$-$H^{\varepsilon2}$ cross-peak visible in H86D CzrA, the blue peak represents His97 $N^{\varepsilon2}$-$H^{\varepsilon2}$ cross-peak visible in H100Q CzrA, and the black peak represents His97 $N^{\varepsilon2}$-$H^{\varepsilon2}$ cross-peak visible in wild-type CzrA. Spectra for D84N, H86N, H97D, and H97N CzrAs were acquired but did not visualize this peak. Solution conditions are the following: pH 6.0 and 0.1 M NaCl, 10% D_2O, and referenced to internal DSS.

DNA binding activities of apo- and Zn-forms of CzrA variants monitored by fluorescence anisotropy. DNA binding experiments were performed with variant CzrA proteins and a fluorescein-labeled 57-bp DNA oligonucleotide that contains the entire region of the czr O/P region footprinted by wild-type CzrA (Chapter II) (Pennella *et al.*, 2003; Singh *et al.*, 1999). Results from representative titration experiments are shown with H86D, H86N, and H97N CzrAs in Figure 4.5. The solid lines through each set of experimental data in Figure 4.5 A-C represent nonlinear least-squares fits to the sequential dimer-binding model described in the Methods and previously described experiments with wild-type CzrA (Chapter II) (Pennella *et al.*, 2003).

These experiments reveal that apo forms of mutant CzrAs have *czr*O/P binding affinities and stoichiometries essentially indistinguishable from that of wild-type CzrA. The lone exception is apoD84N CzrA which binds ≥ 100-fold weaker than wild-type CzrA (data not shown). This suggests that this mutation has either disrupted the DNA binding site directly or destabilized the homodimer; these two possibilities will be distinguished by analytical equilibrium ultracentrifugation. Nevertheless, addition of stoichiometric zinc has no effect on the DNA binding activity of this variant.

To elucidate the regulatory effect of metal ions on the association of CzrA for the fluorescein-labeled czr O/P region, pre-formed zinc:protein complexes were titrated into free DNA in the presence of 2.0 μM zinc to help ensure that these zinc sites would be saturated. Figure 4.5A-C show that zinc complexed forms of H86D and H86N CzrA have much weaker association with the *czr*O/P when compared to their apo forms. The binding isotherms for H86D and H86N CzrAs could be satisfactorily fit with the binding

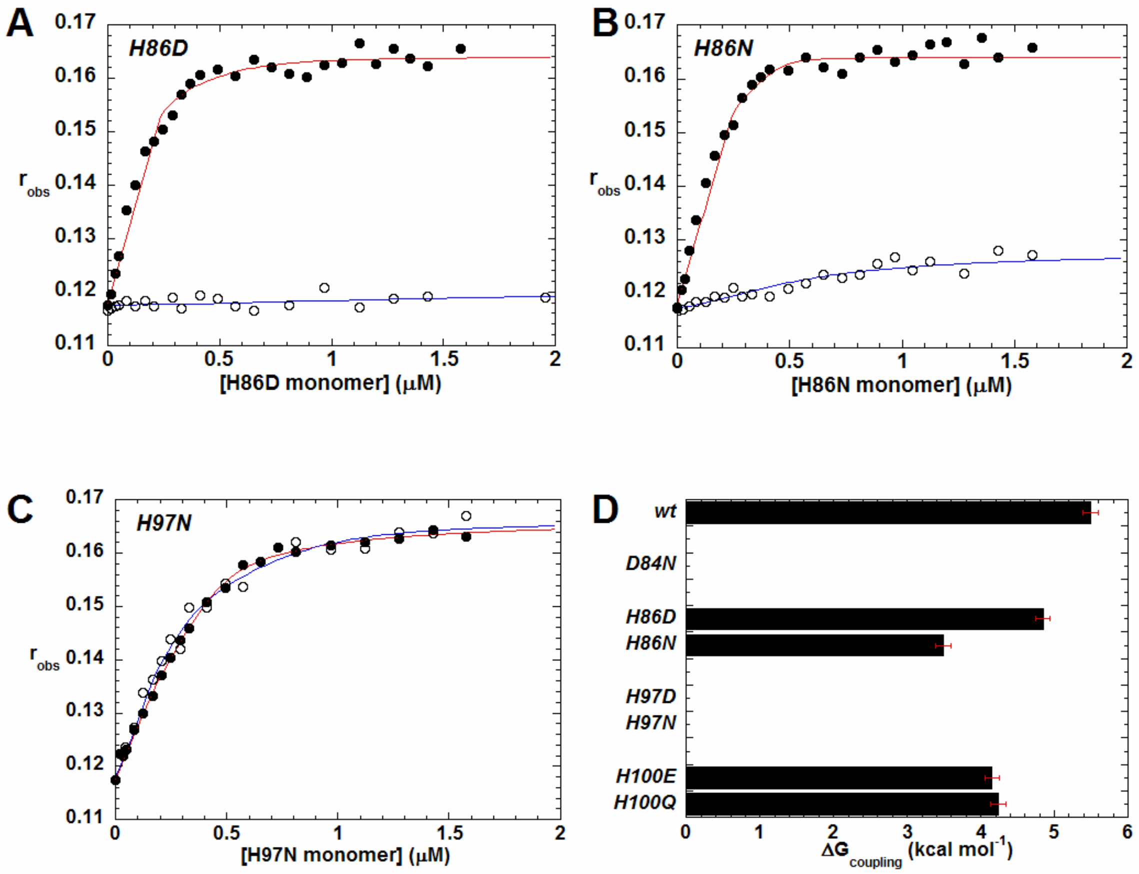

Figure 4.5. Representative binding isotherms of apo and zinc forms of variant CzrAs (H86D, H86N, and H97N) to fluorescein-labeled DNA oligonucleotide containing the czr O/P sequence. The anisotropy, r_{obs}, is plotted vs the total variant monomer concentration for **(A.)** H86D, **(B.)**, H86N, and **(C.)** H97N. The data for binding to the oligonucleotide in the absence (●) or presence of saturating zinc (○) is shown, and the solid red lines for the apo proteins and the blue lines for the zinc forms of the variants represent nonlinear least-squares fits to the binding models described in the text. **(D.)** Bar chart representation of the coupling free energies of variant and wild-type CzrAs. Free energy of binding for apo proteins were calculated by using the first dimer binding affinity only, which was fitted with a lower limit value of K_i = 5 x 10^9 M^{-1}. Free energy of binding for zinc loaded proteins were calculated also by using the first dimer binding affinity only, which gave the following fitted values: K_{wt} = 4.7 (± 0.7) x 10^5 M^{-1}, K_{H86D} = 1.4 (± 0.5) x 10^6 M^{-1}, K_{H86N} = 1.4 (± 0.4) x 10^7 M^{-1}, K_{H100E} = 4.5 (± 0.4) x 10^6 M^{-1}, and K_{H100Q} = 3.9 (± 0.2) x 10^6 M^{-1}. The free energy of binding for zinc saturated H97D and H97N were nearly identical to the apo-proteins, therefore only a lower limit for the first dimer binding affinity was used K_{H97D} = K_{H97N} = 5 x 10^9 M^{-1}. The ΔG coupling for each variant was calculated as follows: $\Delta G_{coupling} = \Delta G_{zinc} - \Delta G_{apo}$.

of a single dimer to the oligonucleotide, with an affinity (K_1, see scheme in Methods of Chapter II) of 1.4 (± 0.5) x 10^6 M^{-1} for H86D CzrA and 1.4 (± 0.4) x 10^7 M^{-1} for H86N CzrA. These are ≥ 3000-fold and ≥ 300-fold reduced relative to apo-H86D and apoH86N, respectively. The *czr*O/P affinity of H100E and H100Q CzrAs were also strongly allosterically regulated by Zn(II). In contrast, both H97 substitutions, H97N and H97D CzrAs, have *czr*O/P affinities that are unaffected by the presence of saturating zinc (Figure 4.5).

Another way to express the extent of allosteric regulation by individual mutants is the coupling free energy, $\Delta G_{coupling}$, i.e., the extent to which Zn(II) binding is negatively coupled to DNA binding of the first dimer. Although only lower limits can be used since the first dimer binds stoichiometrically to the *czr*O/P under these conditions, the trends are nonetheless informative. Wild-type CzrA is characterized by $\Delta G_{coupling} \geq 5.5$ kcal mol^{-1}, while each mutant exhibits weaker coupling free energies. Of the four mutants that maintain tetrahedral symmetry (H86D, H86N, H100E, and H100Q CzrAs), H86D CzrA has the strongest coupling free energy with H86N CzrA the weakest, about 60% of the wild-type protein (see Figure 4.5D). In contrast, H100E and H100Q CzrAs have comparable coupling free energies, ~80% of wild-type CzrA, despite vastly different zinc binding affinities. Notably, all mutants that destroy tetrahedral geometry in the chelate effectively uncouple metal and DNA binding.

DISCUSSION

The structural characterization of α5 zinc sensors SmtB and CzrA reveal a model of how metal binding could affect DNA binding. This model proposes that when metal is bound, an inter-subunit hydrogen bonding network is formed that links the non-ligating face of His97 ($N^{\varepsilon 2}$-$H^{\varepsilon 2}$) from the α5 site, which is within hydrogen bonding distance, to the backbone carbonyl of His67' on the opposing protomer, which is located in the turn between the recognition helix (αR) and β1 (Chapter III) (Eicken *et al.*, 2003). The backbone amide group (N-H) of the adjacent residue L68' is within hydrogen bonding distance of the backbone carbonyl (C=O) of L63' located in the recognition helix and these interactions are proposed to help stabilize a low-affinity, DNA binding conformation (Chapter III) (Eicken *et al.*, 2003). Thus, it is believed that these main-chain and side-chain hydrogen bonding interactions linking the α5 and αR helices play a role in the allosteric coupling of the metal and DNA-binding sites. Therefore, experiments were carried out to probe the functional roles of each ligand (D84, H86, H97, and H100) involved directly with metal binding and their contribution to DNA binding in CzrA.

We show here that two of the four ligands (D84 and H97) from *Staphylococcus aureus* CzrA are absolutely required for maintenance of tetrahedral coordination of cobalt and zinc; furthermore, tetrahedral coordination is necessary and efficient to effect negative allosteric regulation *in vitro*. Substitution of either of the two ligands, with a liganding and/or nonliganding side chain (D84N, H97D, or H97N CzrAs) results in a dramatic perturbation of the Co(II) spectrum of wild-type CzrA (Figure 4.2 B), effectively abolishing tetrahedral metal binding to this site. These variants also bind zinc with a much lower affinity than wild-type CzrA, but still bind two zinc ions with strong negative cooperativity (Figure 4.3). The DNA binding affinity of the zinc-saturated forms of these three mutants is nearly indistinguishable from the apo forms, revealing that these mutants do not allosterically regulate DNA binding.

In contrast, substitution of His86 and His100 with both liganding and nonliganding residues (H86D, H100E and H86N, H100Q, respectively) results in clear Co(II) absorption spectra, consistent with tetrahedral coordination (Figure 4.2 A). The binding affinity of Co(II) for these mutants is ≥ 250-fold weaker than wild-type CzrA. This finding suggests that the amino acid residues of positions H86 and H100 of CzrA in the $\alpha5$ site are somewhat accommodating in terms of maintaining a tetrahedral coordination environment in a way that has some effect on the Co(II) binding affinity (see Figure 4.1A and Figure 4.2). Although these variant CzrAs have lower affinities for zinc compared to wild-type CzrA, they still maintain the property of negative cooperativity (Table 4.1). The zinc forms of these tetrahedral binding mutants also show a lower affinity for the *czr*O/P compared to the apo-forms of these same variants (Figure 4.5). This indicates that they are capable of allosterically regulating DNA binding *in vitro*. The coupling free energies of all the variants tested were lower than wild-type CzrA (see Figure 4.5). Although these tetrahedral coordinating mutants regulate DNA binding in the presence of zinc, whether they are capable of regulation *in vivo* has not been tested.

Negative cooperativity of zinc binding in CzrA. The structural origin of the strong negative cooperativity of zinc binding in CzrA is not known but suggests that when one metal is loaded, the symmetry of the dimer is strongly disrupted. Negative cooperativity of zinc binding is maintained in the functional and non-functional mutant CzrAs. The zinc binding properties of apoCzrA bound to its O/P region are not well-characterized. If these same competitor assays are performed when CzrA is bound to its operator DNA sequence, this negative cooperativity may be lost. If it is maintained, this unusual property may be relevant for CzrA regulating zinc *in vivo*.

Conservation of metal binding ligands in the α5 site. The results presented here provide evidence that D84 and H97 are absolutely required to drive the formation of a tetrahedral coordination site, which then allows H97 to mediate the formation of an inter-subunit hydrogen bonding network. This suggests that these two residues should be absolutely conserved for SmtB/ArsR family members that possess a functioning α5 metal-binding site.

A multiple sequence alignment of fifty-one candidate α5 metal sensing sites is shown in Figure 4.6. Forty-five of these fifty-one sequences possess all four conserved residues of an α5 metal binding site, if one includes both His and Glu in the most C-terminal residue (H100 in CzrA; E120 in SmtB) (Chapter III) (also see Figure 4.1). Five of the six remaining fifty-one sequences contain neither a glutamate nor a histidine in this C-terminal position (this includes AztR from *Anabaena*, CmtR from

CzrA *S. aureus*	DIHVATMLKQAIHHANHPKESGL-----------------
NmtR *M. tuberculosis*	DTHVAQLLDEAIYHSEHLHLGLSDRHPSAG----------
Streptomyces	DDHVAGLLDQAVYHVEHLRLGISDTAE-------------
Rubrobacter	DAHLGVLLREALYHVDHARLGAARREER------------
Staphylococcus	DIHVSTLLKQAIHHAKHPSEGGISNDKS------------
Listeria_monocytogenes	DNHVLELLTQAIRHVHHH----------------------
Bacillus	DEHVLDVLQQMIHHTQHD----------------------
Oceanobacillus	DEHVIKLLEQAIEHMEHTTKEV------------------
Enterococcus	DHHVIDILNQTFEHIEHR----------------------
Oenococcus	DPHIITTLNQLMNHVDHILLGRKHNGQ-------------
Gloeobacter	DEHVLNLLAQGEAHIRHD----------------------
Rubrobacter_xylanophil	DDHVRRLLDLSLEHVRHA----------------------
***Tropheryma whipplei*_TW0827**	DEHIKHVVADCIQHVQHET---------------------
SmtB *Synechococcus PCC7942*	DHHIVALYQNALDHLQECR---------------------
BxmR *O. brevis*	DRHVLELYRAVAEHLDEES---------------------
CadC *S. aureus pI258*	DEHIRQIMMIALAHKKEVKVNV------------------
ZiaR *Synechocystis PCC6803*	DNHVMNLYREVADHLQESD---------------------
***Mycobacterium* Rv2358**	DHHLAHIVLDAVAHAGEDAI--------------------
Mycobacterium paratuberculosis	DHHLAHIVVDAVAHAGEEPRP-------------------
Methanosarcina	DEHVRTLIEMCLEHVEEKA---------------------
Methanosarcina acetivorans	DEHVRTLIEMCLEHVEEKI---------------------
Lactobacillus	DKHIISIFQQVAAHAEEADN--------------------
Streptococcus	DEHIRQIMMIALAHKKEVKINV------------------
Oceanobacillus_iheyensis_HTE83	DDHIRQLVSIALIHHQEVENHVS-----------------
***Bacillus_halodurans*_C_125**	DDHVRTILSMAVVHGKEGKGNG------------------
***Bacillus_cereus*_ATCC_10987_2**	DSHVNGLIELAFSHSSEISKKELNM---------------
Exiguobacterium	DHHISSLVHLAMEHVNEGKASS------------------
COG0640	DEHVRQLFRQALEHVQEER---------------------
Desulfovibrio	DDHVRTLFRQGLEHVRERT---------------------
Chlorobium	DSHIAELIKIGFEHVQER----------------------
Desulfitobacterium	DSHVQELYRQGLEHIDE-----------------------
***Bacillus_cereus*_ATCC_14579**	DQHVIHIFEQAFEHVNEEE---------------------
Fusobacterium	DNHVKEIFEQGLIHIQEDKKGDE-----------------
Clostridium	DDHIKQIFDQGYMHITENESGKQV----------------
Thermoanaerobacter	DDHVKKIFEQGFDHINE-----------------------
Clostridium acetobutylicum	DEHIKEIFNMGLMHINEK----------------------
Wolinella	DEHIKNIFDQGMEHILERQGGEYGEA--------------
Moorella	DEHIVHLIREAQEHFAEYR---------------------
Deinococcus radiodurans	DEHVTTLIRSALDHARE-----------------------
Thermus	DRHVEGLLAEALAHAEENT---------------------
Treponema	DNHVGILYSVGLEHIREGR---------------------
Pyrococcus	DEHIREILRTALNHLSEVR---------------------
Anabaena Nostoc	DNHILELYQAVAEHLDEKD---------------------
Thermosynechococcus elongatus	DHHVLTLYEVVAEHLDEEDPETA-----------------
Lactococcus	DRHILHLLKDVAEHLDEQEGGNHEP---------------
Lactobacillus	?DPDVLSMIDAMIEHVEHTAKEHPSNLY-------------
Geobacter	*DSHVGNLLSEGLDHITAQGGHHDS----------------
Methanococcoides	*DEHVRALLELSRSHVMGCAQ--------------------
Mycobacterium_leprae	?DYHLTHIVVDAVAHAGVDAL--------------------
AztR *Anabaena*	*DSHVINLYRSLVENNTYATGTG------------------
CmtR *M. tuberculosis*	*DSHLARALGELVQVVLAVDTDQPCVAERAASGEAVEMTGS

Figure 4.6. An amino acid sequence alignment of the α5 metal binding sites of selected proteins from the SmtB/ArsR family. 51 sequences of the α5 metal binding site from proteins of the SmtB/ArsR family were aligned using ClustalW (Thompson *et al.*, 1997). Residues colored red represent native amino acid residues which are involved in metal binding. Residues colored blue represent non-native amino acid residues which may or may not be involved in metal binding. Purple colored residues represent amino acids that are proposed to be possible candidates for ligands of metal binding. The (*) symbol represents protein sequences that also possess an additional metal binding site (either α3N or α4C). The (?) symbol represents protein sequences that do not possess another known or characterized metal binding site.

M. tuberculosis, *Geobacter, Methanococcoides,* and *M. leprae*) (see Figure 4.6). Three of these three sequences possess a recognizable α3N site (AztR from *Anabaena*, *Geobacter*, and *Methanococcoides*), suggesting that the α5 sensing site may be destroyed. Previous studies on *Synechococcus PCC7942* SmtB showed that C121 could functionally replace E120 in metal ligation (VanZile *et al.*, 2002b) (see Figure 4.6). The α5 site of *Mycobacterium leprae* and *Methanococcoides* contain metal liganding residues (Cys for *Methanococcoides* and Asp for *M. leprae*) immediately following the residue in the C-terminal position (glycine for *Methanococcoides* and valine for *M. leprae*) (see Figure 4.6). It seems possible that the cysteine and aspartate may function as metal ligands in the α5 metal binding site of *Methanococcoides* and *M. leprae*, respectively.

Finally, there is one α5 sensor sequence from *Lactobacillus* that possesses a naturally occurring aspartate substitution at the position corresponding to His86 in CzrA (see Figure 4.6). Since this protein lacks a candidate α3N or α4C metal binding site, this suggests that this aspartate is functional in the family of α5 sensor sites, a result supported by our characterization of H86D CzrA. All of these proteins would need to be characterized before any assignment of metal binding sites can be made, but based on the experiments presented here, it is clear that D84 and H97 play key roles in functional regulation. As a result, our findings suggest that any substitution of D84 or H97 would result in a non-functional α5 sensing site; this has recently been established in two additional members of the ArsR/SmtB family with AztR from *Anabaena sp.* and CmtR from *M. tuberculosis* (see Figure 4.6) (unpublished observations of Liu, Wang and

Giedroc). They both have naturally occurring nonliganding substitutions at the positions corresponding to H97 and H100 in CzrA (see Figure 4.6). AztR does possess a functional α3N site, and CmtR has a functional α4C site.

CHAPTER V

SUMMARY AND PERSPECTIVES

Summary. Prokaryotic metalloregulatory proteins bind and respond to a wide range of heavy metal ions (Brown *et al.*, 2003; Busenlehner *et al.*, 2003; Hantke, 2001a, 2002; van Vliet *et al.*, 2004). Significant and new insight into the molecular determinants of metal ion specificity and selectivity of prokaryotic metalloregulatory transcriptional repressors/activators, and how metal binding is allosterically linked to specific DNA binding properties has been obtained from work published over the last two years (Chapters II & III) (Changela *et al.*, 2003; Eicken *et al.*, 2003; Glasfeld *et al.*, 2003; Pennella *et al.*, 2003; Pohl *et al.*, 2003; Schreiter *et al.*, 2003). Experiments presented here address these issues directly.

In this work, *Staphylococcus aureus* CzrA was shown to bind Co(II) and Zn(II) with high affinity at the α5 metal binding site found in SmtB/ArsR proteins, and inhibits or negatively regulates specific operator/promoter DNA binding when complexed with Zn(II). This site was previously shown in SmtB from *Synechococcus PCC7942* to regulate zinc binding as well (VanZile *et al.*, 2000; VanZile *et al.*, 2002a, b). This site is comprised of carboxylate- and imidazole-containing ligands that preferentially bind smaller, harder metal ions, e.g., Co(II) and Zn(II). Thiolate-rich sites, such as the α3N or α4C metal binding sites, predominantly comprised of cysteine ligands bind larger, softer metal ions such as Cd(II) and Pb(II) (Busenlehner *et al.*, 2002b; Busenlehner *et al.*, 2003; VanZile *et al.*, 2002b). X-ray crystallography, optical absorption, NMR, and

X-ray absorption spectroscopies reveal that the coordination geometry of the α5 site in homodimeric CzrA is tetrahedral and binds metal with two ligands (D84 and H86) from one protomer and two ligands (H97’ and H100’) from the opposite protomer (Chapters II & III) (Eicken *et al.*, 2003; Pennella *et al.*, 2003). CzrA coordinates Zn(II) and Co(II) with tetrahedral geometry while Ni(II), a non-functional metal ion adopts a five or six-coordinate geometry (Chapter II) (Pennella *et al.*, 2003). Strikingly, in the case of *Mycobacterium tuberculosis* NmtR, optical absorption and X-ray absorption spectroscopies reveal Co(II) and Ni(II) bind with five or six-coordinate geometry, while the poorly-functional Zn(II) ion binds with four-coordinate geometry (Chapter II) (Cavet *et al.*, 2002; Pennella *et al.*, 2003). Thus, NmtR expands the coordination number of the α5 metal binding site to 5- or 6-coordinate by recruitment of two additional histidine ligands not present in other α5 sensors, including CzrA, which are proposed to be C-terminal to the α5 helix. In fact, NmtR, which has been shown to be a Ni(II)/Co(II) regulator, possesses an affinity for Zn(II) that is equivalent to or higher than for Ni(II) (Chapter II) (Cavet *et al.*, 2002). Thus, the metal ion which binds with the highest thermodynamic stability, Zn(II), does not result in strong, allosteric regulation in the case of NmtR. These collective results reveal that metal coordination number and geometry, rather than metal affinity, determine metal specificity, in the case of CzrA vs. NmtR (Chapter II) (Cavet *et al.*, 2002; Pennella *et al.*, 2003).

This finding that coordination geometry determines metal ion specificity was also recently observed in the MerR family of metal-responsive transcriptional regulators, as well (Changela *et al.*, 2003). Crystallographic structures of Cu(I) regulator CueR from *E. coli* and the Zn(II) regulator ZntR from *E. coli* showed that CueR binds one copper ion with two cysteine ligands derived from the same monomer in a linear coordination geometry while ZntR binds two zinc ions with four residues derived from one protomer (C114, C115, H119, and C124), while a phosphate (or sulfate) anion and the side chain of C79' from the other protomer bridge the two zinc ions (see Figure 1.1). The two liganding cysteines in CueR are conserved in ZntR, but the two additional cysteines and histidine which are ligands in ZntR are not present in the sequence of CueR. This again illustrates that metal ion selectivity is determined mainly by coordination number (geometry) in these proteins. *In vivo*, CueR regulates the expression of the *cue* operon in response to monovalent Cu(I) over divalent Zn(II), while the opposite is true for ZntR, the regulator of the *znt* operon (Changela *et al.*, 2003).

The mechanism of metal mediated regulation of DNA binding by ArsR/SmtB metal sensors. The family of SmtB/ArsR proteins now has three well-characterized metal binding sites, that are known as the α3N site, the α4C site, and the α5 site. The α3N site utilizes two cysteine ligands from one protomer located in the N-terminal region of the protein before the first α-helix (see Figure 4.1) and two cysteines located on the opposite protomer on the α3 helix, which is part of the helix-turn-helix motif, the putatively assigned DNA binding site for this family of proteins. This is a very well conserved motif throughout the family and is the major sequence determinant by which proteins are assigned to this family (see Chapter IV, Figure 4.1). The α4C site is proposed to involve coordination by two cysteines from one protomer located within the recognition helix (denoted as αR or α4), and one cysteine from the opposite protomer C-terminal to the α5 helix. Although the molecular details are not yet determined, speculation of how metal binding might influence DNA binding in the α3N and α4C sites is facilitated by the fact that each have ligands in or near the helix-turn-helix (α3-turn-α[R/4]) motif. Metal binding to each of these sites would likely result in direct disruption of protein-DNA interactions, with a quarternary structural change perhaps mediated by allosteric ligands derived from the N-terminal (α3N) (Busenlehner *et al.*, 2002b)or C-terminal (α4C) (Cavet *et al.*, 2003) sites, and therefore lower the affinity of the protein-DNA interaction.

The α5 metal-sensing site is distinct from the α3N and α4C sites in that metal binding ligands for this site are not located in the helix-turn-helix (α3-turn-αR) motif (see Figure 4.1). However, like that proposed for the α3N and α4C sites, the α5 site donates two ligands from opposite protomers (see Chapter I, Figure 1.5). X-ray crystallographic and NMR spectroscopy studies on apo and zinc forms of both CzrA and SmtB are consistent with the hypothesis that an intersubunit hydrogen bonding network originating from the nonliganding face of His97 (H117 in SmtB) ($N^{\varepsilon2}$-$H^{\varepsilon2}$) in the α5 site of CzrA across the subunit to the backbone carbonyl of H67 (R87 in SmtB), continuing from the adjacent backbone amide proton (-N-H) of L68 (L88 in SmtB) of CzrA to the backbone carbonyl of L63 (L83 in SmtB) in the putative recognition helix (αR) is present solely in the Zn_2 forms of these proteins. This network clearly links the metal binding site to the proposed DNA binding site. NMR experiments reveal that this hydrogen bonding network originating from H97 in CzrA appears to be evident in solution as well. A distinct and resolved ^{1}H-^{15}N HSQC cross-peak assigned to His97 N$^{\varepsilon 2}$-H$^{\varepsilon 2}$ correlation is only present in the zinc forms of wild-type CzrA and SmtB (see Chapters III and IV).

However, additional experiments with H97 substitution variants that are expected of coordinating zinc in a tetrahedral manner but do not allosterically regulate DNA binding would provide a key test of this model. One approach would be to substitute a cysteine residue for this histidine. Previous studies on the α5 chelate of SmtB have clearly shown that a Cys substitution of H106 (corresponds to H86 in CzrA) is capable of binding zinc with high affinity (VanZile *et al.*, 2002b). In the case of H97 in CzrA, cysteine would likely coordinate zinc, but would not be capable of hydrogen bonding to the backbone carbonyl oxygen of His67, thus preventing the formation of the intersubunit hydrogen bond. Unfortunately, H97C could not be obtained with this cysteine fully reduced, preventing this key experiment.

An additional experiment that could be done to test this model might be to incorporate non-natural amino acid substitutions of His97. Methodology for these types of experiments have had significant developments during the last few years and allow the opportunity to generate proteins with novel and/or modulated properties (Hodgson and Sanderson, 2004). Recently, Muir and colleagues developed a method that allowed the incorporation of 7-aza-tryptophan (7AW) using Expressed Protein Ligation (EPL) (Muralidharan *et al.*, 2004). In this case, an *E. coli* Trp auxotroph was used to uniformly incorporate 7AW into proteins in place of Trp residues. In combination with *in vivo* incorporation of Trp analogues, EPL allows synthetic or recombinant peptides to be joined together by native chemical ligation. An N-terminal cysteine (Cys) containing protein or peptide, is specifically ligated to the C-terminus of a recombinant α-thioester protein, which is generated using an intein fusion (Muralidharan *et al.*, 2004). To test our model for allosteric coupling in CzrA, we would substitute H97 with the analog 5-de-azahistidine, where the $N^{\varepsilon 2}$ is replaced with a carbon atom and therefore cannot donate a hydrogen bond. Incorporation of this analog may be achieved by a nonsense suppression mutagenesis approaches (Steward and Chamberlin, 1998). An alternate method would generate a chemoselective ligated protein that substitutes a backbone amide (-CONH-) with a backbone ester (-COO-), therefore selectively de-stabilizing backbone hydrogen bonds (Blankenship *et al.*, 2002). This methodology would be incorporated at Leu68 of CzrA, which would disrupt the hydrogen bond between the backbone amide of Leu68 to the backbone carbonyl of Leu63 (located in the recognition helix), but maintain the native CzrA metal binding site.

The evidence collected for the α5 sensors, in particular CzrA, allows a generalized model to be put forth about determinants of specificity and the metal ion regulation of DNA binding (Figure 5.1) (Chapters II and III) (Eicken *et al.*, 2003; Pennella *et al.*, 2003). The coordination environment and ligand set within the α5 metal binding site are predominantly tetrahedral with two ligands donated from opposite protomers (see Chapter IV, Figure 4.6). The results presented here suggest that α5 zinc sensors must contain an aspartate at the position corresponding to Asp84 in CzrA and a histidine at the position corresponding to His97 in CzrA, in order to form tetrahedral or distorted tetrahedral coordination sites, and those metals which are unable to easily adopt

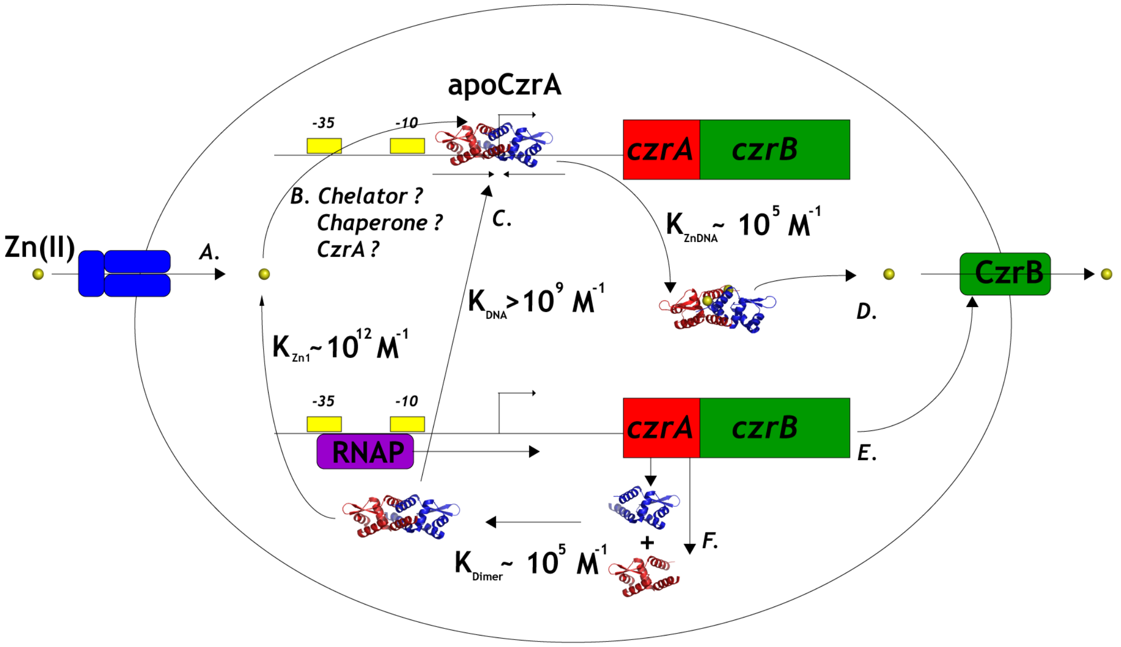
apoCzrA
-35
-10
czrA
czrB
B. Chelator ?
Chaperone ?
CzrA ?
C.
K_{ZnDNA}~ 10^5 M^{-1}
Zn(II)
A.
CzrB
K_{DNA}>10^9 M^{-1}
D.
K_{Zn1}~10^{12} M^{-1}
-35
-10
czrA
czrB
RNAP
E.
+
F.
K_{Dimer}~ 10^5 M^{-1}

Figure 5.1. Model of CzrA regulation of Zn(II). Shown is a schematic depicting how a S. aureus cell responds to elevated intracellular concentrations of Zn(II). **(A.)** Zn(II) enters the cell via an uptake transporter or diffusion through the inner membrane. **(B.)** Zn(II) may be coordinated and transported to other zinc-requiring proteins by an intracellular chelator or a metallo-chaperone specific for zinc. CzrA may also act as a transporter for zinc, but none of these have been demonstrated. **(C.)** Apo-CzrA binds the operator-promoter region of the *czr* operon and **(D.)** binds zinc which results in dissociation from the DNA allowing RNA Polymerase (RNAP) to bind and initiate transcription. The *czrAB* transcript is translated into **(E.)** CzrB, which effluxes excess zinc out of the cell, and **(F.)** CzrA, the repressor , which binds to the *czr O/P* to repress transcription when the excess zinc is completely extruded from the cell.

these geometric constraints (for example Ni(II)) will not be effective as tetrahedral allosteric regulators (Chapter II) (Pennella *et al.*, 2003). In fact, tetrahedral coordination, ligand type, and affinity for zinc appear to be critical for the α5 sensor CzrA to regulate DNA binding. The same applies for other metal sensors sites in this family as well. NmtR is an α5 sensor, which expands the coordination number of the α5 site to 5 or 6, regulates and coordinates Ni(II) and Co(II) with an octahedral geometry but not Zn(II) (Chapter II) (Cavet *et al.*, 2002; Pennella *et al.*, 2003). α3N sensors always contain an N-terminal cysteine and an α3 cysteine (for example *S. aureus* pI258 CadC, Cys7 and Cys60) and form trigonal/tetrahedral thiolate coordination sites and regulate thiophilic metals, for example Cd(II), Pb(II), and Bi(III) (Busenlehner *et al.*, 2002b). α4C sensors use three cysteine ligands which are used to bind and coordinate thiophilic metals Cd(II) and Hg(II) (Brunker *et al.*, 1996; Cavet *et al.*, 2003; Rother *et al.*, 1999).

A striking conclusion from these studies taken collectively is that the ArsR/SmtB family is capable of binding a wide variety of metal ions via three structurally distinct metal binding sites that have appeared independently of one another. However, it seems possible that there may be yet to be identified proteins from this super-family that possess different and specific metal coordination sites other than the ones described here. In fact, another group of metal-responsive proteins that regulate transcription also have members which respond to other environmental stimuli including oxidative stress and antibiotics. These proteins belong to the MerR family of transcriptional activators. This suggests that it is possible there may be members of the ArsR/SmtB family that are not metal-regulators, but responsive to other molecules. The details of the ligand binding and DNA binding properties of these non-metal binding proteins would be facilitated by the work characterizing the metal-responsive family members.

REFERENCES

Andrews, S.C., Robinson, A.K., and Rodriguez-Quinones, F. (2003) Bacterial iron homeostasis. *FEMS Microbiol Rev* **27**: 215-237.

Ansari, A.Z., Chael, M.L., and O'Halloran, T.V. (1992) Allosteric underwinding of DNA is a critical step in positive control of transcription by Hg-MerR. *Nature* **355**: 87-89.

Ansari, A.Z., Bradner, J.E., and O'Halloran, T.V. (1995) DNA-bend modulation in a repressor-to-activator switching mechanism. *Nature* **364**: 371-375.

Anton, A., Weltrowski, A., Haney, C.J., Franke, S., Grass, G., Rensing, C., and Nies, D.H. (2004) Characteristics of zinc transport by two bacterial cation diffusion facilitators from *Ralstonia metallidurans* CH34 and *Escherichia coli*. *J Bacteriol* **186**: 7499-7507.

Arguello, J.M. (2003) Identification of ion-selectivity determinants in heavy-metal transport P1B-type ATPases. *J Membr Biol* **195**: 93-108.

Auld, D.S. (2001) Zinc coordination sphere in biochemical zinc sites. *Biometals* **14**: 271-313.

Banerjee, S., Wei, B., Bhattacharyya-Pakrasi, M., Pakrasi, H.B., and Smith, T.J. (2003) Structural determinants of metal specificity in the zinc transport protein ZnuA from *Synechocystis* 6803. *J Mol Biol* **333**: 1061-1069.

Barkay, T., Miller, S.M., and Summers, A.O. (2003) Bacterial mercury resistance from atoms to ecosystems. *FEMS Microbiol Rev* **27**: 355-384.

Bear, C.A., Duggen, K.A., and Freeman, H.C. (1975) Tetraimidazolezinc(II) perchlorate. *Acta Crystallogr. Sec. B* **31**: 2713.

Benoit, S., Posey, J.E., Chenoweth, M.R., and Gherardini, F.C. (2001) *Treponema pallidum* 3-phosphoglycerate mutase is a heat-labile enzyme that may limit the maximum growth temperature for the spirochete. *J Bacteriol* **183**: 4702-4708.

Berg, J.M., and Shi, Y. (1996) The galvanization of biology: a growing appreciation for the roles of zinc. *Science* **271**: 1081-1085.

Berg, J.M., and Godwin, H.A. (1997) Lessons from zinc-binding peptides. *Annu Rev Biophys Biomol Struct* **26**: 357-371.

Bird, A.J., McCall, K., Kramer, M., Blankman, E., Winge, D.R., and Eide, D.J. (2003) Zinc fingers can act as Zn2+ sensors to regulate transcriptional activation domain function. *Embo J* **22**: 5137-5146.

Blankenship, J.W., Balambika, R., and Dawson, P.E. (2002) Probing backbone hydrogen bonds in the hydrophobic core of GCN4. *Biochemistry* **41**: 15676-15684.

Blencowe, D.K., and Morby, A.P. (2003) Zn(II) metabolism in prokaryotes. *FEMS Microbiol Rev* **27**: 291-311.

Brocklehurst, K.R., Hobman, J.L., Lawley, B., Blank, L., Marshall, S.J., Brown, N.L., and Morby, A.P. (1999) ZntR is a Zn(II)-responsive MerR-like transcriptional regulator of *zntA* in *Escherichia coli*. *Mol Microbiol* **31**: 893-902.

Brown, N.L., Stoyanov, J.V., Kidd, S.P., and Hobman, J.L. (2003) The MerR family of transcriptional regulators. *FEMS Microbiol Rev* **27**: 145-163.

Brunger, A.T., Adams, P.D., Clore, G.M., DeLano, W.L., Gros, P., Grosse-Kunstleve, R.W., Jiang, J.S., Kuszewski, J., Nilges, M., Pannu, N.S., Read, R.J., Rice, L.M., Simonson, T., and Warren, G.L. (1998) Crystallography & NMR system: a new software suite for macromolecular structure determination. *Acta Crystallogr D Biol Crystallogr* **54 (Pt 5)**: 905-921.

Brunker, P., Rother, D., Sedlmeier, R., Klein, J., Mattes, R., and Altenbuchner, J. (1996) Regulation of the operon responsible for broad-spectrum mercury resistance in *Streptomyces lividans* 1326. *Mol Gen Genet* **251**: 307-315.

Busenlehner, L.S., Cosper, N.J., Scott, R.A., Rosen, B.P., Wong, M.D., and Giedroc, D.P. (2001) Spectroscopic properties of the metalloregulatory Cd(II) and Pb(II) sites of *S. aureus* pI258 CadC. *Biochemistry* **40**: 4426-4436.

Busenlehner, L.S., Apuy, J.L., and Giedroc, D.P. (2002a) Characterization of a metalloregulatory bismuth(III) site in *Staphylococcus aureus* pI258 CadC repressor. *J Biol Inorg Chem* **7**: 551-559.

Busenlehner, L.S., Weng, T.C., Penner-Hahn, J.E., and Giedroc, D.P. (2002b) Elucidation of primary (alpha(3)N) and vestigial (alpha(5)) heavy metal-binding sites in *Staphylococcus aureus* pI258 CadC: evolutionary implications for metal ion selectivity of ArsR/SmtB metal sensor proteins. *J Mol Biol* **319**: 685-701.

Busenlehner, L.S., Pennella, M.A., and Giedroc, D.P. (2003) The SmtB/ArsR family of metalloregulatory transcriptional repressors: structural insights into prokaryotic metal resistance. *FEMS Microbiol Rev* **27**: 131-143.

Carrington, P.E., Chivers, P.T., Al-Mjeni, F., Sauer, R.T., and Maroney, M.J. (2003) Nickel coordination is regulated by the DNA-bound state of NikR. *Nat Struct Biol* **10**: 126-130.

Castagnetto, J.M., Hennessy, S.W., Roberts, V.A., Getzoff, E.D., Tainer, J.A., and Pique, M.E. (2002) MDB: the Metalloprotein Database and Browser at The Scripps Research Institute. *Nucleic Acids Res* **30**: 379-382.

Cavet, J.S., Meng, W., Pennella, M.A., Appelhoff, R.J., Giedroc, D.P., and Robinson, N.J. (2002) A nickel-cobalt-sensing ArsR-SmtB family repressor. Contributions of cytosol and effector binding sites to metal selectivity. *J Biol Chem* **277**: 38441-38448.

Cavet, J.S., Graham, A.I., Meng, W., and Robinson, N.J. (2003) A cadmium-lead-sensing ArsR-SmtB repressor with novel sensory sites. Complementary metal discrimination by NmtR AND CmtR in a common cytosol. *J Biol Chem* **278**: 44560-44566.

Changela, A., Chen, K., Xue, Y., Holschen, J., Outten, C.E., O'Halloran, T.V., and Mondragon, A. (2003) Molecular basis of metal-ion selectivity and zeptomolar sensitivity by CueR. *Science* **301**: 1383-1387.

Chivers, P.T., and Sauer, R.T. (1999) NikR is a ribbon-helix-helix DNA-binding protein. *Protein Sci* **8**: 2494-2500.

Chivers, P.T., and Sauer, R.T. (2000) Regulation of high affinity nickel uptake in bacteria. Ni2+-Dependent interaction of NikR with wild-type and mutant operator sites. *J Biol Chem* **275**: 19735-19741.

Chivers, P.T., and Sauer, R.T. (2002) NikR repressor: high-affinity nickel binding to the C-terminal domain regulates binding to operator DNA. *Chem Biol* **9**: 1141-1148.

Christopher, J.A. (1998) SPOCK: The Structural Properties Observations and Calculation Kit. The Center for Macromoleuclar Design, Texas A&M University. College Station, TX

Cook, W.J., Kar, S.R., Taylor, K.B., and Hall, L.M. (1998) Crystal structure of the cyanobacterial metallothionein repressor SmtB: a model for metalloregulatory proteins. *J Mol Biol* **275**: 337-346.

Corwin, D.T., Jr., Fikar, R., and Koch, S.A. (1987) Four- and Five-coordinate cobalt(II) thiolate complexes: models for the catalytic site of alcohol dehydrogenase. *Inorg. Chem.* **26**: 3079-3080.

Cosper, N.J., Stalhandske, C.M., Iwasaki, H., Oshima, T., Scott, R.A., and Iwasaki, T. (1999) Structural conservation of the isolated zinc site in archaeal zinc-containing ferredoxins as revealed by x-ray absorption spectroscopic analysis and its evolutionary implications. *J Biol Chem* **274**: 23160-23168.

Cowtan, K. (1994) No title. *Joint CCP4 and ESF-EACBM Newslatter on Protein Crystallography* **31**: 34-38.

De Pina, K., Desjardin, V., Mandrand-Berthelot, M.A., Giordano, G., and Wu, L.F. (1999) Isolation and characterization of the nikR gene encoding a nickel-responsive regulator in *Escherichia coli*. *J Bacteriol* **181**: 670-674.

Delaglio, F., Grzesiek, S., Vuister, G.W., Zhu, G., Pfeifer, J., and Bax, A. (1995) NMRPipe: a multidimensional spectral processing system based on UNIX pipes. *J Biomol NMR* **6**: 277-293.

Ding, H., and Demple, B. (1996) Glutathione-mediated destabilization in vitro of [2Fe-2S] centers in the SoxR regulatory protein. *Proc.Natl.Acad.Sci.USA* **93**: 9449-9453.

Eicken, C., Pennella, M.A., Chen, X., Koshlap, K.M., VanZile, M.L., Sacchettini, J.C., and Giedroc, D.P. (2003) A metal-ligand-mediated intersubunit allosteric switch in related SmtB/ArsR zinc sensor proteins. *J Mol Biol* **333**: 683-695.

Eide, D.J. (2003) Multiple regulatory mechanisms maintain zinc homeostasis in *Saccharomyces cerevisiae*. *J Nutr* **133**: 1532S-1535S.

Endo, G., and Silver, S. (1995) CadC, the transcriptional regulatory protein of the cadmium resistance system of *Staphylococcus aureus* plasmid pI258. *J Bacteriol* **177**: 4437-4441.

Ferreira, G.C., Franco, R., Mangravita, A., and George, G.N. (2002) Unraveling the substrate-metal binding site of ferrochelatase: an X-ray absorption spectroscopic study. *Biochemistry* **41**: 4809-4818.

Fingerman, I., Nagaraj, V., Norris, D., and Vershon, A.K. (2003) Sfp1 plays a key role in yeast ribosome biogenesis. *Eukaryot Cell* **2**: 1061-1068.

Finney, L.A., and O'Halloran, T.V. (2003) Transition metal speciation in the cell: insights from the chemistry of metal ion receptors. *Science* **300**: 931-936.

Frausto da Silva, J., and Williams, R. (2001) *The Biological Chemistry of Elements: The Inorganic Chemistry of Life.* Oxford: Oxford University Press.

Gajiwala, K.S., and Burley, S.K. (2000) Winged helix proteins. *Curr Opin Struct Biol* **10**: 110-116.

Giedroc, D.P., Chen, X., and Apuy, J.L. (2001) Metal response element (MRE)-binding transcription factor-1 (MTF-1): structure, function, and regulation. *Antioxid Redox Signal* **3**: 577-596.

Glasfeld, A., Guedon, E., Helmann, J.D., and Brennan, R.G. (2003) Structure of the manganese-bound manganese transport regulator of *Bacillus subtilis*. *Nat Struct Biol* **10**: 652-657.

Goddard, T.D., and Kneller, D.G. Sparky 3. University of California, San Francisco.

Godsey, M.H., Baranova, N.N., Neyfakh, A.A., and Brennan, R.G. (2001) Crystal structure of MtaN, a global multidrug transporter gene activator. *J Biol Chem* **276**: 47178-47184.

Gonzalez de Peredo, A., Saint-Pierre, C., Adrait, A., Jacquamet, L., Latour, J.M., Michaud-Soret, I., and Forest, E. (1999) Identification of the two zinc-bound cysteines in the ferric uptake regulation protein from *Escherichia coli*: chemical modification and mass spectrometry analysis. *Biochemistry* **38**: 8582-8589.

Grass, G., Fan, B., Rosen, B.P., Franke, S., Nies, D.H., and Rensing, C. (2001) ZitB (YbgR), a member of the cation diffusion facilitator family, is an additional zinc transporter in *Escherichia coli*. *J Bacteriol* **183**: 4664-4667.

Guedon, E., and Helmann, J.D. (2003) Origins of metal ion selectivity in the DtxR/MntR family of metalloregulators. *Mol Microbiol* **48**: 495-506.

Guffanti, A.A., Wei, Y., Rood, S.V., and Krulwich, T.A. (2002) An antiport mechanism for a member of the cation diffusion facilitator family: divalent cations efflux in exchange for K+ and H+. *Mol Microbiol* **45**: 145-153.

Hantke, K. (2001a) Bacterial zinc transporters and regulators. *Biometals* **14**: 239-249.

Hantke, K. (2001b) Iron and metal regulation in bacteria. *Curr Opin Microbiol* **4**: 172-177.

Hantke, K. (2002) Members of the Fur protein family regulate iron and zinc transport in *E. coli* and characteristics of the Fur-regulated fhuF protein. *J Mol Microbiol Biotechnol* **4**: 217-222.

Hardham, J.M., Stamm, L.V., Porcella, S.F., Frye, J.G., Barnes, N.Y., Howell, J.K., Mueller, S.L., Radolf, J.D., Weinstock, G.M., and Norris, S.J. (1997)

Identification and transcriptional analysis of a *Treponema pallidum* operon encoding a putative ABC transport system, an iron-activated repressor protein homolog, and a glycolytic pathway enzyme homolog. *Gene* **197**: 47-64.

Hazlett, K.R., Rusnak, F., Kehres, D.G., Bearden, S.W., La Vake, C.J., La Vake, M.E., Maguire, M.E., Perry, R.D., and Radolf, J.D. (2003) The *Treponema pallidum* tro operon encodes a multiple metal transporter, a zinc-dependent transcriptional repressor, and a semi-autonomously expressed phosphoglycerate mutase. *J Biol Chem* **278**: 20687-20694.

Heldwein, E.E., and Brennan, R.G. (2001) Crystal structure of the transcription activator BmrR bound to DNA and a drug. *Nature* **409**: 378-382.

Hendrickson, W.A., Horton, J.R., and LeMaster, D.M. (1990) Selenomethionyl proteins produced for analysis by multiwavelength anomalous diffraction (MAD): a vehicle for direct determination of three-dimensional structure. *Embo J* **9**: 1665-1672.

Hodgson, D.R., and Sanderson, J.M. (2004) The synthesis of peptides and proteins containing non-natural amino acids. *Chem Soc Rev* **33**: 422-430.

Horrocks, W.D., Jr., Ishley, J.N., Holmquist, B., and Thompson, J.S. (1980) Structural and electronic mimics of the active site of cobalt(II)-substituted zinc metalloenzymes. *J Inorg Biochem* **12**: 131-141.

Hotz, C., Lowe, N.M., Araya, M., and Brown, K.H. (2003) Assessment of the trace element status of individuals and populations: the example of zinc and copper. *J Nutr* **133**: 1563S-1568S.

Huckle, J.W., Morby, A.P., Turner, J.S., and Robinson, N.J. (1993) Isolation of a prokaryotic metallothionein locus and analysis of transcriptional control by trace metal ions. *Mol Microbiol* **7**: 177-187.

Huyghues-Despointes, B.M., Scholtz, J.M., and Pace, C.N. (1999) Protein conformational stabilities can be determined from hydrogen exchange rates. *Nat Struct Biol* **6**: 910-912.

Huyghues-Despointes, B.M., Pace, C.N., Englander, S.W., and Scholtz, J.M. (2001) Measuring the conformational stability of a protein by hydrogen exchange. *Methods Mol Biol* **168**: 69-92.

Huyghues-Despointes, B.M., Thurlkill, R.L., Daily, M.D., Schell, D., Briggs, J.M., Antosiewicz, J.M., Pace, C.N., and Scholtz, J.M. (2003) pK values of histidine residues in ribonuclease Sa: effect of salt and net charge. *J Mol Biol* **325**: 1093-1105.

Idea, N. (1994) The collaborative CCP4 suite: programs for protein crystallography. *Acta Crystallogr D Biol Crystallogr* **50**: 760-763.

Jacquamet, L., Aberdam, D., Adrait, A., Hazemann, J.L., Latour, J.M., and Michaud-Soret, I. (1998) X-ray absorption spectroscopy of a new zinc site in the fur protein from *Escherichia coli*. *Biochemistry* **37**: 2564-2571.

Jantz, D., Amann, B.T., Gatto, G.J., Jr., and Berg, J.M. (2004) The design of functional DNA-binding proteins based on zinc finger domains. *Chem Rev* **104**: 789-799.

Jefferson, J.R., Hunt, J.B., and Ginsburg, A. (1990) Characterization of indo-1 and quin-2 as spectroscopic probes for Zn2(+)-protein interactions. *Anal Biochem* **187**: 328-336.

Jones, T.A., Zou, J.Y., Cowan, S.W., and Kjeldgaard (1991) Improved methods for building protein models in electron density maps and the location of errors in these models. *Acta Crystallogr A* **47 (Pt 2)**: 110-119.

Jubier-Maurin, V., Rodrigue, A., Ouahrani-Bettache, S., Layssac, M., Mandrand-Berthelot, M.A., Kohler, S., and Liautard, J.P. (2001) Identification of the nik gene cluster of *Brucella suis*: regulation and contribution to urease activity. *J Bacteriol* **183**: 426-434.

Kantardjieff, K.A., Hochtl, P., Segelke, B.W., Tao, F.M., and Rupp, B. (2002) Concanavalin A in a dimeric crystal form: revisiting structural accuracy and molecular flexibility. *Acta Crystallogr D Biol Crystallogr* **58**: 735-743.

Kar, S.R., Adams, A.C., Lebowitz, J., Taylor, K.B., and Hall, L.M. (1997) The cyanobacterial repressor SmtB is predominantly a dimer and binds two Zn2+ ions per subunit. *Biochemistry* **36**: 15343-15348.

Katz, R.A., and Jentoft, J.E. (1989) What is the role of the cys-his motif in retroviral nucleocapsid (NC) proteins? *Bioessays* **11**: 176-181.

Kay, L.E., Keifer, P., and Saarinen, T. (1992) Pure absorption gradient-enhanced heteronuclear single quantum correlation spectroscopy with improved sensitivity. *Journal of the American Chemical Society* **114**: 10663-10665.

Kehres, D.G., and Maguire, M.E. (2003) Emerging themes in manganese transport, biochemistry and pathogenesis in bacteria. *FEMS Microbiol Rev* **27**: 263-290.

Khan, S., Brocklehurst, K.R., Jones, G.W., and Morby, A.P. (2002) The functional analysis of directed amino-acid alterations in ZntR from *Escherichia coli*. *Biochem Biophys Res Commun* **299**: 438-445.

Konopelski, J.P., Reimann, C.W., Hubbard, C.R., D., M.A., and Santoro, A. (1976) Hexakis(imidazole)nickel(II) chloride tetrahydrate. *Acta Crystallogr. Sec. B* **32**: 2911-2913.

Krishna, S.S., Majumdar, I., and Grishin, N.V. (2003) Structural classification of zinc fingers: survey and summary. *Nucleic Acids Res* **31**: 532-550.

Kuroda, M., Hayashi, H., and Ohta, T. (1999) Chromosome-determined zinc-responsible operon czr in *Staphylococcus aureus* strain 912. *Microbiol Immunol* **43**: 115-125.

Kuzmic, P. (1996) Program DYNAFIT for the analysis of enzyme kinetic data: application to HIV proteinase. *Anal Biochem* **237**: 260-273.

Laue, T., Shaw, D., Ridgeway, T., and Pelletier, S. (1991) *Analytical Ultracentrifugation in Biochemistry and Polymer Science.* Cambridge, UK: Royal Society of Chemistry.

Lee, Y.H., Deka, R.K., Norgard, M.V., Radolf, J.D., and Hasemann, C.A. (1999) *Treponema pallidum* TroA is a periplasmic zinc-binding protein with a helical backbone. *Nat Struct Biol* **6**: 628-633.

Lee, Y.H., Dorwart, M.R., Hazlett, K.R., Deka, R.K., Norgard, M.V., Radolf, J.D., and Hasemann, C.A. (2002) The crystal structure of Zn(II)-free *Treponema pallidum* TroA, a periplasmic metal-binding protein, reveals a closed conformation. *J Bacteriol* **184**: 2300-2304.

Liu, T., Nakashima, S., Hirose, K., Shibasaka, M., Katsuhara, M., Ezaki, B., Giedroc, D.P., and Kasamo, K. (2004) A novel cyanobacterial SmtB/ArsR family repressor regulates the expression of a CPx-ATPase and a metallothionein in response to both Cu(I)/Ag(I) and Zn(II)/Cd(II). *J Biol Chem* **279**: 17810-17818.

Lohr, F., Katsemi, V., Betz, M., Hartleib, J., and Ruterjans, H. (2002 Feb) Sequence-specific assignment of histidine and tryptophan ring 1H, 13C and 15N resonances in 13C/15N- and 2H/13C/15N-labelled proteins. *J Biomol NMR* **22**: 153-164.

Mager, W.H., and De Kruijff, A.J. (1995) Stress-induced transcriptional activation. *Microbiol Rev* **59**: 506-531.

Maret, W. (2001) Zinc biochemistry, physiology, and homeostasis-recent insights and current trends. *Biometals* **14**: 187-190.

Marion, D., Kay, L.E., Sparks, S.W., Torchia, D.A., and Bax, A. (1989) Three-dimensional heteronuclear NMR of 15N-labeled proteins. *J.Am.Chem.Soc.* **111**: 1515-1517.

Matthews, J.M., and Sunde, M. (2002) Zinc fingers--folds for many occasions. *IUBMB Life* **54**: 351-355.

McCall, K.A., Huang, C., and Fierke, C.A. (2000) Function and mechanism of zinc metalloenzymes. *J Nutr* **130**: 1437S-1446S.

McCall, K.A., and Fierke, C.A. (2004) Probing determinants of the metal ion selectivity in carbonic anhydrase using mutagenesis. *Biochemistry* **43**: 3979-3986.

Morby, A.P., Turner, J.S., Huckle, J.W., and Robinson, N.J. (1993) SmtB is a metal-dependent repressor of the cyanobacterial metallothionein gene smtA: identification of a Zn inhibited DNA-protein complex. *Nucleic Acids Res* **21**: 921-925.

Muralidharan, V., Cho, J., Trester-Zedlitz, M., Kowalik, L., Chait, B.T., Raleigh, D.P., and Muir, T.W. (2004) Domain-specific incorporation of noninvasive optical probes into recombinant proteins. *J Am Chem Soc* **126**: 14004-14012.

Murshudov, G.N., Vagin, A.A., Lebedev, A., Wilson, K.S., and Dodson, E.J. (1999) Efficient anisotropic refinement of macromolecular structures using FFT. *Acta Crystallogr D Biol Crystallogr* **55 (Pt 1)**: 247-255.

Navarro, C., Wu, L.F., and Mandrand-Berthelot, M.A. (1993) The nik operon of *Escherichia coli* encodes a periplasmic binding-protein-dependent transport system for nickel. *Mol Microbiol* **9**: 1181-1191.

Nies, D., and Brown, N. (1998) *Metal Ions in Gene Regulation.* New York: Chapman & Hall.

O'Halloran, T.V. (1993) Transition metals in control of gene expression. *Science* **261**: 715-725.

Otwinowski, Z. (1993) Oscillation data reduction program. In *Proceedings of the CCP4 Study Weekend: Data Collection and Processing*. Sawyer, L., Isaacs, N. and Bailey, S. (eds). Warrington, UK: SERC Daresbury Laboratory, pp. 56-62.

Outten, C.E., Outten, F.W., and O'Halloran, T.V. (1999) DNA distortion mechanism for transcriptional activation by ZntR, a Zn(II)-responsive MerR homologue in *Escherichia coli*. *J Biol Chem* **274**: 37517-37524.

Outten, C.E., Tobin, D.A., Penner-Hahn, J.E., and O'Halloran, T.V. (2001) Characterization of the metal receptor sites in *Escherichia coli* Zur, an ultrasensitive zinc(II) metalloregulatory protein. *Biochemistry* **40**: 10417-10423.

Pace, C.N., Vajdos, F., Fee, L., Grimsley, G., and Gray, T. (1995) How to measure and predict the molar absorption coefficient of a protein. *Protein Sci* **4**: 2411-2423.

Patzer, S.I., and Hantke, K. (1998) The ZnuABC high-affinity zinc uptake system and its regulator Zur in *Escherichia coli*. *Mol Microbiol* **28**: 1199-1210.

Patzer, S.I., and Hantke, K. (2000) The zinc-responsive regulator Zur and its control of the znu gene cluster encoding the ZnuABC zinc uptake system in *Escherichia coli*. *J Biol Chem* **275**: 24321-24332.

Pennella, M.A., Shokes, J.E., Cosper, N.J., Scott, R.A., and Giedroc, D.P. (2003) Structural elements of metal selectivity in metal sensor proteins. *Proc Natl Acad Sci USA* **100**: 3713-3718.

Pohl, E., Holmes, R.K., and Hol, W.G. (1999) Crystal structure of a cobalt-activated diphtheria toxin repressor-DNA complex reveals a metal-binding SH3-like domain. *J Mol Biol* **292**: 653-667.

Pohl, E., Haller, J.C., Mijovilovich, A., Meyer-Klaucke, W., Garman, E., and Vasil, M.L. (2003) Architecture of a protein central to iron homeostasis: crystal structure and spectroscopic analysis of the ferric uptake regulator. *Mol Microbiol* **47**: 903-915.

Poiarkova, A.V., and Rehr, J.J. (1999) Multiple-scattering x-ray absorption fine-structure Debye-Waller factor calculations. *Phys. Rev. B* **59**: 948-957.

Posey, J.E., Hardham, J.M., Norris, S.J., and Gherardini, F.C. (1999) Characterization of a manganese-dependent regulatory protein, TroR, from *Treponema pallidum*. *Proc Natl Acad Sci USA* **96**: 10887-10892.

Rensing, C., Sun, Y., Mitra, B., and Rosen, B.P. (1998) Pb(II)-translocating P-type ATPases. *J Biol Chem* **273**: 32614-32617.

Rosa, D.T., Krause Bauer, J.A., and Baldwin, M.J. (2001) Structural and spectroscopic studies of the versatile coordination chemistry of the chiral ligand N,N-bis(1-

propan-2-onyl oxime)-L-methionine N'-methylamide with Ni(II) and Zn(II). *Inorg Chem* **40**: 1606-1613.

Rosenzweig, A.C. (2002) Metallochaperones: bind and deliver. *Chem Biol* **9**: 673-677.

Rother, D., Mattes, R., and Altenbuchner, J. (1999) Purification and characterization of MerR, the regulator of the broad-spectrum mercury resistance genes in *Streptomyces lividans* 1326. *Mol Gen Genet* **262**: 154-162.

Rutherford, J.C., Cavet, J.S., and Robinson, N.J. (1999) Cobalt-dependent transcriptional switching by a dual-effector MerR-like protein regulates a cobalt-exporting variant CPx-type ATPase. *J Biol Chem* **274**: 25827-25832.

Schreiter, E.R., Sintchak, M.D., Guo, Y., Chivers, P.T., Sauer, R.T., and Drennan, C.L. (2003) Crystal structure of the nickel-responsive transcription factor NikR. *Nat Struct Biol* **10**: 794-799.

Scott, R.A. (1985) Measurement of metal-ligand distances by EXAFS. *Methods Enzymol.* **117**: 414-459.

Shi, W., Wu, J., and Rosen, B.P. (1994) Identification of a putative metal binding site in a new family of metalloregulatory proteins. *J Biol Chem* **269**: 19826-19829.

Silver, S., and Phung, L.T. (1996) Bacterial heavy metal resistance: new surprises. *Annu Rev Microbiol* **50**: 753-789.

Singh, V.K., Xiong, A., Usgaard, T.R., Chakrabarti, S., Deora, R., Misra, T.K., and Jayaswal, R.K. (1999) ZntR is an autoregulatory protein and negatively regulates the chromosomal zinc resistance operon znt of *Staphylococcus aureus*. *Mol Microbiol* **33**: 200-207.

Spolar, R.S., and Record, M.T., Jr. (1994) Coupling of local folding to site-specific binding of proteins to DNA. *Science* **263**: 777-784.

Steward, L.E., and Chamberlin, A.R. (1998) Protein engineering with nonstandard amino acids. *Methods Mol Biol* **77**: 325-354.

Sun, Y., Wong, M.D., and Rosen, B.P. (2001) Role of cysteinyl residues in sensing Pb(II), Cd(II), and Zn(II) by the plasmid pI258 CadC repressor. *J Biol Chem* **276**: 14955-14960.

Tapiero, H., and Tew, K.D. (2003) Trace elements in human physiology and pathology: zinc and metallothioneins. *Biomed Pharmacother* **57**: 399-411.

Terwilliger, T.C., and Berendzen, J. (1999) Automated MAD and MIR structure solution. *Acta Crystallogr D Biol Crystallogr* **55 (Pt 4)**: 849-861.

Terwilliger, T.C. (2000) Maximum-likelihood density modification. *Acta Crystallogr D Biol Crystallogr* **56 (Pt 8)**: 965-972.

Thelwell, C., Robinson, N.J., and Turner-Cavet, J.S. (1998) An SmtB-like repressor from *Synechocystis* PCC 6803 regulates a zinc exporter. *Proc Natl Acad Sci USA* **95**: 10728-10733.

Thompson, J.D., Gibson, T.J., Plewniak, F., Jeanmougin, F., and Higgins, D.G. (1997) The CLUSTAL_X windows interface: flexible strategies for multiple sequence alignment aided by quality analysis tools. *Nucleic Acids Res* **25**: 4876-4882.

Turner, J.S., Glands, P.D., Samson, A.C.R., and Robinson, N.J. (1996) Zn2+-sensing by the cyanobacterial metallothionein repressor SmtB: different motifs mediate metal-induced protein-DNA dissociation. *Nucl.Acids Res.* **19**: 3714-3721.

van Vliet, A.H., Poppelaars, S.W., Davies, B.J., Stoof, J., Bereswill, S., Kist, M., Penn, C.W., Kuipers, E.J., and Kusters, J.G. (2002) NikR mediates nickel-responsive transcriptional induction of urease expression in *Helicobacter pylori*. *Infect Immun* **70**: 2846-2852.

van Vliet, A.H., Ernst, F.D., and Kusters, J.G. (2004) NikR-mediated regulation of *Helicobacter pylori* acid adaptation. *Trends Microbiol* **12**: 489-494.

VanZile, M.L., Cosper, N.J., Scott, R.A., and Giedroc, D.P. (2000) The zinc metalloregulatory protein *Synechococcus* PCC7942 SmtB binds a single zinc ion per monomer with high affinity in a tetrahedral coordination geometry. *Biochemistry* **39**: 11818-11829.

VanZile, M.L., Chen, X., and Giedroc, D.P. (2002a) Allosteric negative regulation of smt O/P binding of the zinc sensor, SmtB, by metal ions: a coupled equilibrium analysis. *Biochemistry* **41**: 9776-9786.

VanZile, M.L., Chen, X., and Giedroc, D.P. (2002b) Structural characterization of distinct alpha3N and alpha5 metal sites in the cyanobacterial zinc sensor SmtB. *Biochemistry* **41**: 9765-9775.

Walkup, G.K., and Imperiali, B. (1997) Fluorescent chemosensors for divalent zinc based on zinc finger domains. Enhanced oxidative stability, metal binding affinity, and structural and functional characterization. *J Am Chem Soc* **119**: 3443-3450.

White, A., Ding, X., vanderSpek, J.C., Murphy, J.R., and Ringe, D. (1998) Structure of the metal-ion-activated diphtheria toxin repressor/tox operator complex. *Nature* **394**: 502-506.

Wishart, D.S., and Sykes, B.D. (1994) Chemical shifts as a tool for structure determination. *Methods Enzymol.* **239**: 363-392.

Wishart, D.S., Bigam, C.G., Yao, J., Abildgaard, F., Dyson, H.J., Oldfield, E., Markley, J.L., and Sykes, B.D. (1995) 1H, 13C and 15N chemical shift referencing in biomolecular NMR. *J Biomol NMR* **6**: 135-140.

Wong, M.D., Lin, Y.F., and Rosen, B.P. (2002) The soft metal ion binding sites in the *Staphylococcus aureus* pI258 CadC Cd(II)/Pb(II)/Zn(II)-responsive repressor are formed between subunits of the homodimer. *J Biol Chem* **277**: 40930-40936.

Wu, J., and Rosen, B.P. (1993) Metalloregulated expression of the ars operon. *J Biol Chem* **268**: 52-58.

Xiong, A., and Jayaswal, R.K. (1998) Molecular characterization of a chromosomal determinant conferring resistance to zinc and cobalt ions in *Staphylococcus aureus*. *J Bacteriol* **180**: 4024-4029.

Xu, C., Zhou, T., Kuroda, M., and Rosen, B.P. (1998) Metalloid resistance mechanisms in prokaryotes. *J Biochem (Tokyo)* **123**: 16-23.

Yamaguchi, K., Cosper, N.J., Stalhandske, C., Scott, R.A., Pearson, M.A., Karplus, P.A., and Hausinger, R.P. (1999) Characterization of metal-substituted *Klebsiella aerogenes* urease. *J Biol Inorg Chem* **4**: 468-477.

Yoon, K.P., Misra, T.K., and Silver, S. (1991) Regulation of the cadA cadmium resistance determinant of *Staphylococcus aureus* plasmid pI258. *J Bacteriol* **173**: 7643-7649.

Yoon, K.P., and Silver, S. (1991) A second gene in the *Staphylococcus aureus* cadA cadmium resistance determinant of plasmid pI258. *J Bacteriol* **173**: 7636-7642.

Zabinsky, S.I., Rehr, J.J., Ankudinov, A., Albers, R.C., and Eller, M.J. (1995) Multiple-scattering calculations of x-ray-absorption spectra. *Phys. Rev. B* **52**: 2995-3009.

VITA

NAME: Mario Antonio Pennella

BIRTHDAY: August 5, 1975

BIRTHPLACE: Bartlesville, Oklahoma

EDUCATION: B.S., Biochemistry (1997)
University of Oklahoma
Norman, Oklahoma

Ph.D., Biochemistry (2005)
Texas A&M University
College Station, TX

PUBLICATIONS: Cavet JS, Meng W, Pennella MA, Appelhoff RJ, Giedroc DP and Robinson NJ. (2002) A nickel-cobalt-sensing ArsR-SmtB family repressor. Contributions of cytosol and effector binding sites to metal selectivity. *Journal of Biological Chemistry* 277:38441-38448.

Pennella MA, Shokes JE, Cosper NJ, Scott RA and Giedroc DP. (2003) Structural elements of metal selectivity in metal sensor proteins. *Proc. Natl. Acad. Sci. USA* 100: 3713-3718.

Busenlehner LS, Pennella MA and Giedroc DP (2003) The SmtB/ArsR family of metalloregulatory transcriptional repressors: structural insights into prokaryotic metal resistance. *FEMS Microbiology Reviews* 27: 131-143.

*Eicken C, *Pennella MA, Chen X, Koshlap KM, VanZile ML, Sacchettini JC and Giedroc DP. (2003) A Metal-Ligand-mediated Intersubunit Allosteric Switch in Related SmtB/ArsR Zinc Sensor Proteins. *Journal of Molecular Biology* 333: 683-695.

*Denotes joint first authorship

PERMANENT ADDRESS: Department of Biochemistry and Biophysics
College Station, TX 77843-2128